Institutionen för vattenbyggnad
Chalmers Tekniska Högskola

Department of Hydraulics
Chalmers University of Technology

BARRIER-TYPE BREAKWATERS

TRANSMISSION, REFLECTION AND FORCES

by

Mickey Johansson

Submitted to the School of Civil Engineering, Chalmers University of Technology
in partial fulfillment of the requirements for the degree of Doctor of Philosophy.

Report
Series A:19
ISSN 0348-1050

Göteborg 1989

Address: Department of Hydraulics
Chalmers University of Technology
S-412 96 Göteborg, Sweden
Telephone: 031 - 72 10 00

SUMMARY

This is a study of partly submerged breakwaters with a gap between the bottom of the breakwater and the sea bottom. Mainly fixed breakwaters, built up from the sea bottom with columns or piles, are treated. Floating breakwaters are also covered to some extent.

The study consists of a theoretical and an experimental part. The calculated and measured main parameters are: reflected and transmitted waves, forces and moments, and pressure.

In the theoretical study the structure/fluid interaction problem is solved by assuming a linear model and a non–viscous fluid. Three solution procedures have been developed; one for breakwaters with a rectangular cross section, a second for breakwaters with a rectangular cross section and a protruding bottom plate facing the incident waves and a third for breakwaters of more general cross section*. The breakwaters are modelled to be impermeable.

The experimental part deals mainly with a fixed breakwater with rectangular cross section. For regular wave excitations, transmitted and reflected waves, forces and moments, and pressure at the bottom of the breakwater were measured. The transmitted waves were also measured for irregular wave excitations. In addition, the transmitted waves were measured for the breakwater with a protruding bottom plate.

The generation of irregular waves was performed using a technique in which faster wave components were successively delayed. This allowed for longer recordings of responses before the problem of reflected waves arose.

The measured transmitted and reflected waves agree reasonably well with the calculated ones. The maximum to minimum values of the horizontal force also agree well with theory, while the vertical force is significantly contaminated by a double harmonic (component at twice the frequency of wave generation). The double harmonic characteristic of the vertical force is especially pronounced for short and steep waves.

* first and second solutions being applications of Principality of Monaco's patented process "waterwall" (no. PCT/MC/86/00003 and no. F8515938).

It is shown how the wave protection can be significantly improved by using a breakwater with a protruding bottom plate rather than a rectangular one. This is confirmed both by potential theory and measurements.

PREFACE

Research concerning wave/structure interaction has been performed at the Department of Hydraulics, Chalmers University of Technology, since the mid 70s. Wave energy devices, offshore structures and harbour units have been included. Since 1980 the National Swedish Board of Technical Development (STU) has sponsored the activities in the project "Offshore Structures – Wave Forces and Motions".

This thesis is the result of a part of the project concerning surface oriented breakwaters with a gap between the bottom of the breakwater and the sea bottom. The work has been carried out at the Department of Hydraulics and is submitted in partial fulfillment of the requirements for the degree of Doctor of Philosophy.

The project was initiated as a Ph.D. study when the Department of Hydraulics became involved in an experimental study ordered by the Principality of Monaco in order to precise the optimal characteristics of a breakwater implementing their own patented process "waterwall" (see second reference in list of references) and suitable to their La Condamine Harbour extension project. It should be emphasized that the configurations studied in the thesis are patented by the Principality of Monaco in patents Nos. PCT/MC/86/00003 and F 85 15938. In this connection, I am especially grateful to the Government of the Principality of Monaco, who addressed and interesting concept to be studied and agreed to the publication of the experimental data.

I am indebted to my colleagues at the Department of Hydraulics for their valuable contributions and for creating a stimulating work environment. I especially wish to express gratitude to my advisor, Professor Lars Bergdahl, who has supported and encouraged me throughout the study, to Professor Anders Sjöberg, Gösta Lindvall, Bengt Carlsson and Karl–Oskar Djärv for their contributions in the experimental part of the study and to Anne–Marie Hellgren and Yvonne Young for patiently typing the manuscript.

Lastly I wish to thank Dr. Wojciech Sulisz for giving me valuable advice concerning the theoretical part of the study.

Göteborg, April 1989

Mickey Johansson

CONTENTS

INTRODUCTION

1.1 Background

Breakwaters are used in order to protect a certain location from waves, for example a harbour. The breakwater is meant to prevent the energy of the incident waves from entering a harbour. This can be effected either by reflecting the energy or converting it into heat.

The most common type of breakwater is the mound type with a sloped front facing the incident waves. This structure may be constructed of natural rock, prefabricated concrete elements or a combination. A typical rubble mound breakwater, placed at the seabottom and piercing the free water surface, is built with a front slope inclined about 1:1.5 (Figure 1.1). In deep water the volume of material needed for such breakwaters is large, and therefore they are expensive to build.

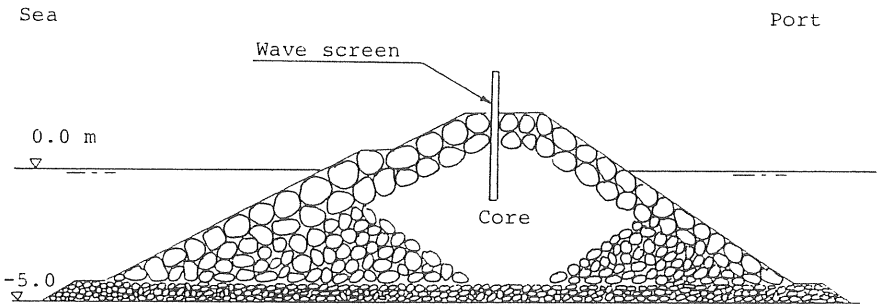

Figure 1.1 Example of a rubble mound breakwater.

In the present study an alternative type of breakwater is studied. The breakwater is located in the free water surface with a gap between the bottom of the breakwater and the sea bottom. The concept is presented schematically in Figure 1.2. Such a concept has been proposed and patented by the Principality of Monaco for its own Port de la Condamine project, see Bouchet and Manzone (1986). The coast in the vicinity of the Principality is extremely steep and, even close to the shore, the water depth is considerable.

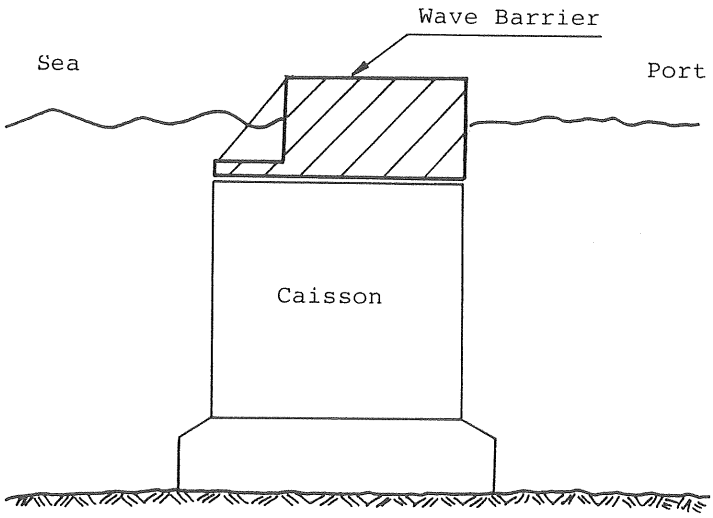

Figure 1.2 Alternative type of breakwater.

In the present study mainly fixed breakwaters, built up from the sea bottom with caissons or piles according to the patented concept, are treated. To some extent also floating breakwaters, assumed to be kept in position by mooring systems, are covered.

The breakwaters are assumed to be impermeable which, according to non–viscous theory, means that the energy of the incident waves is partly reflected against the breakwater and partly transmitted through the gap. Since most of the energy in waves is concentrated to the upper part of the sea, near the free surface, the types of breakwater discussed can be rather effective in terms of wave reduction, at least if the wave length is not too long.

1.2 Scope of the study

It has been noted that the choice of cross section of the breakwater significantly influences the transmission of wave energy. Three different solution procedures have been developed to solve the hydrodynamic problem of the surface oriented type of breakwater. Assuming the incident wave has crests parallel with the breakwater and neglecting the influence from any columns or piles, the problem can be treated as two–dimensional.

All three solution procedures are two–dimensional. They are based on the linear wave theory and the assumption that the fluid is non–viscous. The mathematical formulation of the problem is outlined in Chapter 2.

The first procedure is for a fixed breakwater of rectangular cross section with a protruding bottom plate facing the incident waves, see Figure 1.3a. The second procedure is for a fixed or floating breakwater of rectangular cross section, see Figure 1.3b. In the third procedure fixed and floating 2D structures of more general geometry are considered, and the formulation also allows the water depth in the vicinity of the structure to vary, see Figure 1.3.c. In procedures I and II the field quantities such as fluid velocities and pressure are solved as continuous functions throughout fluid sub domains whereas in procedure III the boundaries enclosing the fluid domain are discretized into elements assuming the field quantities to be constant across each element. The three solving procedures mentioned above are outlined briefly in Chapter 3. A more detailed description of the procedures is given in Appendices I, II and III.

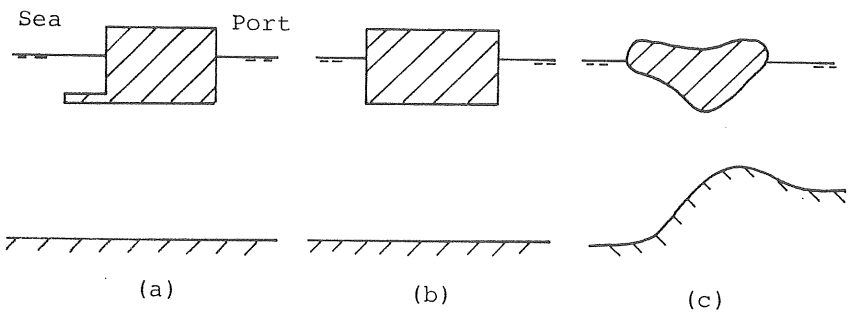

Figure 1.3 Geometries associated with the three solution procedures presented.

The experimental study presented here is primarily for a fixed breakwater with a rectangular cross section. For regular wave excitations, transmitted and reflected waves, forces and moments as well as pressure at the bottom of the breakwater were measured. The transmitted waves were also evaluated from experiments in irregular waves. In addition, transmitted waves for the breakwater with a protruding bottom plate were measured. The performance and methodology of the experimental study are described in Chapter 4.

In Chapter 5 results obtained from the theoretical study and the experimental study are presented. Comparisons are made between the different solution procedures as well as with findings of other authors. It is shown how a breakwater with a protruding bottom plate significantly reduces the transmission coefficient in comparison with a rectangular breakwater. Comparisons between theoretical and experimental data are presented. Agreements and discrepancies are discussed.

Conclusions drawn from the study are summarized in Chapter 6.

2 MATHEMATICAL FORMULATION

2.1 Fundamentals

The mathematical formulation presented below is first reviewed for 3D structures and subsequently discussed for the 2D case. Both the problem of fixed structures and floating structures are described.

To justify use of a linear hydrodynamic theory, both small structural motions and small wave amplitudes are assumed. The structures are assumed to be rigid, and therefore any motion of the structure can be described by motions in six modes, i.e. three translations and three rotations. A Cartesian coordinate system, Oxyz, is defined with its origin in the free mean water surface and its z–axis positive upwards and oriented through the center of gravity. The vector of motion is denoted by $\underline{x}$ and contains the following elements:

x_1 = translation in the x–direction	= surge motion
x_2 = translation in the y–direction	= sway motion
x_3 = translation in the z–direction	= heave motion
x_4 = rotation about the x–axis	= roll motion
x_5 = rotation about the y–axis	= pitch motion
x_6 = rotation about the z–axis	= yaw motion

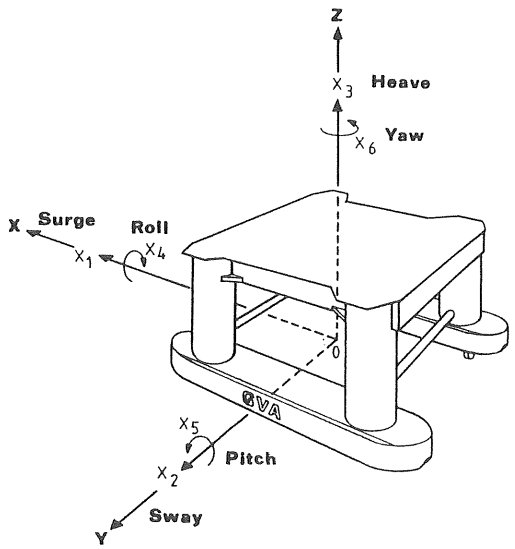

Figure 2.1 Definition of coordinate system and modes of motion.

The fluid is assumed to be ideal (non–viscous) and the flow to be irrotational. The assumption that the flow can be considered irrotational is important to the formulation of the problem. Generally, the flow is described using the velocity vector, but when the flow is irrotational it can be described using a single scalar, the velocity potential $\Phi(x,y,z,t)$.

For irrotational flow, also called potential flow, a velocity potential exists such that

$$\underline{u} = \nabla\Phi \tag{2.1}$$

where the velocity vector $\underline{u}$ is given by

$$\underline{u} = u\underline{i} + v\underline{j} + w\underline{k}$$

and the operator, ∇, by

$$\nabla = \frac{\partial}{\partial x}\underline{i} + \frac{\partial}{\partial y}\underline{j} + \frac{\partial}{\partial z}\underline{k}$$

where $\underline{i}$, $\underline{j}$ and $\underline{k}$ are unit vectors along the x, y and z axis respectively.

If the fluid is assumed to be incompressible the continuity equation may be written

$$\nabla \cdot \underline{u} = 0 \tag{2.2}$$

and if Eq. (2.1) is substituted into Eq. (2.2) one obtains

$$\nabla^2\Phi = 0 \tag{2.3}$$

which is the Laplace equation, expressing conservation of fluid mass for potential flow. From this it is clear that the velocity potential is related to the velocity vector in a simple way, and in fact it is equally simply related to pressure distribution and wave elevation. Therefore, the main problem is to solve the Laplace equation with appropriate boundary conditions.

Consider a regular wave propagating in a direction towards the structure. The incident wave is disturbed by the presence of the structure and this results in a diffracted wave. The diffracted wave causes a change in the dynamic pressure which, integrated over the wet surface of the structure, gives the wave exciting force. Consistent with the linear theory, even for a floating structure, the wave exciting force is calculated when the structure is fixed in its equilibrium position.

The problem associated with the wave exciting force is referred to as the diffraction problem. If the structure is free to move, the wave exciting force will force the structure to oscillate. The movement forces the fluid mass adjacent to the structure to accelerate and decelerate and creates a radiated wave. This influence on the system is accounted for by the hydrodynamic reaction force which, in a linear formulation, is determined when the structure is forced to oscillate in the absence of an incident wave. This latter problem is referred to as the radiation problem.

In fact, the diffraction problem and the radiation problems associated with motions in different modes are mathematically similar. This because the moving boundary conditions are applied when the structure is in its equilibrium position, which, in turn, is justified by the assumption of small structural motions.

The formulation below assumes that the solution is time harmonic with the angular frequency ω. Before proceeding with the boundary conditions for the problems described above it is convenient to decompose the velocity potential $\Phi(x,y,z,t)$ into a spatial component and a time harmonic component. Using complex notation the decomposition may be set as

$$\Phi(x,y,z,t) = \phi^{(l)}(x,y,z)\dot{x}_l(t), \quad l=1,2,..,6 \tag{2.4}$$

where $\phi^{(l)}(x,y,z)$ is the spatial velocity potential associated with the radiation problem in the l:th mode of motion and

$$x_l(t) = x_l\, e^{-i\omega t},$$

the structural motion in the corresponding mode. The velocity potential of the diffraction problem, $\phi^{(7)}(x,y,z)$, is simply decomposed by

$$\Phi(x,y,z,t) = \phi^{(7)}(x,y,z)\, e^{-i\omega t} \tag{2.5}$$

It should be emphasized that complex notation implies that harmonic quantities such as velocities, pressure, etc., are complex and thereby include information of both amplitudes and phases. The corresponding physical quantities are simply obtained by taking the real part of the complex value. The spatial velocity potential $\phi^{(l)}(x,y,z)$ has to satisfy the Laplace equation throughout the fluid domain. At the

boundaries enclosing the fluid domain, various boundary conditions are applied. At the free water surface both a kinematic and a dynamic boundary condition are required. The kinematic condition states that the normal velocity of the fluid and the boundary surface must be equal. The dynamic condition states that the pressure at the free water surface must be atmospheric. Expressed in terms of the spatial velocity potential, the two conditions, combined and linearized, give the free surface condition

$$\frac{\partial \phi^{(l)}}{\partial z} - \frac{\omega^2}{g} \phi^{(l)} = 0 \qquad (2.6)$$

It is consistent with the linear assumption to apply this condition at the mean water level, i.e. z=0. For further details see, for example, Newman (1977). At the sea bottom the condition

$$\frac{\partial \phi^{(l)}}{\partial n} = 0 \qquad (2.7)$$

is applied, which states that the sea bottom is assumed to be impermeable and therefore that the velocity normal to the sea bottom equals zero. The surface of the structure is also assumed to be impermeable and consequently the boundary condition at the surface of the fixed structure is identical to the sea bottom condition, i.e.

$$\frac{\partial \phi^{(7)}}{\partial n} = 0 \qquad (2.8a)$$

while for a moving structure the normal velocity of the structure should equal the normal velocity of the adjacent fluid particle and hence,

$$\frac{\partial \phi^{(l)}}{\partial n} = n_l, \quad l=1,...,6 \qquad (2.8b)$$

where

$n_1 = n_x$ = x–component of the normal vector (2.9)
$n_2 = n_y$ = y–component of the normal vector
$n_3 = n_z$ = z–component of the normal vector
$n_4 = yn_3 - zn_2$
$n_5 = zn_1 - xn_3$
$n_6 = xn_2 - yn_1$

Finally, to give the problem a unique solution, a boundary condition must be applied at a surface connecting the free water surface and the sea bottom at some distance from the structure. If the fluid domain is taken to be infinitly large this radiation condition becomes

$$\frac{\partial \phi^{(l)}}{\partial r} = (-\frac{1}{2r} + ik)\phi^{(l)}, \quad r \to \infty \tag{2.10a}$$

where r is the polar radius in the horizontal plane and k the wave number given by the dispersion relation

$$k \tanh kh = \frac{\omega^2}{g} \tag{2.10b}$$

The radiation condition above assumes that the water depth h is constant for $r \to \infty$ and states that the waves behave like restricted outwards propagating waves. The main problem is now to solve the Laplace equation under consideration of the boundary conditions. It should be pointed out that the only differences between the radiation problems and the diffraction problem appears in the boundary condition applied at the surface of the structure.

One of the objectives in the present work is to study how well the horizontal cylinder works as protection against waves. Therefore we need know how to calculate reflected waves and transmitted waves respectively. In fact, the free surface elevation is simply related to the velocity potential by

$$\zeta = -\frac{1}{g}\frac{\partial \Phi}{\partial t}, \quad z = 0 \tag{2.11}$$

The expression is obtained from the dynamic free surface boundary condition which states that the pressure is atmospheric at the free surface.

Before proceeding with the next section let us discuss the 2D case when all variations along the y–axis are omitted as in Figure 2.2.

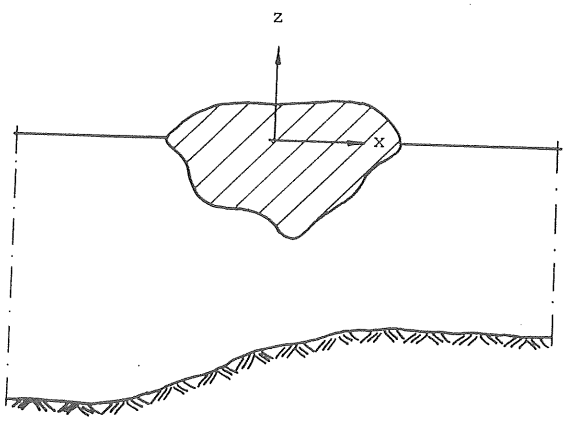

Figure 2.2 2D structure with no variations along the y–axis.

For such a geometry the force vector and the motion vector will be reduced and only contain quantities in surge, heave and pitch. The only change in the formulation above worth mentioning appears in the radiation condition which reduces to

$$\frac{\partial \phi^{(l)}}{\partial x}(x,z) - ik_r \phi^{(l)} = 0, \quad x \to \infty \tag{2.12a}$$

$$\frac{\partial \phi^{(l)}}{\partial x}(x,z) + ik_l \phi^{(l)} = 0, \quad x \to -\infty \tag{2.12b}$$

where k_l, k_r are the wave number associated with the water depth far away from the structure at the left and right side respectively.

2.2 Forces and moments

If we proceed from the Navier–Stokes equation for a viscous fluid, the Bernoulli equation for irrotational flow can be derived. Expressed in terms of the velocity potential it becomes

$$\frac{\partial \Phi}{\partial t} + \frac{1}{2}\nabla\Phi \cdot \nabla\Phi + \frac{p}{\rho} = 0 \tag{2.13}$$

and gives the pressure throughout the fluid domain. Since we are interested in a linear solution the second term is neglected. The Bernoulli equation then becomes

$$p = -\rho \frac{\partial \Phi}{\partial t} - \rho g z \tag{2.14}$$

where the first term represents the hydrodynamic pressure and the second term the hydrostatic pressure. From the Bernoulli equation the pressure distribution is known throughout the fluid, and by integrating the pressure over the wet surface of the structure, forces and moments are obtained. They can be expressed as

$$F_j = \iint_S p n_j \, dS, \quad j=1,2,....,6 \tag{2.15}$$

where the elements n_j are defined by Eq. (2.9) and

F_1 = force along the x–axis
F_2 = force along the y–axis
F_3 = force along the z–axis
F_4 = moment about the x–axis
F_5 = moment about the y–axis
F_6 = moment about the z–axis

The wave exciting force obtained from the solution of the diffraction problem is calculated directly in accordance with Eq. (2.15) while for the radiation problems the hydrodynamic reaction force is usually written as

$$F_i = -\sum_{j=1}^{6} (a_{ij} \ddot{x}_j + b_{ij} \dot{x}_j), \quad i = 1,2, ...,6 \tag{2.16}$$

where the hydrodynamic coefficients a_{ij} and b_{ij} are taken as real and known as the added mass and damping coefficients respectively. Physically, the added mass coefficients can be thought of as masses of water being accelerated by the motion of the structure and the damping coefficients as the effect of damping of the structure introduced when the motion of the structure creates radiated waves. The damping is often referred to as potential damping or radiation damping. Expressed in terms of the spatial velocity potential the hydrodynamic coefficients become

$$a_{ij} + \frac{i\ b_{ij}}{\omega} = \rho \iint_S \phi^{(j)} n_i \, dS \qquad (2.17)$$

Finally, it should be mentioned that the forces of the diffraction problem can be solved using an alternative approach called the Haskind relation, see Newman (1962). This relation is a consequence of Green's theorem and makes it possible to calculate the wave exciting force without having solved the potentials of the diffraction problem. A form of Haskind's relation is

$$F_i = i\omega\rho \iint_{S_\infty} \left[\phi^{(i)} \frac{\partial \phi_I}{\partial n} - \phi_I \frac{\partial \phi^{(i)}}{\partial n} \right] dS\, e^{-i\omega t} \qquad (2.18)$$

where ϕ_I is the spatial velocity potential of the undisturbed incident wave which, for water of constant depth, is given by

$$\phi_I = -\frac{igA}{\omega} e^{ikx} \frac{\cosh k(z+h)}{\cosh kh} \qquad (2.19)$$

where

a = wave amplitude
k = wave number
h = water depth

The surface of integration S_∞ is a surface connecting the free water surface and the sea bottom and is often conveniently chosen far away from the structure.

It should be emphasized that only the wave exciting forces and not the pressure distribution or the pattern of the diffracted wave, can be obtained using the Haskind relation. If the pressure or the wave pattern is of interest the velocity potential of the diffraction problem must be solved. Nevertheless, the Haskind relation is an excellent tool for use in checking computer codes.

2.3 Motions

The motions of the structure are calculated from Newton's second law which, if the generalized force vector includes forces and moments and the generalized

motion vector includes translation and rotations, becomes

$$\sum_{j=1}^{6} (m_{ij} + a_{ij})\ddot{x}_j + b_{ij}\dot{x}_j + c_{ij}x_j = F_i, \quad i = 1,...,6 \qquad (2.20)$$

where

m_{ij} = elements of the mass matrix

a_{ij} = elements of the added mass matrix, defined by Eq. (2.17)

b_{ij} = elements of the damping matrix, defined by Eq. (2.17)

c_{ij} = elements of the hydrostatic matrix

If we only consider the two dimensional horizontal cylinder given in Figure 2.2 the equation of motion reduces to

$$\sum_{j=1,3,5} (m_{ij} + a_{ij})\ddot{x}_j + b_{ij}\dot{x}_j + c_{ij}x_j = F_i, \quad i = 1,3,5 \qquad (2.21)$$

If it is assumed that the z–axis points through the center of gravity of the cylinder the only non–zero elements of the mass matrix and the hydrostatic matrix are

$$m_{11} = m$$
$$m_{15} = mz_G$$
$$m_{33} = m$$
$$m_{51} = mz_G$$
$$m_{55} = mr_p^2$$

$$c_{33} = \rho g A_w$$
$$c_{35} = -\rho g x_c A_w$$
$$c_{53} = -\rho g x_c A_w$$
$$c_{55} = \rho g \forall z_B - mgz_G + \rho g J$$

where

m = mass of cylinder

z_G = center of gravity

r_p = pitch radius of gyration

ρ = density of water

x_c = center of gravity of the water plane area

A_w = water plane area

$\forall$ = water volume displaced by the structure

z_B = center of buoyancy

J = moment of inertia at the water plane area about the y–axis

For further insight in the linear theory see, for example, Newman (1977), Sarpkaya and Isaacson (1981), Mei (1983) and Chakrabarti (1987).

3. SOLUTION PROCEDURES

The main problem in the theoretical study is to solve the Laplace equation under consideration of appropriate boundary conditions. There are a variety of solution procedures to choose among. For structures of simpler geometries the field quantities such as fluid velocity and pressure can be solved as continuous functions througout fluid sub domains. This can be achieved using the method of separation of variables. This method has been used extensively for axisymmetrical three–dimensional problems, for example by Garret (1971), Yeung (1981) and Guoping (1987). For two–dimensional problems it has been used, for example, by McIver (1986) and Wu and Liu (1988). For structures of more complex geometry some type of numerical method including discretization has to be used. In a Finite Element Method (FEM) the fluid domain is discretized into elements while in a Boundary Element Method (BEM) the boundary enclosing the fluid domain is discretized. For two–dimensional structures the Finite Element Method has been used, for example, by Bai and Yeung (1974) and Leonard et al (1983). The Boundary Element Method seems to be the most common type of method used for two–dimensional wave/structure interaction problems. In this method Green's theorem is applied to a source function. Either a fundamental source function can be used or a more complex Green function that satisfies all boundary conditions except the one at the surface of the structure. When using a fundamental source function the surface enclosing the fluid domain has to be discretized, while when using the more complex Green function only the surface of the structure has to be discretized. The method of using fundamental source functions has been used for two–dimensional structures by Bai and Yeung (1974), Ijima et al (1976), Finnigan and Yamamoto (1979), Jones et al (1979) and Liu and Abbaspour (1982). The Green's function procedure has been used, for example, by Garrison (1984) and Wu and Price (1987).

In the present study three different solution procedures have been developed. In two of the procedures the method of separation of variables is used while in the third procedure the Boundary Element Method with a fundamental source function is used. In the present chapter the three solution procedures are briefly outlined. A more detailed description is given in Appendices I, II and III respectively.

Results obtained from the solutions, including comparisons with the findings of other authors are presented in Chapter 5.

3.1 Solution procedure I

The first solution procedure concerns the diffraction problem of a breakwater of rectangular cross section with a protruding bottom plate facing the incident waves, see Figure 3.1. The solution gives the field quantities such as fluid velocity, and dynamic pressure as continuous functions throughout fluid regions.

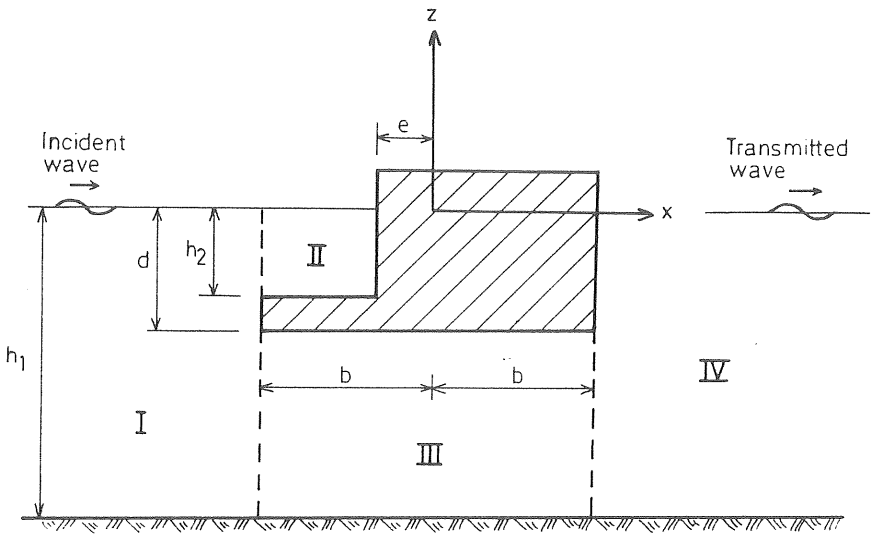

Figure 3.1 Definition of fluid regions and geometrical properties of solution procedure I.

The fluid domain is divided into four regions. The method of separation of variables is then applied in each region in order to obtain expressions for the unknown function, i.e. the velocity potential. Expressions valid in each respective region are obtained as infinite series of orthogonal functions. These expressions are developed to satisfy all boundary conditions except those at the common boundaries between the regions. It then remains to determine a number of unknown coefficients in the series. This is done by imposing the condition of continuity of pressure and normal velocity at the common boundary between the regions. Mathematically, this is fulfilled by matching the potentials and the normal derivatives of the respective potential. A more detailed description is given in Appendix I.

3.2 Solution procedure II

The second solution procedure concerns the diffraction and the radiation problems of a breakwater of rectangular cross section, see Figure 3.2.

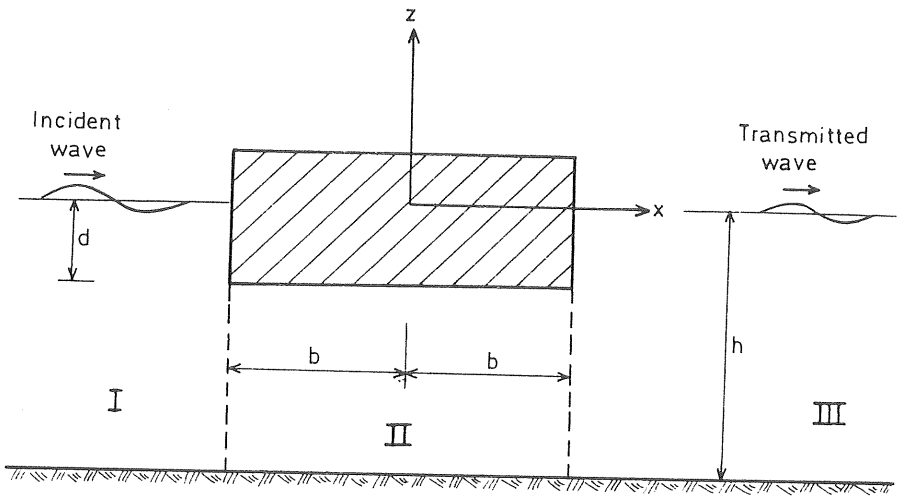

Figure 3.2 Definition of fluid regions and geometrical properties of solution procedure II.

The fluid domain is divided into three regions. The solution procedure applied is basically the same as in section 3.1. The field quantities such as fluid velocity and dynamic pressure are obtained as continuous functions throughout the fluid regions.

The difference between the diffraction problem and the radiation problem appears in the type of excitation applied. In the diffraction problem the excitation is caused by an incident propagating wave while in the radiation problem the excitation is introduced by moving boundaries. The solution of the diffraction and the radiation problems makes it possible to study fixed as well as floating breakwaters. A more detailed description is given in Appendix II.

3.3 Solution procedure III

The third solution procedure concerns the diffraction and the radiation problems of breakwaters of general cross section. The formulation also allows the water depth to vary in the vicinity of the breakwater, see Figure 3.3.

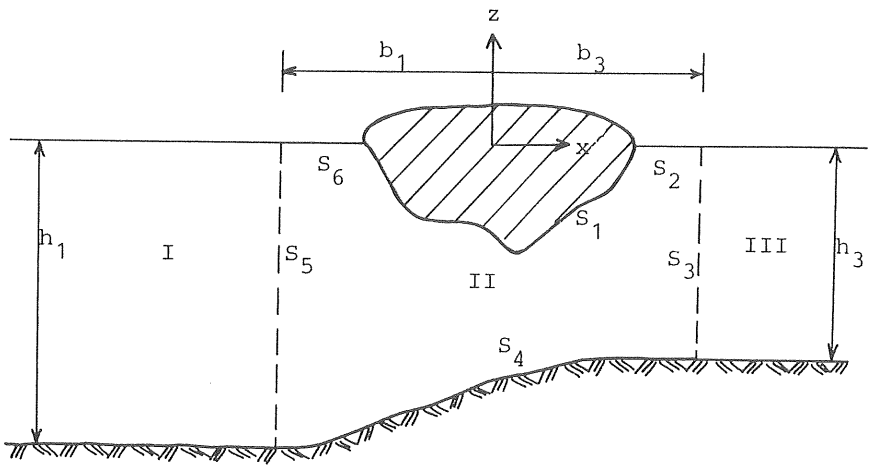

Figure 3.3 Definition of fluid regions and geometrical properties of solution procedure III.

The method used is the Boundary Element Method with fundamental source functions. Green's theorem is applied in a fluid region close to the cylinder (region II). Outside this region, at each side, the water depth is assumed to be constant. Analytical series solutions are developed in the outer regions and subsequently introduced as boundary conditions at the common boundaries S_3 and S_5 respectively. The resulting integral equation is solved after discretizing the boundary enclosing region II into elements and assuming the potential to be constant across each element.

The solution procedure makes it possible to study fixed and floating breakwaters of complex geometries. In Chapter 5 the quality of the numerical procedure is analysed by comparisons with solution procedures I and II as well as with findings of other authors. A more detailed description of the solution procedure is given in Appendix III.

4 EXPERIMENTAL STUDY

4.1 General

In the experimental study the main interest was focused on a fixed breakwater with rectangular cross section (Principality of Monaco's patent no. PCT/MC/86/00003). The width of the breakwater (along the wave tank) was 615 mm, the draught 154 mm and the water depth 769 mm. When exposed to regular waves, transmitted and reflected waves, forces and moments as well as pressure at the bottom of the breakwater were measured. The transmitted waves were also evaluated from experiments in irregular waves. In addition, transmitted waves were measured in regular and irregular waves for the type of breakwater with a protruding bottom plate(Principality of Monaco's patent no. F 85 15938). The width, the draught and the water depth were the same as for the rectangular breakwater. The height of the plate was 18 mm and the length of the protruding part either 123 or 246 mm. The shapes of the structures included in the measuring program are shown in Figure 4.1

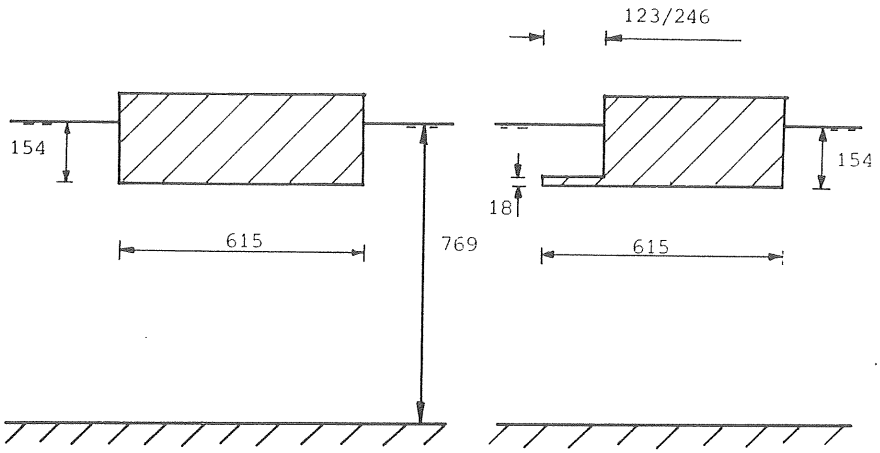

Figure 4.1 Geometries included in the test program. Dimensions in mm.

In the present chapter the performance of the experiments is reviewed. The results of the experiments and comparisons with theoretical results are presented in Chapter 5.

The experiments were performed in a wave tank, 80 m long, 2 m wide, and with a maximum depth of 0.95 m. The wave tank was equipped with a wave generator hinged so that the plane blade could both translate in the direction of wave

propagation and rotate. A wave absorbing slope was supplied at the end of the tank opposite the wave generator. The distance between the generator and the slope was 73 m.

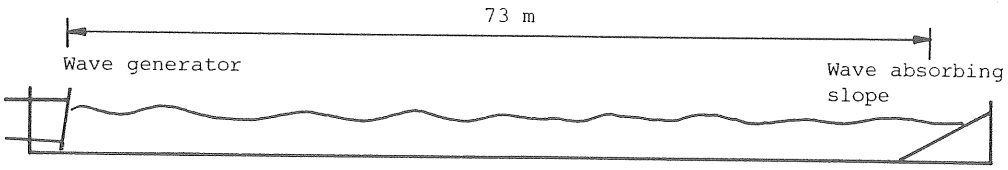

Figure 4.2 Wave tank.

4.2 Generation of regular waves

The regular waves were generated by giving the piston a sinusoidal input signal. The piston was connected to the wave blade by a mechanism which allowed the blade to translate in the direction of wave propagation and also to rotate. The magnitude of the translation was adjusted so that it increased for longer waves. Consequently, the wave generator acts as a flap type for deep water waves and more as a piston type for shallow water waves.

Starting from zero, the magnitude of the input signal was gradually increased to a final value. A sufficient length of recording was obtained before reflected waves disturbed the measurements. Experiments were performed with wave frequency, f, in the range 0.67 – 1.35 Hz and steepness H/L in the range 0.02 – 0.05.

4.3 Generation of irregular waves

When studying fixed structures, it could be an advantage to perform the experiments in irregular waves. If the measured quantities are considered reasonably linear, at least in principle, only a single run is necessary to obtain the quantities in the desired range of frequencies. This is achieved by frequency analysis of measured time series.

Some difficulties arise, however, when performing experiments in irregular waves. The main problem is that the measuring time should be long enough to give reasonable conditions for the frequency analysis of the measured time series. When measuring over a long period, the problem of reflected waves arises. The incident wave is first reflected by the structure and subsequently by the wave generator. If the waves are generated for a sufficiently long time, the multiple reflected wave system between the wave generator and the structure reaches a state of equilibrium. One possibility of handling the problem of reflected waves is to record the waves and the responses of interest after equilibrium has been reached. This procedure then requires an algorithm to separate the waves propagating towards the structure from those propagating towards the wave generator. This technique has been used by several investigators, including Kajima (1969), Thornton and Calhoun (1972) and Yamamoto (1981).

A related problem concerning irregular waves is that the waves consist of several components propagating along the wave tank at different speeds. If the wave generator starts at a certain instant at one end of the wave tank, the wave components with the highest celerities have already been reflected and re–reflected, and have reached the structure a second time before the components with the lowest celerities have reached the structure at all. A second concievable method in which it is not necessary to separate waves travelling in different directions, is to generate the waves in such a way that the generation of wave components with high celerities is successively delayed. In the present study this method has been used. The principle underlaying the method is described below.

The irregular wave train was created from a wave spectrum. Such a spectrum (if multiplied by a constant) gives the energy content corresponding to a specific sea state, as a function of frequency. In order to obtain time series of the wave elevation, the continuous spectrum is discretized using the frequency spacing Δf.

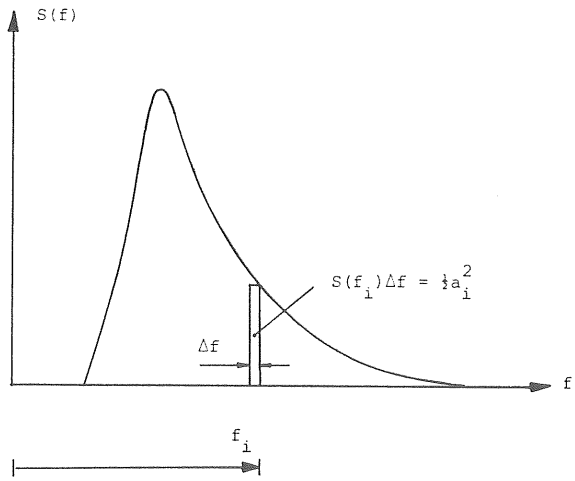

Figure 4.3 Discretization of continuous wave spectrum.

The energy content of the i:th component of the spectrum is then set equal to the energy content of a regular wave of frequency f_i. The time realization of the wave elevation is subsequently obtained as a series of superimposed regular waves with different frequencies, f_i. Furthermore, if a standard wave spectrum is used, nothing is known about the phases of the components. A common approach is to assume random phase angles, uniformly distributed in the interval $[0,2\pi]$. We can then express the wave elevation created from the wave spectrum as

$$\zeta(t) = \sum_{i=1}^{N} a_i \cos(2\pi f_i t + \theta_i) \qquad (4.1)$$

where

a_i $= \sqrt{2\ S(f_i)\Delta f}$ = amplitude of wave component
$S(f)$ = wave spectrum
Δf = frequency spacing
f_i $= i\Delta f$
θ_i = phase angle randomly chosen in the interval $[0,2\pi]$
N = number of components in spectrum

It should be pointed out that the time series given above repeats itself at the return period

$$T_r = \frac{1}{\Delta f} \tag{4.2}$$

The frequency spacing was chosen so that the return period became equal to the period of recording, i.e. equal to the period which started when all generated wave components had reached the measuring point and terminated when the re–reflected waves caused disturbances.

It is convenient at this point to define a transfer function, R(f), as the ratio between amplitude of the input signal of the wave generator and the wave amplitude. This frequency dependent function was originally determined in regular waves and subsequently adjusted slightly after calibration in irregular waves, see Figure 4.4.

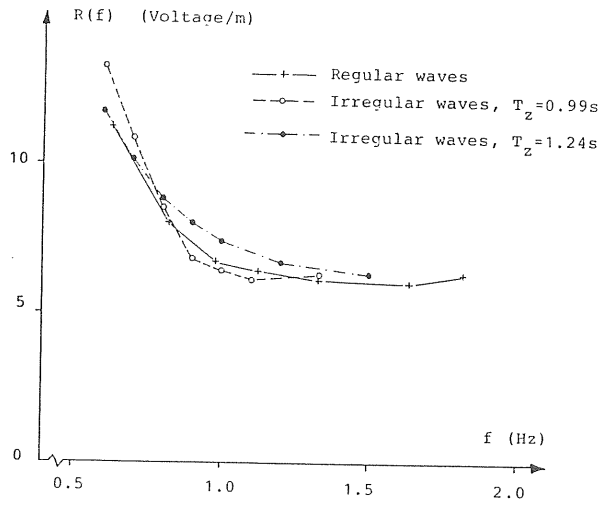

Figure 4.4 Ratio between amplitude of input signal fed into the wave generator and wave amplitude. Water depth h=0.77 m.

When using the transfer function defined above, the time series of the input signal of the wave generator becomes

$$r(t) = \sum_{i=1}^{N} R(f_i) a_i \cos(2\pi f_i t + \theta_i) \qquad (4.3)$$

The expression given above could be used directly as an input signal to the wave generator. Theoretically, it then would give the spectrum at the point of generation. However, we are not interested in the wave condition at the point of generation but rather at a measuring point some distance from the wave generator.

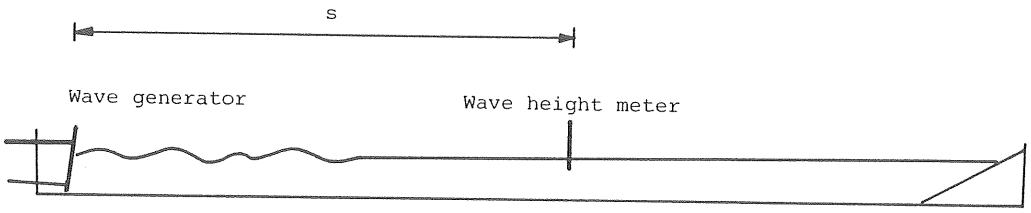

Figure 4.5 Schematically drawn wave elevation a short time after the wave generator has been started.

Since the fronts of the wave components of the irregular wave propagate at different velocities the total energy content generated does not reach the measuring point until the slowest wave component has propagated the distance s, see Figure 4.5. It is not appropriate to start measuring before this instant.

The length of measuring time is limited by the time it takes for the fastest wave component to be re–reflected and cause disturbances. In order to extend the length of the measuring period, the faster wave components were successively delayed. The front of each component was then assumed to propagate at the group velocity c_g. At water of finite depth the group velocity of a regular wave is given by

$$c_g = \frac{1}{2}\left[1 + \frac{2kh}{\sinh(2kh)}\right] c \qquad (4.4)$$

where

c = phase velocity
k = wave number
h = water depth.

The components in the time series were then delayed so that, theoretically they should reach the measuring point at the same time. This was achieved by using a delay function defined by

$$\theta(\tau_i) = \begin{cases} 0 \text{ for } \tau_i < 0 \\ 1 \text{ for } \tau_i \geq 0 \end{cases} \qquad (4.5)$$

where

τ_i = $t - (T_{sN} - T_{si})$
T_{si} = $\frac{s}{c_{gi}}$ = time for the i:th wave component to reach the measuring point
s = distance from wave generator to measuring point
c_{gi} = group velocity of the i:th wave component.
T_{sN} = time for the slowest wave component to reach the measuring point

Waves exhibiting this delay characteristic should then be generated using the following input signal

$$r(t) = \sum_{i=1}^{N} \theta(\tau_i)\, R(f_i) a_i \cos(2\pi f_i t + \theta_i) \qquad (4.6)$$

According to theory, if Eq. (4.6) is used as input signal to the wave generator, the wave components should reach the measuring point at the same time. This means that there should be no waves at all at the measuring point before the time it takes for the slowest component to propagate the distance s. In Figure 4.6 a recording of the wave elevation is shown. The time for the waves to reach the measuring point was calculated to be 88 s. The time for the fastest wave component to reach the test object a second time was calculated to be 130 s. Consequently, the period available for recording, with all wave component present and without disturbances from re–reflected waves, was calculated to be 42 s. It is clear from the figure that even if some waves occur before 88 s the energy content is quite small. It is believed that the proposed method significantly reduces the negative effects of wave reflection. .

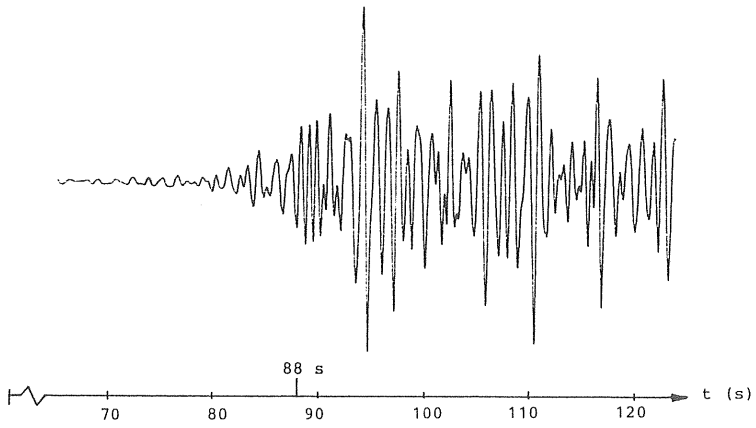

Figure 4.6 Wave elevation at the measuring point as a function of time. The wave generator has been started at t=0 and the waves should, theoretically, reach the measuring point at t=88 s.

The irregular waves were created from what is known as an ISSC–spectrum, as suggested by the International Ship Structures Congress (1964). The spectrum is a two parameter spectrum determined by the significant wave height H_s and the zero upcrossing period T_z. The ISSC–spectrum reads

$$S(f) = \frac{1}{4\pi}\left[\frac{H_s}{T_z}\right]^2 f^{-5} e^{-\left[\frac{T_z f}{\pi}\right]^{-4}} \qquad (4.7)$$

From this spectrum the input signal to the wave generator, Eq. (4.6), was created. The spectrum was truncated for frequencies with a spectral density of less than 5% of the peak value. In the test program, spectra for two different values of T_z were used, 0.99 and 1.240 s respectively. The wave generation approach previously described gives available periods of recording of 42 and 35 s respectively. With the return period set equal to the period of recording this gives a frequency spacing of 0.024 and 0.029 Hz respectively.

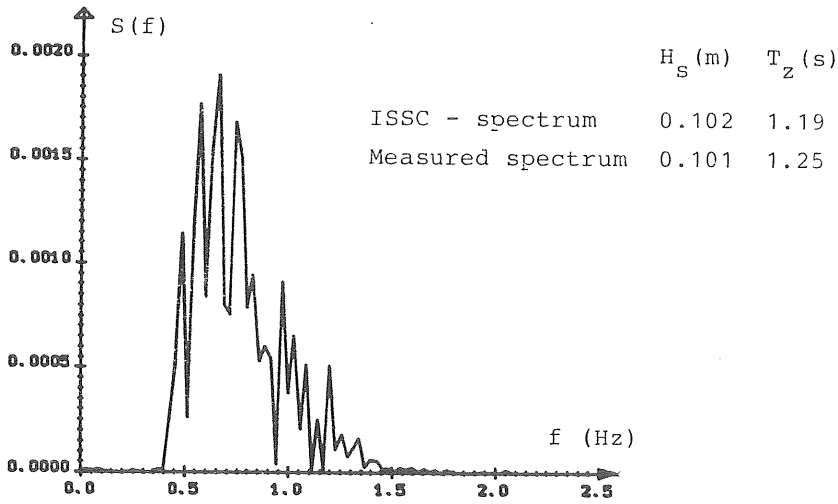

Figure 4.7 Example of measured raw spectrum.

Figure 4.7 shows an example of a spectrum obtained by Fourier analysis of a recorded wave elevation. The agreement between the measured spectrum and the one used to create the input signal fed into the wave generator was generally satisfactory. If the experiments in irregular waves are used to evaluate responses in a certain frequency range, it is of little importance that the generated spectrum agrees with the original one, as long as the energy content in the frequency range of interest is not too small. When the experiments are used to directly evaluate significant values of the response, agreement is of course more important. In the present investigation the tests in irregular waves were mainly used to measure responses at different frequencies.

4.4 Transmission coefficient

The wave elevation was measured using resistance type wave height meters, i.e. the resistance in the water between two parallel electrodes was measured in a Wheatstone type bridge.

The wave elevation was measured at a point 37 m from the wave generator. In a first run the incident wave was measured without any disturbing structure in the wave tank. The transmitted wave was measured in a second run in which the structure was placed at position about 2–3 m in front of the measuring point. In regular waves the transmission coefficient was then simply received as the ratio of the wave height in the second run to the wave height in the first run.

In irregular waves the procedure of splitting the measurements into two runs is justified by the fact that the reproducibility of the waves was virtually total. This is shown in Figure 4.8 where the wave elevation has been recorded for two runs using the same input signal.

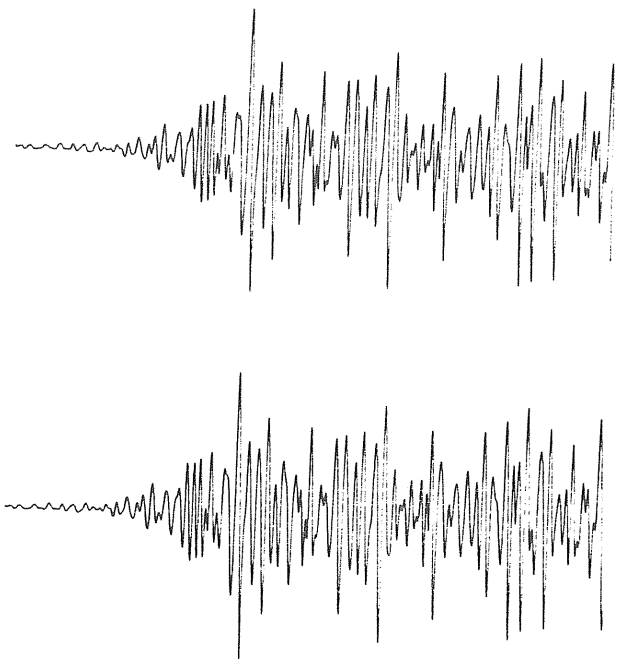

Figure 4.8 The wave elevation measured in two different runs using identical input signals.

In irregular waves the measured time series of the incident wave and the transmitted wave were frequency analyzed using a Fast Fourier Transform (FFT). The analysis gave the wave spectra associated with the incident wave and the transmitted wave respectively. Before evaluating the transmission coefficients the wave spectra were made slightly smoother by using

$$\bar{S}(f_i) = 0.25\, S(f_{i-1}) + 0.5\, S(f_i) + 0.25\, S(f_{i+1}) \qquad (4.8)$$

where

$\bar{S}(f_i)$ = the smooth spectrum of the measured wave
$S(f_i)$ = the raw spectrum of the measured wave

The transmission coefficients were then evaluated frequency by frequency from

$$K_T(f_i) = \sqrt{\frac{\bar{S}_T(f_i)}{\bar{S}_I(f_i)}} \qquad (4.9)$$

Without this light smoothing, it occasionally happened that the energy content at some frequency was close to zero and hence gave unrealistic values of the transmission coefficient. However, this was avoided by using the smoothing procedure and it became possible process the data in a more efficient and automatic manner. Figure 4.9 shows an example of raw spectra associated with the incident wave and the transmitted wave respectively. In Figure 4.10 the transmission coefficient, evaluated from Eq. (4.9), is plotted. Although only the slight smoothing effected by Eq. (4.8) was used, the transmission coefficient does not show much scattering. Note that frequencies below approximately 0.4 Hz and above 1.35 Hz are of no interest since the input energy was negligible at these frequencies.

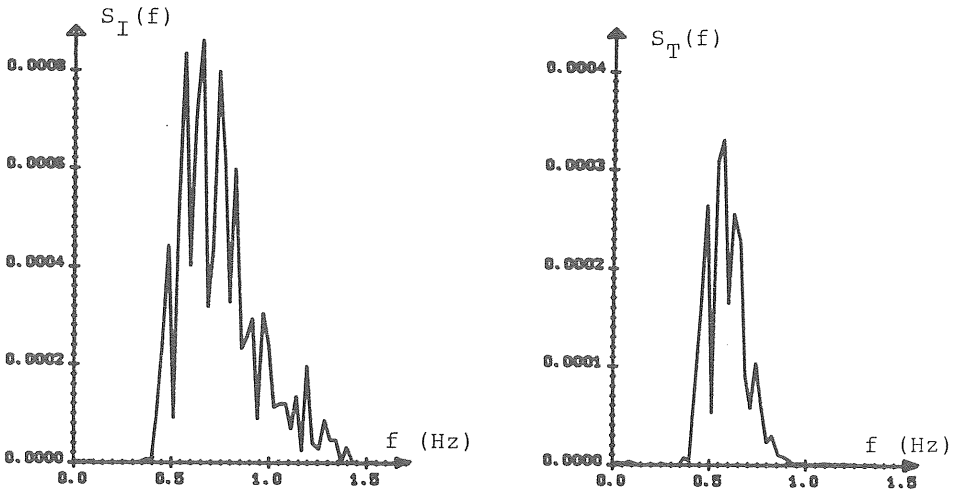

Figure 4.9 Raw spectrum of measured incident and transmitted waves.

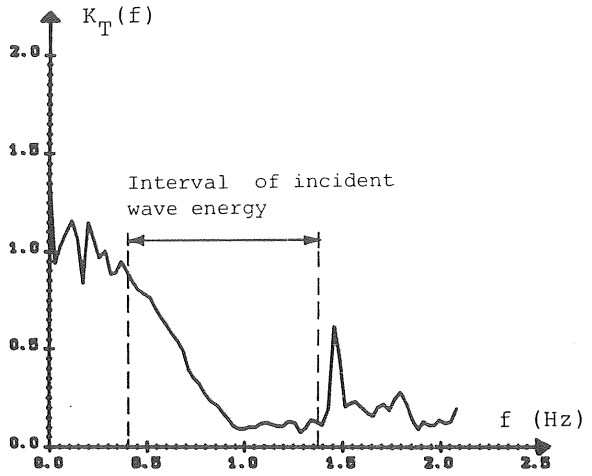

Figure 4.10 Transmission coefficent evaluated from experiments in irregular waves using Eq. (4.9).

It might be argued that it would be safer to base the measurements on averaged spectral values. However, for the present spectra the length of the recording times at full energy content and without disturbing reflected waves were in the range of $35<T_m<42$ s. This gives a frequency spacing for the spectral values $0.024<\Delta f<0.029$ Hz. For a single run and a given measuring period, any averaging procedure of spectral values will give larger frequency spacing Δf. Since the spectral values of the responses gave values without much scattering, a preference was given to keeping the frequency spacing small.

The option of using averaging procedures for a number of different runs remains. This option was, however, not considered necessary.

The principles used for measuring and evaluating the transmission coefficient in irregular waves are summarized in Figure 4.11.

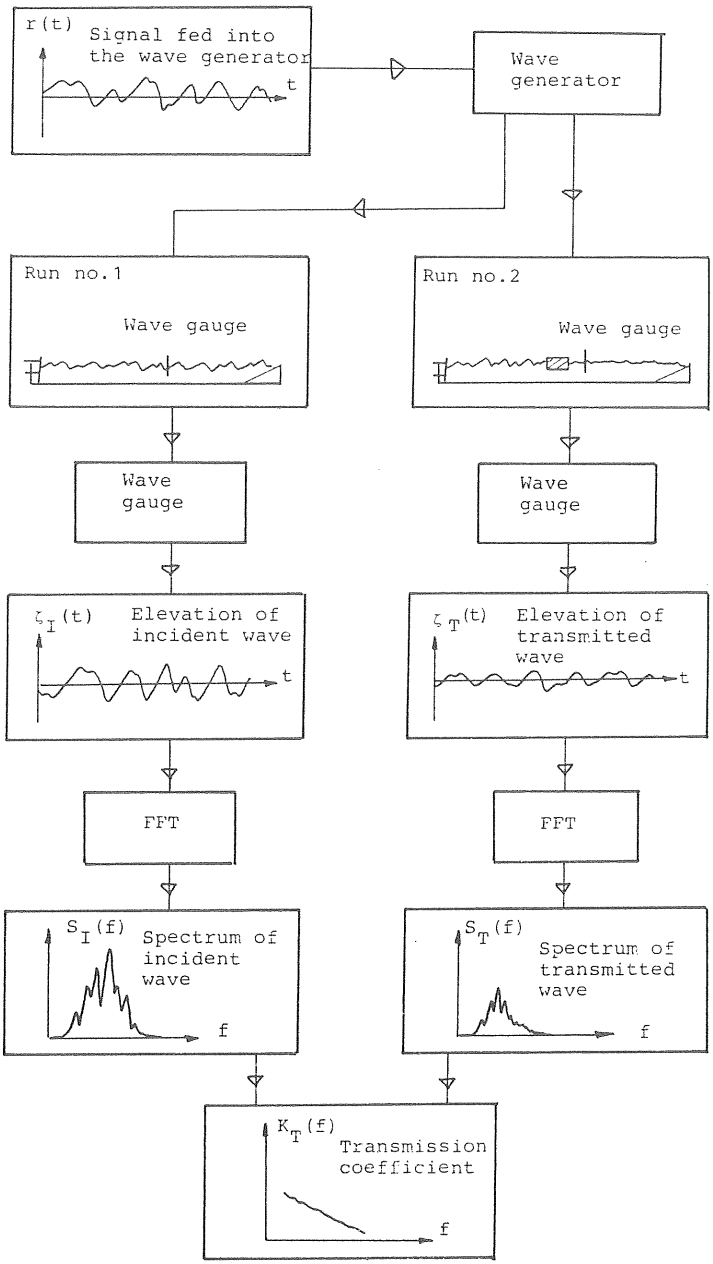

Figure 4.11 Principles for measuring and evaluating transmission coefficients in irregular waves.

4.5 Reflection coefficient

The reflection coefficient is somewhat more complicated to evaluate from experimental data than is the transmission coefficient. The latter is conveniently obtained using a single wave height meter. In a first run the incident wave is measured with no structure in the wavetank. Subsequently, in a second run, when the breakwater has been located in front of the recorder, the transmitted wave is measured. This simple procedure cannot be used for reflected waves since the reflected wave is superimposed on the incident wave and it therefore is impossible to measure it in isolation. Obviously, the two superimposed waves, propagating in opposite directions, have to be measured and subsequently somehow separated.

For both regular and irregular waves it is possible to separate the two waves using two fixed wave height meters.

An FFT (Fast Fourier Transform) is used to evaluate amplitudes and phases of the superimposed waves (or components). This is the key information necessary to separate the reflected wave from the incident wave. Such a separation technique has been used in different applications by several investigators, for example Jolas (1962), Kajima (1969), Thornton and Calhoun (1972), Goda and Suzuki (1976) Mansard and Funke (1980), Gaillard et al. (1980) and Yamamoto (1981).

For regular waves a more straightforward approach can be used with a single movable wave height meter. In this procedure the wave heights in the node and in the antinode are evaluated from the envelope of the measured time series. The reflection coefficient is then easily obtained from the following relation

$$K_R = \frac{H_R}{H_I} = \frac{(H_A - H_N)/2}{(H_A + H_N)/2} \qquad (4.10)$$

where

H_R = reflected wave height

H_I = incident wave height

H_A = wave height of antinode

H_N = wave height of node

In the present study the method using the Fourier analysis was chosen. This procedure provides information on energy content in periods other than the one generated. The method also has the advantage that it can be used both for regular as well as irregular waves. In the present study the reflection coefficient was evaluated only in regular waves. The method is outlined briefly below.

Using complex notation the elevation of the incident wave, propagating in the positive x–direction, can be written

$$\zeta_I(x,t) = A_I e^{i(\omega t - kx)} \tag{4.11}$$

where

A_I = complex amplitude of the incident wave

ω = angular frequency

k = wave number

Similarly, the elevation of the reflected wave propagating in the negative x–direction is written

$$\zeta_R(x,t) = A_R e^{i(\omega t + kx)} \tag{4.12}$$

where

A_R = complex amplitude of the reflected wave.

The total wave elevation is then given by

$$\zeta(x,t) = A_I e^{i(\omega t - kx)} + A_R e^{i(\omega t + kx)} \tag{4.13}$$

Now, assume the j:th measured time series to be time harmonic. It can then be written in the form

$$\zeta_j^m(t) = C_j e^{i\omega t} \tag{4.14}$$

where the complex amplitude C_j is obtained by an FFT (Fast Fourier Transform) of the time series. Let the x–coordinate of the j:th wave height meter be denoted by x_j. For $x=x_j$ Eq. (4.13) should then be equal to Eq. (4.14) and hence

$$A_I e^{-ikx_j} + A_R e^{ikx_j} = C_j \tag{4.15}$$

Once the complex amplitude of the measured time series is known, Eq. (4.15) contains two unknowns, that is the complex wave amplitudes A_I and A_R. Consequently, it takes two wave height meters (equations) to solve for the unknowns. Assuming $x_1=0$ we obtain

$$A_I = \frac{C_2 - C_1 e^{ikx_2}}{e^{-ikx_2} - e^{ikx_2}} \tag{4.16a}$$

$$A_R = C_1 - A_I \tag{4.16b}$$

In short, the important steps of the procedure are: first the complex amplitudes of the time series, C_1 and C_2, are evaluated using an FFT analysis. Second, the amplitudes of the incident wave and the reflected wave are obtained using Eqs. (4.16a,b)

If more than two wave height meters are used, more equations than unknowns are obtained. Then the separation can be applied to each pair of meters or alternatively a least square formulation applied. It should be pointed out that the separation procedure fails if the distance between two wave height meters equals a multiple of half a wave length. Distances close to these critical values should be avoided, see for example Goda and Suzuki (1976), Mansard and Funke (1980), and Gaillard et al (1980).

4.6 Force and pressure measurements

The force measurements were performed with excitations of regular waves. Compared with the transmitted waves, the forces were of a more non–linear nature and it was believed therefore that results based on a frequency analysis would not be meaningful.

The measurements were performed for the breakwater with a rectangular cross section and dimensions in accordance with Figure 4.12.

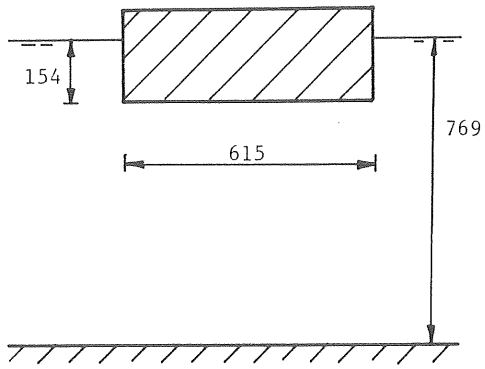

Figure 4.12 Breakwater for which forces were measured (mm).

The breakwater was mounted with six articulated supports, three of them oriented vertically, two horizontally in the direction of wave propagation and one horizontally perpendicular to the direction of wave propagation; see Figure 4.13. All supports except the horizonal one perpendicular to the direction of the waves, were equipped with force probes.

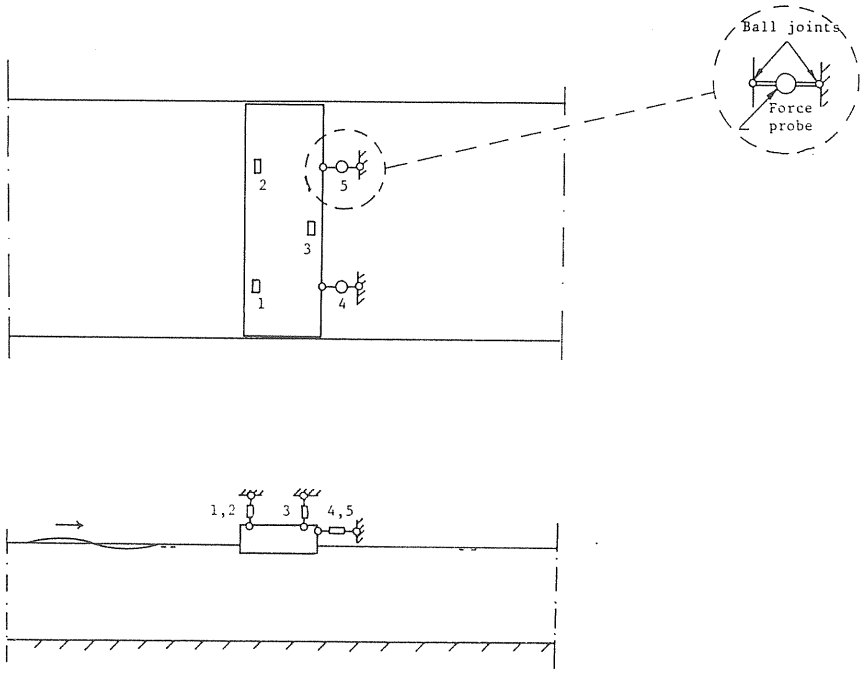

Figure 4.13 Experimental set up for force measurements.

$$A_I e^{-ikx_j} + A_R e^{ikx_j} = C_j \tag{4.15}$$

Once the complex amplitude of the measured time series is known, Eq. (4.15) contains two unknowns, that is the complex wave amplitudes A_I and A_R. Consequently, it takes two wave height meters (equations) to solve for the unknowns. Assuming $x_1=0$ we obtain

$$A_I = \frac{C_2 - C_1 e^{ikx_2}}{e^{-ikx_2} - e^{ikx_2}} \tag{4.16a}$$

$$A_R = C_1 - A_I \tag{4.16b}$$

In short, the important steps of the procedure are: first the complex amplitudes of the time series, C_1 and C_2, are evaluated using an FFT analysis. Second, the amplitudes of the incident wave and the reflected wave are obtained using Eqs. (4.16a,b)

If more than two wave height meters are used, more equations than unknowns are obtained. Then the separation can be applied to each pair of meters or alternatively a least square formulation applied. It should be pointed out that the separation procedure fails if the distance between two wave height meters equals a multiple of half a wave length. Distances close to these critical values should be avoided, see for example Goda and Suzuki (1976), Mansard and Funke (1980), and Gaillard et al (1980).

4.6 Force and pressure measurements

The force measurements were performed with excitations of regular waves. Compared with the transmitted waves, the forces were of a more non–linear nature and it was believed therefore that results based on a frequency analysis would not be meaningful.

The measurements were performed for the breakwater with a rectangular cross section and dimensions in accordance with Figure 4.12.

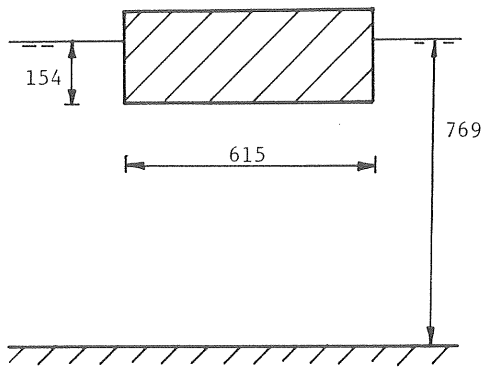

Figure 4.12 Breakwater for which forces were measured (mm).

The breakwater was mounted with six articulated supports, three of them oriented vertically, two horizontally in the direction of wave propagation and one horizontally perpendicular to the direction of wave propagation; see Figure 4.13. All supports except the horizonal one perpendicular to the direction of the waves, were equipped with force probes.

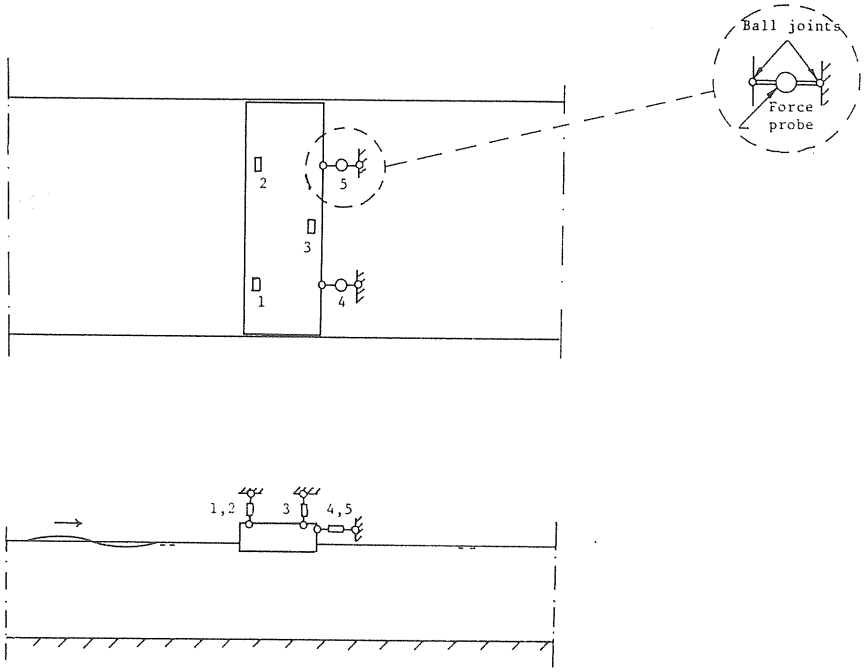

Figure 4.13 Experimental set up for force measurements.

The forces were measured for waves with frequencies in the range 0.67 – 1.35 Hz and steepness, H/L, in the range 0.02 – 0.05. The frequency range corresponds to a wave length in the range 3.14 – 0.87 m.

The vertical force was obtained by adding together the forces measured with force probes 1, 2 and 3 at each time step and the horizontal force was similarly obtained by adding the forces from probes 4 and 5. The moment about the centre of the bottom of the breakwater was also evaluated

In a first series of experiments only forces were measured. After evaluation of these experiments, the vertical forces were found to contain a significant component at twice the frequency of wave generation. This was especially pronounced for short and steep waves as is further discussed in Chapter 5.

In order to verify the vertical forces it was decided to measure the pressure at the bottom of the breakwater simultaneously with the vertical forces. This second series of experiments included two frequencies, 0.81 and 1.15 Hz, corresponding to wave lengths of 2.33 and 1.17 m respectively. The same steepnesess as before were tested.

In the first series of experiments the breakwater had a frame structure covered with plywood walls. The breakwater was partly submerged, with water inside. The lowest resonance frequency of the breakwater/suspension system was estimated to be about 10 Hz.

In the second series of experiments, the breakwater was rebuilt, using the same frame but replacing the plywood walls with PVC, since the pressure transducers mounted at the bottom of the breakwater required an interior without water. Six resistance type pressure transducers were used and were placed in line with the direction of wave propagation as shown in Figure 4.14.

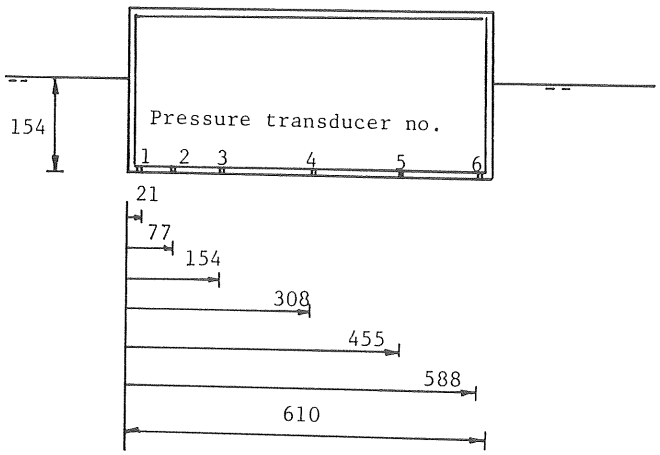

Figure 4.14 Pressure transducers.

The pressure transducers were calibrated hydrostatically when mounted on the breakwater. The force probes were calibrated individually before being mounted and were subsequently checked using 20 kg masses. No checks gave deviations larger than 1% from the individual calibrations.

As is shown in Chapter 5, there was excellent agreement between vertical forces measured directly by force probes and those obtained by integrating the pressure.

5 ANALYSIS OF RESULTS

5.1 Theoretical results

5.1.1 Theoretical validation

In order to check the quality of the solution procedures the result of procedures I and II are compared with those of procedure III. In addition comparisons are made with results collected from other authors.

Solution procedures II and III

In Figure 5.1 the results of procedures II and III are compared. The breakwater with a rectangular cross section is defined by h/d = h/b = 2.0. All quantities are plotted versus kb. In procedure II the number of components in the orthogonal series is N=10 while the total number of elements in procedure III is N_6=180. In procedure III the number of elements of the boundaries S_1, S_2, S_3, S_4, S_5 and S_6 was 120, 10, 10, 20, 10 and 10 respectively, see Figure 3.3. At each respective boundary the size of the elements was equal. The agreement is seen to be quite satisfactory. When expressed as percentage of the maximum value the deviation, in the range 0.3<kb<1.3, is less than 0.2% for the reflection and transmission coefficients, less than 1% for F_1, F_3, a_{11}, a_{33}, b_{11}, b_{33}, less than 2% for F_5, less than 3% for a_{15}, a_{51}, b_{15}, b_{51}, and less than 4% for a_{55} and b_{55}.

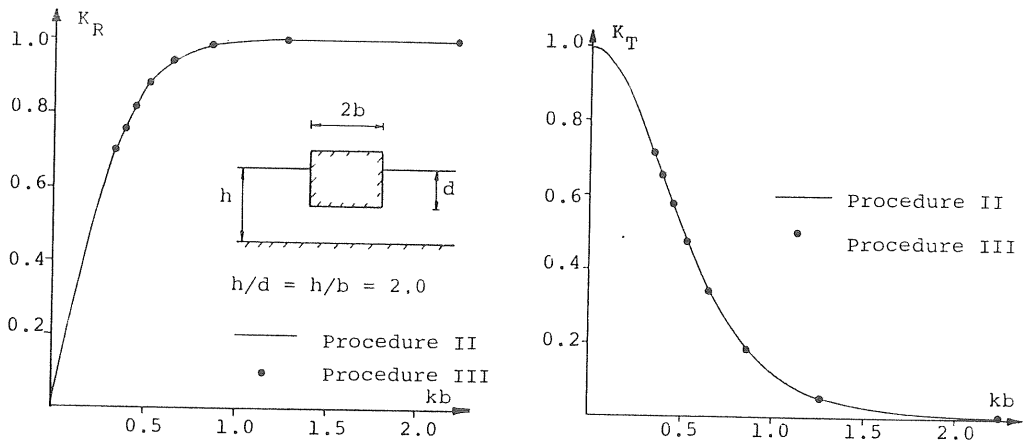

Figure 5.1a Reflection and transmission coefficients for a breakwater with a rectangular cross section defined by h/d = h/b = 2.0.

The largest deviations appear for the pitch quantities, i.e. moment, added mass, and damping in pitch. When the number and length of the elements in procedure III were varied it was noticed that the pitch quantities were more sensitive to changes than the others. However, it seems that all quantities calculated using procedure III are close to those calculated by procedure II when the number of elements is increased.

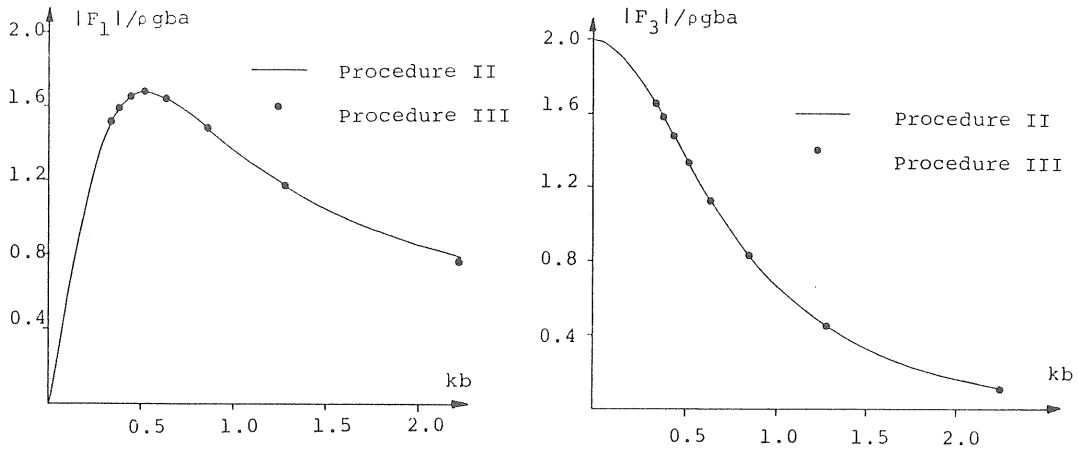

Figure 5.1b Forces for a breakwater with a rectangular cross section defined by h/d = h/b = 2.0.

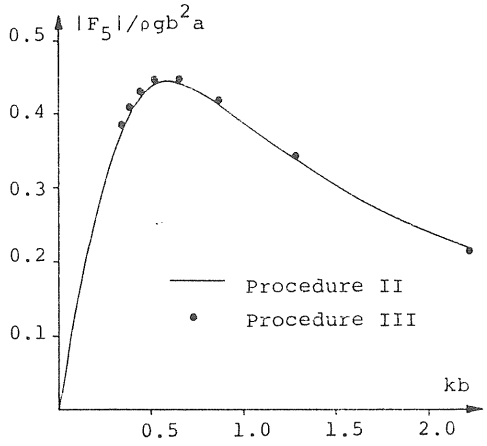

Figure 5.1c Pitch moment for a breakwater with a rectangular cross section defined by h/d = h/b = 2.0.

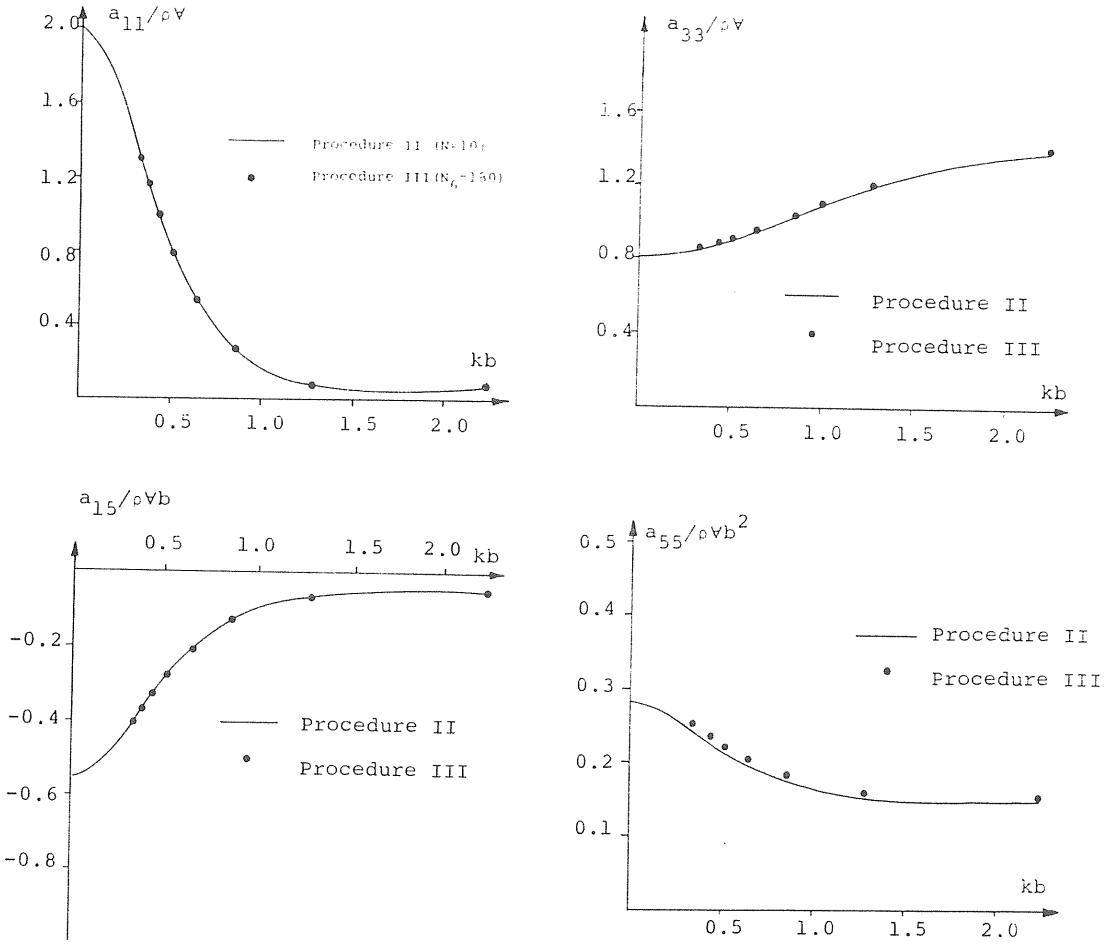

Figure 5.1d Added mass coefficients for a breakwater with a rectangular cross section defined by h/d = h/b = 2.0.

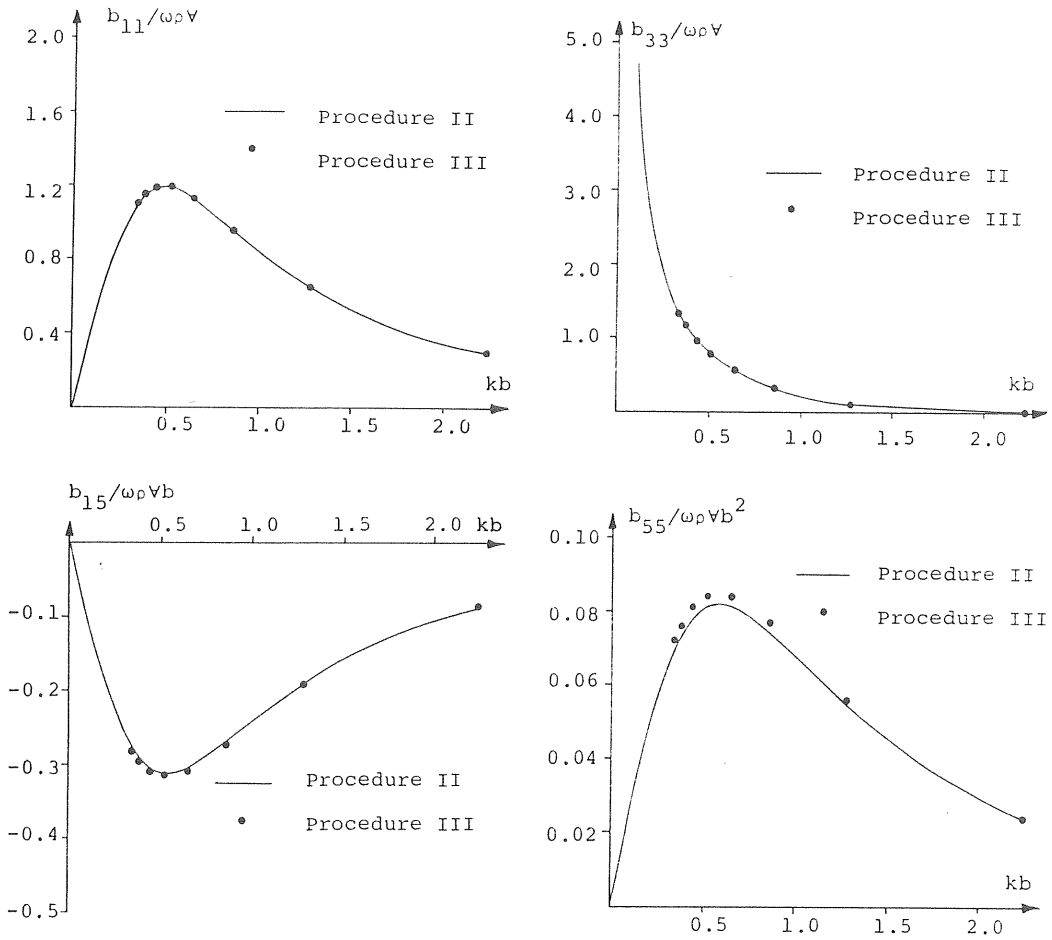

Figure 5.1e Potential damping for a breakwater with a rectangular cross section defined by h/d = h/b = 2.0.

As an additional check of the results, the coupling elements of the added mass and potential damping matrices can be compared, as the matrices should be symmetrical, i.e. a_{15} should equal a_{51} and b_{15} should equal b_{51}. In Table 5.1 a comparison of the coupling elements is made for solution procedures II and III.

Table 5.1 Comparison of the coupling coefficients of the added mass and potential damping matrices. Solution procedures II and III. Rectangular cross section with h/d = h/b = 2.0.

kb	Solution procedure II (N=10)				Solution procedure III (N_6=180)			
	$a_{15}/\rho\forall b$	$a_{51}/\rho\forall b$	$b_{15}/\omega\rho\forall b$	$b_{51}/\omega\rho\forall b$	$a_{15}/\rho\forall b$	$a_{51}/\rho\forall b$	$b_{15}/\omega\rho\forall b$	$b_{51}/\omega\rho\forall b$
0.030	-0.551	-0.551	-0.034	-0.034	-0.565	-0.565	-0.035	-0.035
0.080	-0.542	-0.542	-0.111	-0.111	-0.556	-0.556	-0.086	-0.086
0.160	-0.509	-0.509	-0.162	-0.162	-0.522	-0.522	-0.166	-0.166
0.340	-0.394	-0.394	-0.276	-0.276	-0.404	-0.404	-0.282	-0.282
0.385	-0.362	-0.362	-0.291	-0.291	-0.371	-0.371	-0.297	-0.297
0.445	-0.321	-0.321	-0.304	-0.304	-0.329	-0.329	-0.310	-0.310
0.525	-0.268	-0.268	-0.310	-0.310	-0.275	-0.275	-0.317	-0.316
0.650	-0.202	-0.202	-0.303	-0.303	-0.208	-0.207	-0.309	-0.309
0.860	-0.126	-0.126	-0.267	-0.267	-0.130	-0.130	-0.273	-0.272
1.275	-0.063	-0.063	-0.190	-0.190	-0.064	-0.064	-0.192	-0.192
2.235	-0.051	-0.051	-0.087	-0.087	-0.057	-0.057	-0.084	-0.084

From Table 5.1 it is seen that the coupling coefficients of procedure II are practically identical. The coefficients of procedure III also exhibit excellent agreement. However, when comparing the coefficients of procedure II with those of procedure III a slight discrepancy is noted.

A further check of the results can be made using the Haskind relation, Eq. (2.18). The Haskind relation is a consequence of Green's theorem and existing boundary conditions which makes it possible to calculate the wave exciting forces having solved the radiation problems but not the diffraction problem. In Table 5.2 the wave exciting forces of procedure II are shown, calculated both by solving the diffraction problem and by using the Haskinds relation.

Table 5.2 The wave exciting forces of procedure II calculated by solving the diffraction problem and by using the Haskind relation.

kb	Diffraction problem			Haskinds relation		
	$\frac{\lvert F_1 \rvert}{\rho g b a}$	$\frac{\lvert F_3 \rvert}{\rho g b a}$	$\frac{\lvert F_5 \rvert}{\rho g b^2 a}$	$\frac{\lvert F_1 \rvert}{\rho g b a}$	$\frac{\lvert F_3 \rvert}{\rho g b a}$	$\frac{\lvert F_5 \rvert}{\rho g b^2 a}$
0.340	1.507	1.658	0.378	1.507	1.658	0.378
0.385	1.585	1.582	0.401	1.585	1.582	0.401
0.445	1.649	1.478	0.423	1.649	1.478	0.423
0.525	1.681	1.333	0.439	1.681	1.333	0.439
0.650	1.642	1.126	0.441	1.642	1.126	0.441
0.860	1.482	0.832	0.413	1.482	0.832	0.413
1.275	1.174	0.455	0.339	1.174	0.455	0.339
2.235	0.792	0.125	0.220	0.792	0.125	0.220

It is seen that the wave exciting forces of procedure II, calculated in the two different ways, are virtually identical. The wave exciting forces of procedure III are presented in Table 5.3. Again excellent agreement is obtained.

Table 5.3 Comparison of forces of procedure III ($N_6 = 180$) calculated by solving the diffraction problem and by using the Haskind relation

kb	Diffraction problem			Haskinds relation		
	$\frac{\lvert F_1 \rvert}{\rho g b a}$	$\frac{\lvert F_3 \rvert}{\rho g b a}$	$\frac{\lvert F_5 \rvert}{\rho g b^2 a}$	$\frac{\lvert F_1 \rvert}{\rho g b a}$	$\frac{\lvert F_3 \rvert}{\rho g b a}$	$\frac{\lvert F_5 \rvert}{\rho g b^2 a}$
0.340	1.513	1.658	0.385	1.512	1.656	0.385
0.385	1.590	1.581	0.409	1.590	1.580	0.409
0.445	1.655	1.477	0.431	1.654	1.476	0.431
0.525	1.686	1.332	0.447	1.685	1.331	0.447
0.650	1.648	1.125	0.448	1.648	1.124	0.449
0.860	1.486	0.829	0.419	1.488	0.830	0.420
1.275	1.170	0.448	0.342	1.177	0.452	0.344
2.235	0.766	0.111	0.215	0.784	0.121	0.221

It is important to emphasize that when the coupling coefficients or the forces calculated in the two different ways are compared not much could be said about the quality of the results. For example, the deviation of the coupling coefficients from symmetry within procedure III is negligible but when comparing them with those of procedure II the deviation becomes noticeable. Nevertheless, the above mentioned

comparisons are important tools for eliminating errors in the derivation of equations and computer implementations.

Solution procedures I and III

In Figure 5.2 the results of procedures I and III are compared. The breakwater is defined by $h_1/d=h_1/b=2.0$, $h_1/d-h_2=20.0$, and $h_1/(b-e)=5.0$. In procedure I the number of components in the orthogonal series is N=12 while the total number of elements in procedure III is $N_6=180$. In procedure III the number of elements at the boundaries S_1, S_2, S_3, S_4, S_5 and S_6 was 120, 10, 10 ,20, 10 and 10 respectively, see Figure 3.3. The comparison is made for the quantities obtained from the solution of the diffraction problem. When expressed as a percentage of the maximum value the deviation, in the range $0.3<kb<1.3$, is less than 0.3% for the reflection and transmission coefficients, less than 1% for F_1 and F_3, and less than 1.5% for F_5, i.e. the magnitude of the deviations is similar to that of the comparison between procedures II and III.

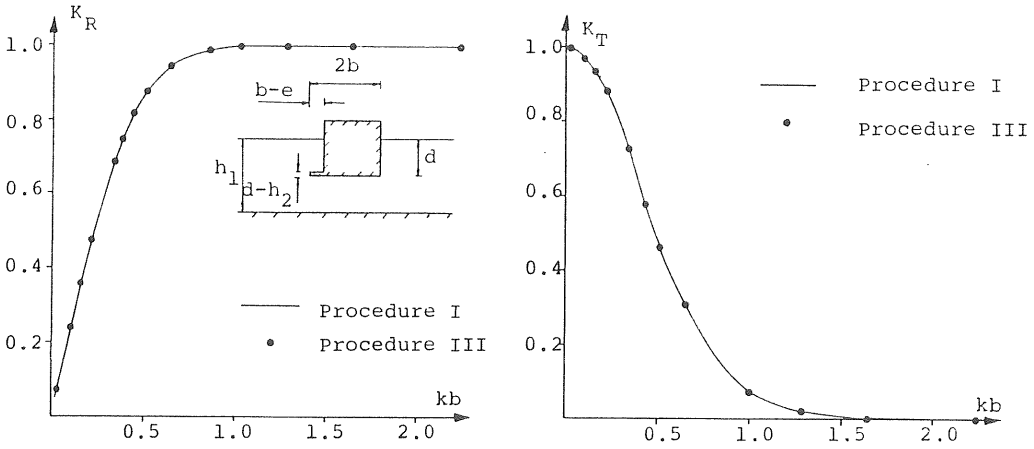

Figure 5.2a Reflection and transmission coefficients for the breakwater with a protruding bottom plate defined by $h_1/d=h_1/b=2.0$, $h_1/(d-h_2)=20.0$, and $h_1/(b-e)=5.0$.

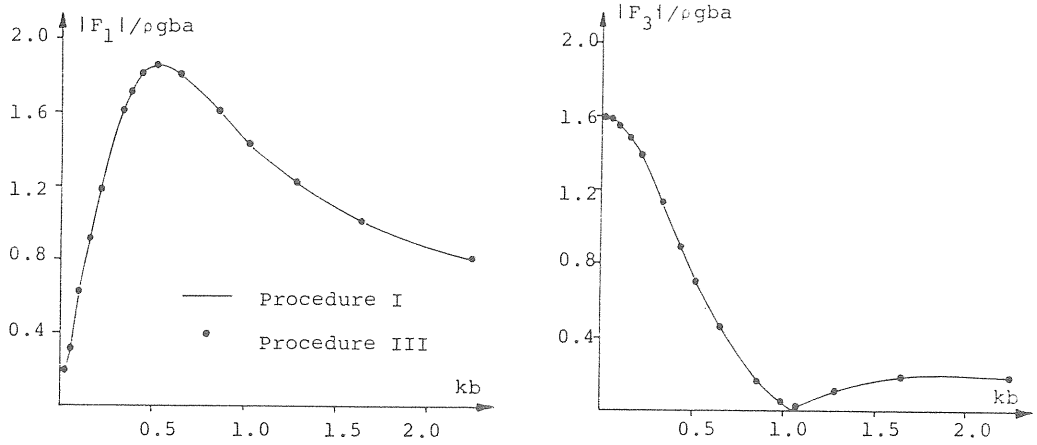

Figure 5.2b Forces for the breakwater with a horizontal protruding bottom plate defined by $h_1/d=h_1/b=2.0$, $h_1/(d-h_2)=20.0$, and $h_1/(b-e)=5.0$.

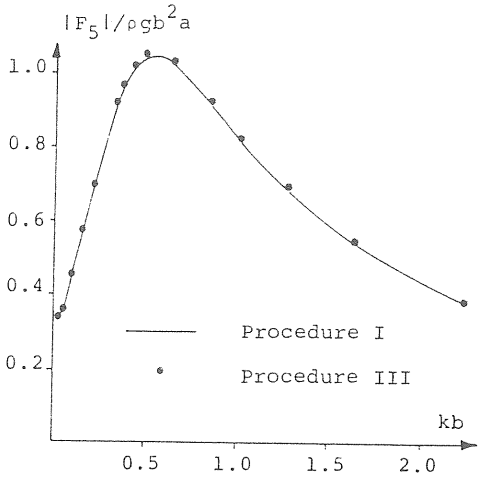

Figure 5.2c Pitch moment for the breakwater with a protruding bottom plate defined by $h_1/d=h_1/b=2.0$, $h_1/(d-h_2)=20.0$, and $h_1/(b-e)=5.0$.

A comparison of the wave exciting forces of solution procedure III obtained by solving the diffraction problem and by using the Haskind relation yields results similar to those obtained for the breakwater with a rectangular cross section.

Comparisons with results of other authors

The next step in the verification is to compare the results with those of other authors. It would have been suitable to compare the pitch quantities since they exhibit the largest scatter in the present work. However, such results are rare in the literature. Most of the published results only discuss one or a few quantities included in a solution. Therefore, some of the comparisons below are for added mass and damping coefficients and others are for transmission and reflection coefficients.

In Figure 5.3 a comparison is made of the added mass and potential damping for a rectangular cylinder in heave. The figure is taken from Bai and Yeung (1974). They contributed two solution procedures, one a finite element solution and the other using an approach similar to that used in solution procedure III in the present study. The main difference between procedure III and the approach of Bai and Yeung appears in the radiation condition applied. They extend the fluid domain sufficiently far from the structure to allow simple propagating wave conditions to be applied at the vertical boundaries connecting the free surface and the sea bottom. (In solution procedure III complete series solutions are applied at the vertical boundaries and they could therefore be positioned close to the structure.) Results of an integral equation solution of Lebreton and Margnac, as cited by Bai and Yeung, are also shown in the figure.

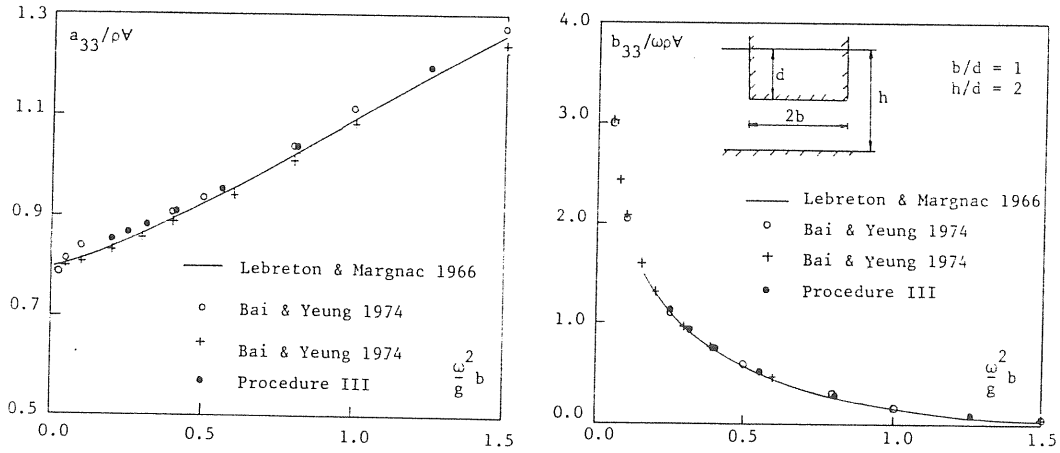

Figure 5.3 Added mass and potential damping coefficients of a rectangular cylinder in heave. Redrawn from Bai and Yeung (1974).

From Figure 5.3 it is seen that the added mass and potential damping of the rectangular cylinder in heave agree reasonably well with the results of Bai and Yeung , and Lebreton and Margnac.

In Figure 5.4 a comparison of the added mass coefficient for a semi–submerged circular cylinder in heave is shown. The graph is redrawn from Keil (1974) and also shows the results of Bai and Yeung. The agreement with the results of solution procedure III is seen to be excellent. The results for the circular cylinder were less sensitive to a variation of the number of elements than the results obtained for the rectangular cylinder.

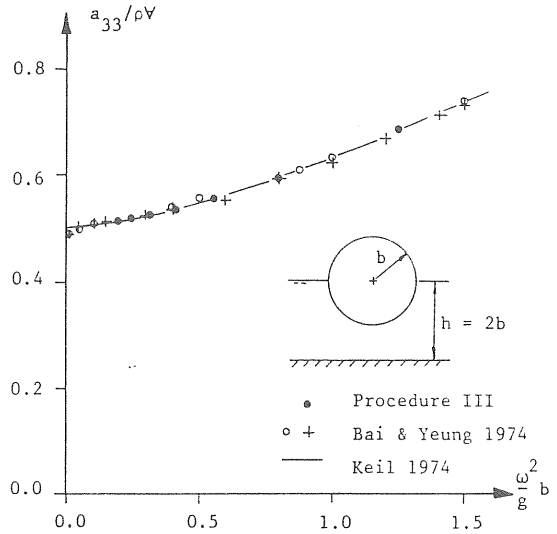

Figure 5.4 Added mass coefficient for a semi–submerged circular cylinder in heave. From Keil (1974).

Solution procedure III can be used to analyse not only floating structures but also effects due to variations in water depth. In Figure 5.6 a comparison is made of the transmission and reflection coefficients of a sea bottom trench according to Figure 5.5.

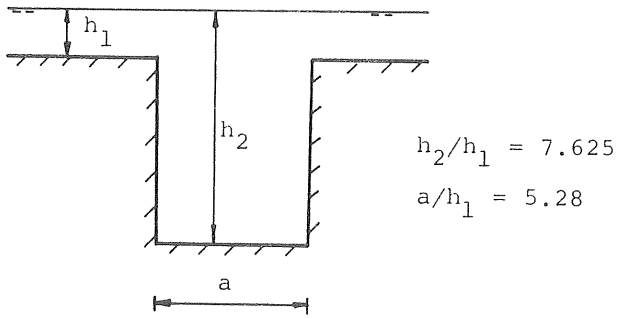

Figure 5.5 Geometry of sea bottom trench.

Figure 5.6. is redrawn from Kirby and Dalrymple (1983). They used a method based on matching of orthogonal series in a similar way as in procedures I and II in the present study. Results of Kirby and Dalrymple, solution procedure III, as well as Lee and Ayer (1981) are compared in Figure 5.6. The agreement is satisfactory.

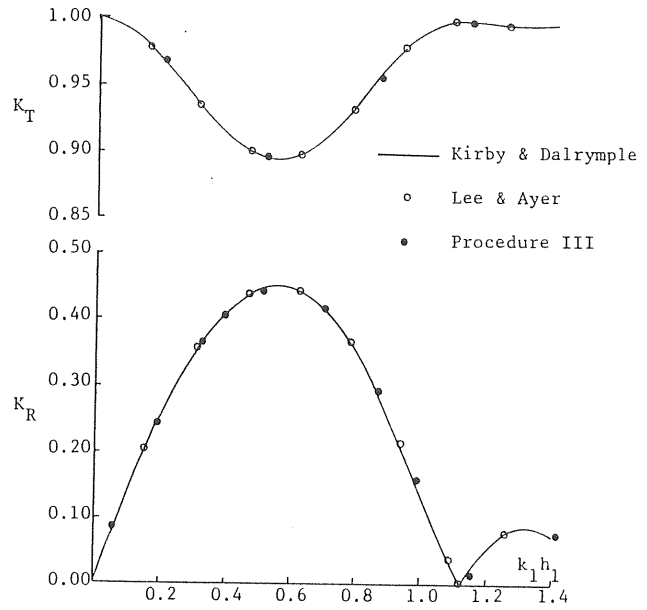

Figure 5.6 Transmission and reflection coefficients for a sea bottom trench.

5.1.2 The effect of the protruding bottom plate.

As an illustration of the effect of the protruding bottom plate, the transmission coefficient of a breakwater with a rectangular cross section is compared with the transmission coefficient obtained if the front wall facing the incident waves is moved as indicated in Figure 5.7.

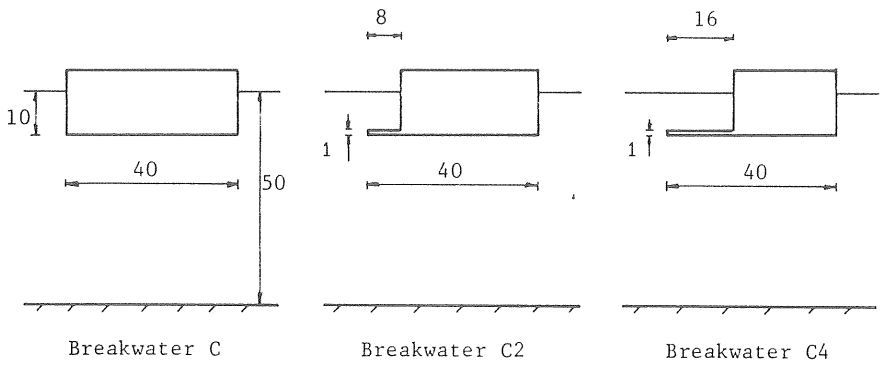

Figure 5.7 Breakwaters included in the comparison performed to illustrate the effect of the protruding bottom plate. Dimensions in m.

The geometry of the breakwater and the wave characteristics were chosen with the breakwater concept of Port de la Condamine in the Principality of Monaco in mind. This means a rather large gap between the bottom of the breakwater and the sea bottom. The depth of submergence was one–fifth of the water depth. The reductions of the width of the breakwater at the still water level correspond to 20% and 40%, respectively, of the total width. In Figure 5.8 the transmission coefficients are shown. They are plotted versus wave period.

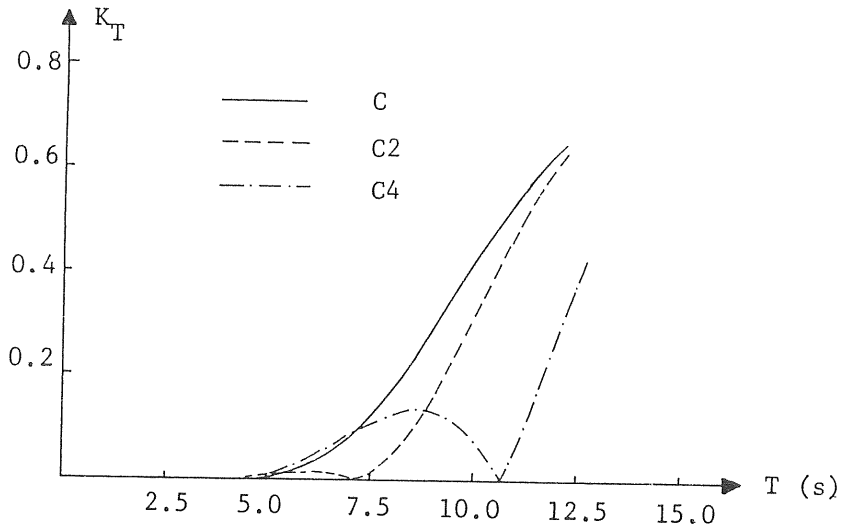

Figure 5.8 Illustration of the effect of the protruding bottom plate on the transmission coefficient.

Breakwaters (C2) and (C4) exhibit clear anti–resonance characteristics. Comparing (C2) with (C), the transmission coefficient is reduced in practically the whole range of plotted periods. However, when (C4) is compared with (C2), the transmission coefficient increases for periods lower than 8.8 but decreases for higher periods. Consequently, the proper length of the protruding plate should be decided with the wave climate in mind.

5.2 Experimental results

In the experimental part of the study the prototype breakwaters presented in Figure 5.7 were scaled to model dimensions. The length scale of the models was 1:65 and the time scale $1:(65)^{1/2}$ = 1:8.06, which gives model dimensions as described in Figure 5.9. The three breakwaters included in the measuring program will be referred to as C, C2 and C4 respectively.

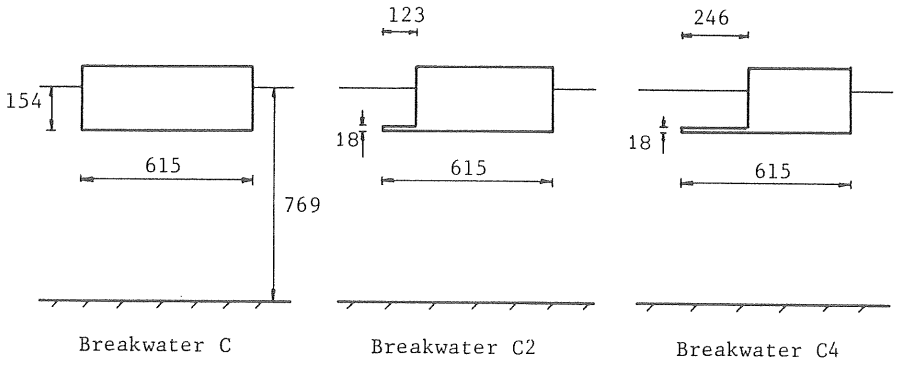

Figure 5.9 Model dimensions in mm of breakwaters included in the measuring program.

In the following sections, the results of the measurements performed as described in Chapter 4 are presented. The results are generally presented in prototype quantities except in a few cases when raw data are presented as they were measured in the models. In Table 5.4 the wave characteristics for regular waves are listed in both prototype and model quantities.

Table 5.4 Wave characteristics for regular waves in prototype and model.

T_p(s)	T_m(s)	f_p(Hz)	f_m(Hz)	L_p(m)	L_m(m)
6	0.744	0.167	1.344	56.3	0.866
7	0.868	0.143	1.152	76.4	1.175
8	0.992	0.125	1.008	99.4	1.529
9	1.116	0.111	0.896	124.6	1.917
10	1.240	0.100	0.806	151.1	2.325
11	1.364	0.091	0.733	177.9	2.737
12	1.488	0.083	0.672	204.4	3.145

5.2.1 Transmission coefficient

The measurements included breakwaters C, C2 and C4. For regular waves the prototype period, T_p, was varied in the range of 6 to 12 s, each period having steepnesses of 2,3,4 and 5%. The transmission coefficient was evaluated as the ratio between transmitted wave height and incident wave height. The wave heights were taken as maximum to minimum values in the time series of the wave elevation.

The transmission coefficient was also measured in irregular waves. Four irregular wave trains were selected. The amplitudes of the components of the spectrum were obtained from the ISSC–spectrum given by Eq. (4.7), which is a two parameter spectrum defined by H_s and T_z. Table 5.5 shows the parameters of the irregular waves used in the study. The parameters were evaluated both directly from the measured time series and from spectral moments. From the time series H_s was taken as the mean of the one–third highest waves and T_z as the mean of the zero up–crossing periods. From the spectral moments the parameters were evaluated as

$$H_s = 4\sqrt{m_0} \tag{5.1}$$

$$T_z = \sqrt{\frac{m_0}{m_2}} \tag{5.2}$$

where

$$m_n = \int_0^\infty f^n S(f)df \tag{5.3}$$

The table also indicates that spectra nos. 1, 2, 3 and 4 were used for breakwater C and spectra nos. 1 and 4 for breakwaters C2 and C4.

Table 5.5 Parameters of irregular waves

Spectr. no.	Break–water	Prototype				Model			
		Spectral moments		Time series		Spectral moments		Time Series	
		T_z	H_s	T_z	H_s	T_z	H_s	T_z	H_s
1	C, C2, C4	8.03	3.45	8.47	3.51	1.00	0.053	1.05	0.054
2	C	8.01	3.32	8.55	2.99	0.99	0.051	1.06	0.046
3	C	10.06	6.57	9.35	6.11	1.25	0.101	1.16	0.094
4	C, C2, C4	10.30	4.36	10.32	4.03	1.28	0.067	1.28	0.062

In order to get an overall idea of the quality of the breakwaters as wave protectors the transmission coefficient based on significant wave heights was evaluated. Based on spectral moments this coefficient becomes

$$K_T^S = \frac{H_{ST}}{H_{SI}} = \sqrt{\frac{m_{0T}}{m_{0I}}} \tag{5.4}$$

where

H_{ST} = significant wave height of transmitted wave train

H_{SI} = significant wave height of incident wave train

m_{0T} = zeroth order spectral moment of transmitted wave train

m_{0I} = zeroth order spectral moment of incident wave train

In Table 5.6 the transmission coefficient, K_T^S, is presented. A significant reduction is obtained for breakwaters C2 and C4 compared with C. For spectrum no.1, K_T^S is reduced from 0.383 for breakwater C to 0.184 for breakwater C4, and for spectrum no.4, from 0.562 to 0.375.

Table 5.6 Transmission coefficient based on significant wave height

Spect. no.	Breakwater		
	C	C2	C4
1	0.383	0.276	0.184
2	0.387	–	–
3	0.560	–	–
4	0.562	0.481	0.375

It should be emphasized that the transmission for a spectrum with a given zero up–crossing period, for example T_z=10 s, is much higher than the transmission obtained for a regular wave with the period T=10 s. This is caused by the high transmission of the low frequency content of the spectrum. A regular design wave is therefore a poor description of the wave climate when studying transmission through the gap underneath the breakwaters.

Another characteristic of the transmitted waves is that the zero upcrossing period increases compared with that of the incident wave. In the tests it increased between 23 and 36%.

The main purpose of running the experiments in irregular waves was to evaluate a presumed linear response in a range of frequencies. In Figures 5.10, 5.11 and 5.12 a comparison is made between the theoretically obtained transmission coefficients and those obtained in irregular and regular wave tests. In the graphs the

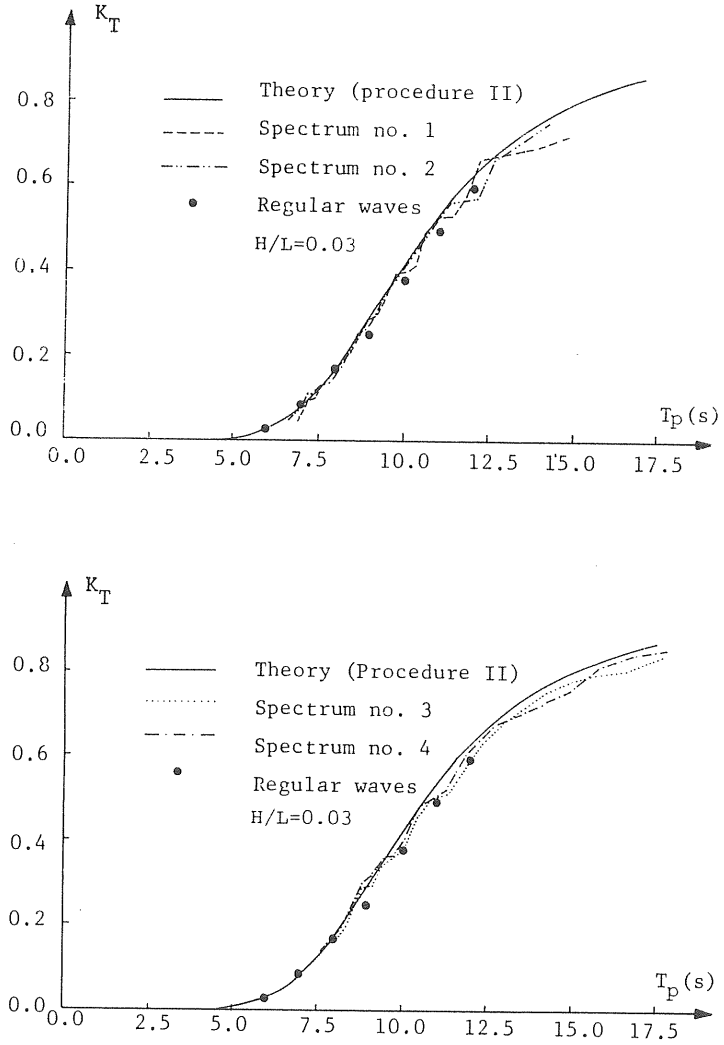

Figure 5.10 Transmission coefficients of breakwater C

transmission coefficient of the regular wave tests is shown for the steepness, H/L= 3%. Figure 5.10 shows the results for breakwater C. For all four spectra, the agreement between the results of regular and irregular wave tests as well as the agreement between model tests and theory are satisfactory. Figure 5.11 shows the results for breakwater C2. The difference between theory and experiments is somewhat larger than for breakwater C. The difference is most pronounced for long periods. The agreement between the results of regular and irregular wave tests is satisfactory.

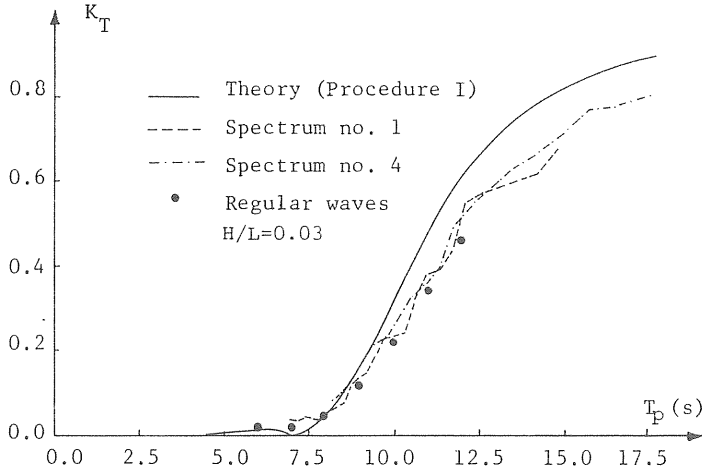

Figure 5.11 Transmission coefficient of breakwater C2

Figure 5.12 shows the results for breakwater C4. The theoretical results show a cancellation period of about 10.5 – 10.6 seconds during which the transmission coefficient tends towards zero. This anti–resonance characteristic is hardly noticeable in the experiments. The deviation between theoretical and experimental results has now become large in a wide range of frequencies. The agreement between the irregular and regular wave test results is, however, still satisfactory.

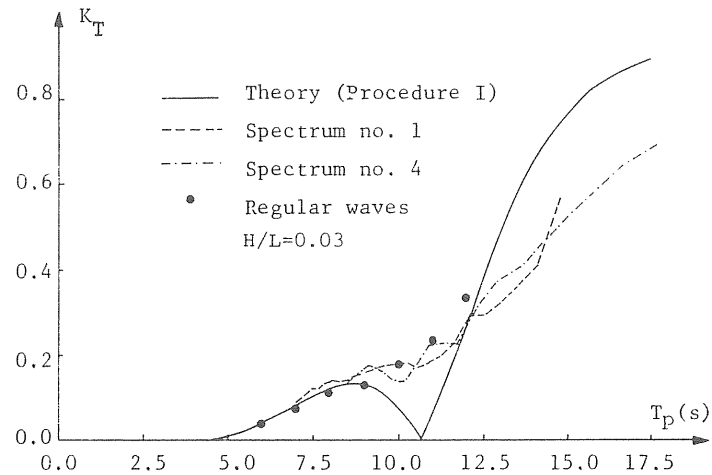

Figure 5.12 Transmission coefficient of breakwater C4.

It is concluded that regular and irregular wave test results are in good agreement and that the theoretical model is a valuable tool for selecting the profile of the breakwater. The experiments confirm that, for breakwater C4, the transmission increases for short periods when compared with C2, see Figure 5.13.

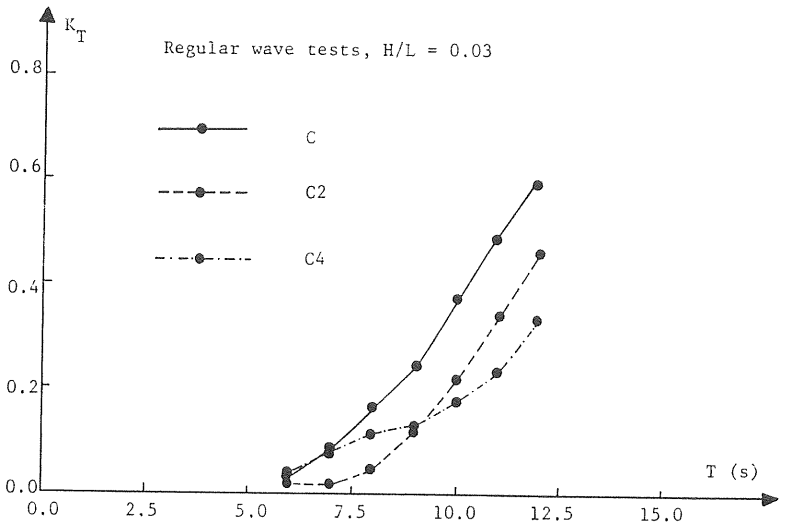

Figure 5.13 Transmission coefficient of breakwater C, C2 and C4 when exposed to regular waves. H/L= 0.03

Finally, in Table 5.7, the transmission coefficients obtained in regular waves are presented. They are listed for different steepnesses together with the theoretical values. For breakwater C the dependence on wave steepness is slight and only noticeable for prototype periods higher than 10 seconds. For these periods the transmission tends to decrease with increasing steepness. The C2 breakwater exhibits a similar characteristic for periods longer than 10 seconds. The decrease of transmission for increasing steepness is somewhat larger. Furthermore, for waves with periods of 8 and 9 seconds, the transmission tends to increase for increasing steepness. This is probably associated with the cancellation which appears in the theory. The ideal situation without viscous effects giving the appearance of cancellation is probably increasingly disturbed with increasing steepness, thus giving increasing transmission. This characteristic is even stronger for the C4 breakwater, and is noticeable for virtually all periods investigated. For the periods 10, 11 and 12 seconds the increase in transmission with increasing steepness is significant.

Table 5.7 Transmission coefficient obtained from regular wave tests.

T_p(s)	Wave steepness H/L 0.01	0.02	0.03	0.04	0.05	Theory
Breakwater C						
6	-	0.02	0.02	0.03	0.03	0.027
7	-	0.08	0.08	0.08	0.08	0.079
8	-	0.18	0.17	0.17	0.17	0.169
9	-	0.28	0.26	0.26	0.26	0.290
10	-	0.39	0.38	0.38	0.38	0.420
11	-	0.50	0.48	0.48	0.46	0.538
12	-	0.60	0.60	0.58	0.54	0.633
Breakwater C2						
6	-	-	0.02	0.02	0.02	0.014
7	-	-	0.02	0.02	0.02	0.004
8	-	0.04	0.05	0.06	0.07	0.047
9	-	0.10	0.11	0.15	0.15	0.157
10	0.24	0.22	0.22	0.24	0.23	0.315
11	0.39	0.35	0.34	0.34	-	0.477
12	0.51	0.48	0.46	0.44	-	0.610
Breakwater C4						
6	-	-	0.04	0.04	0.04	0.040
7	-	-	0.07	0.07	0.08	0.084
8	-	0.10	0.11	0.11	0.12	0.125
9	-	0.12	0.12	0.13	0.14	0.135
10	0.13	0.15	0.18	0.20	0.20	0.082
11	0.15	0.21	0.24	0.26	-	0.056
12	0.25	0.32	0.34	-	-	0.267

5.2.2. Reflection coefficient

In the present study the principle described in section 4.5 was used to separate the incident wave and the reflected wave. Three wave height meters were placed in front of the breakwater and an additional meter was placed on the port side, see Figure 5.14.

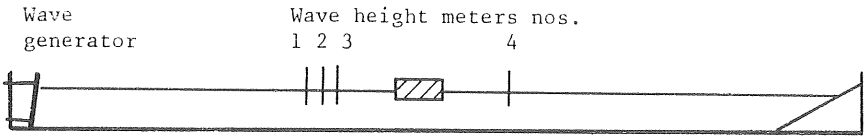

Figure 5.14 Location of wave height meters.

The three wave height meters on the wave–exposed side were used to separate the incident wave and the reflected wave. Three meters will give three sets of pairs so that, in each run, it is possible to estimate the incident wave, the reflected wave, and the reflection coefficient three times. The additional wave height meter on the port side was used to measure the transmitted wave simultaneously.

Since the results evaluated in this section include an FFT analysis of the measured time series, the transmission coefficients are not evaluated as those presented for regular waves in section 5.2.1 (they were evaluated directly from the time series). In this section, results of transmission measured simultaneously with the reflection are therefore presented.

The separation technique seems to give reasonsable results for the tested wave steepnesses. For the steep waves the scatter in the results became somewhat larger. The method also gave larger scatter if the distance between the meters was equal to or close to a multiple of half a wave length.

For practical reasons the wave height meters were kept fixed during a series of runs at different wave periods including T_p = 7, 8, 9, 10, 11, and 12 seconds. Since the wave length varies for different periods, sometimes the distance between the gauges became close to a multiple of half a wave length. These results were omitted from further evaluation. The evaluated quantities in each run were then chosen as the mean of the remaining estimates. For example, the incident wave for a single run

was evaluated as the mean of one, two or three estimates depending on how many estimates had been omitted.

As a quality check of how well the waves were separated the evaluated incident waves were compared with those measured with no structure in the wave tank (henceforth referred to as undisturbed incident waves). For breakwater C, the incident wave and the reflected wave were separated in a total of 25 runs (19 of them with a wave steepness close to 3% and 6 of them with a wave steepness close to 5%).

The mean of the ratio between the evaluated incident wave and the undisturbed incident wave was 0.993 for the flatter waves (H/L = 3%) and 0.998 for the steeper waves (H/L = 5%). The corresponding standard deviation was 0.026 and 0.040 respectively. Consequently, the mean of the ratio was close to 1 for both steepnesses but the scattering of the results somewhat larger for the steeper waves.

The reflection coefficient and the transmission coefficient, evaluated using the separated incident wave, are presented in Table 5.8. The coefficients are presented in terms of mean values and standard deviations for each period and each steepness. For the smaller waves the scattering of the coefficients is rather small, especially for the transmission coefficients. For the steeper waves the number of runs is too few to give a reliable view of the scattering.

Table 5.8 Transmission coefficient and reflection coefficient evaluated using the separated incident wave.

T_p (s)	H/L (%)	N	$\bar{K}_T$	s	$\bar{K}_R$	s	$\bar{K}_T^2+\bar{K}_R^2$
7	3	3	0.086	0.004	0.954	0.025	0.918
8	3	1	0.181	–	0.926	–	0.890
9	3	6	0.252	0.009	0.918	0.025	0.906
10	3	3	0.383	0.009	0.827	0.019	0.831
11	3	3	0.483	0.007	0.788	0.011	0.854
12	3	3	0.576	0.013	0.753	0.025	0.899
9	5	1	0.282	–	0.900	–	0.890
10	5	1	0.360	–	0.775	–	0.730
11	5	2	0.465	0.011	0.745	0.045	0.771
12	5	1	0.569	–	0.669	–	0.771

In the rightmost column the sum of the square of the transmission and reflection coefficients are given. This quantity should equal 1 if there is no mechanical energy transformed into heat. For the 3% steepness, the losses vary in the range of 8.2 to 16.9% of the energy of the incident waves. For the steeper waves (H/L = 5%) the losses are in the range of 11.0 to 27.0%. From the experiments described above it seems that the reflection coefficient is more dependent on the steepness than the transmission coefficient.

In Figure 5.15 the measured reflection coefficients (mean value) are compared to calculated values. For the lower waves the deviation between measurements and theory was less than 9%, while for the steeper waves it was less than 15%.

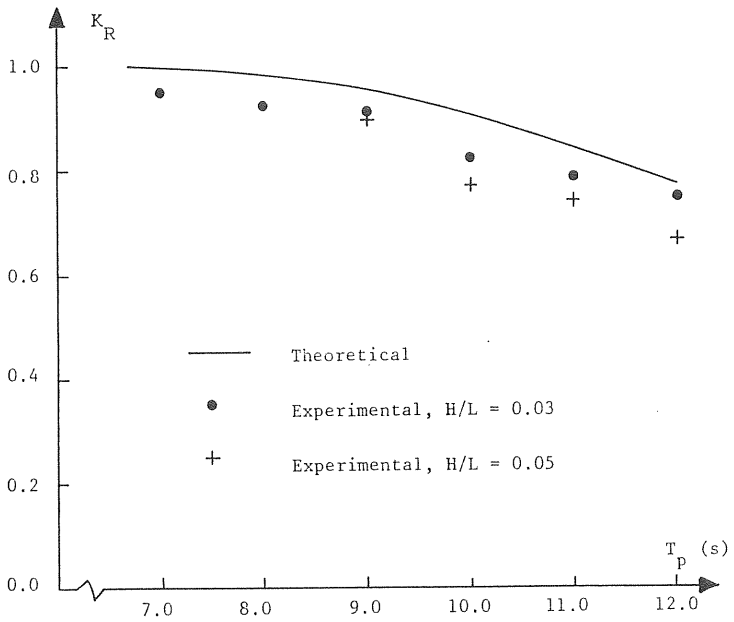

Figure 5.15 Measured and calculated reflection coefficients for breakwater C

In addition to the results obtained above the transmission coefficient was evaluated using the undisturbed incident wave. The results of this evaluation are presented in Table 5.9.

Table 5.9 Transmission coefficient based on the undisturbed incident wave.

T_p(s)	H/L = 3%			H/L = 5%		
	N	$\bar{K}_T$	s	N	$\bar{K}_T$	s
7	3	0.085	0.006	2	0.087	0.020
8	3	0.166	0.008	3	0.171	0.002
9	6	0.250	0.008	1	0.260	–
10	3	0.380	0.005	1	0.369	–
11	3	0.492	0.000	3	0.470	0.002
12	3	0.594	0.004	3	0.565	0.003

It is clear from the table that the standard deviation is small for the flatter waves as well as the steeper ones (except for H/L=5% and T_p=7 s). A dependence on the steepness is noticed, although it is not very pronounced. The agreement with the transmission coefficients presented in Table 5.7 is satisfactory.

5.2.3 Forces and pressure

The forces were measured for the breakwater of geometry type C. As is discussed in this section, the forces calculated using a linear theoretical model do not properly describe all features of the measured forces.

Examples of time series of the measured horizontal forces, vertical forces and moments about the centre of the bottom of the breakwater are presented in Figures 5.16a, b and c. The time series are given as measured on a 1.99 m long model section of the breakwater. The left and right columns of the figures correspond to prototype periods T_p=7 and 10 s respectively (model periods T_m=0.87 and 1.24 s).

As far as one can see from the figures the oscillation of the horizontal force and the moment is closely sinusoidal in time, while the vertical force oscillates in a more complex way. An FFT–analysis confirm that the higher order components of the horizontal force and of the moment are rather small while the vertical force contains a component of significant amplitude at twice the frequency of wave generation.

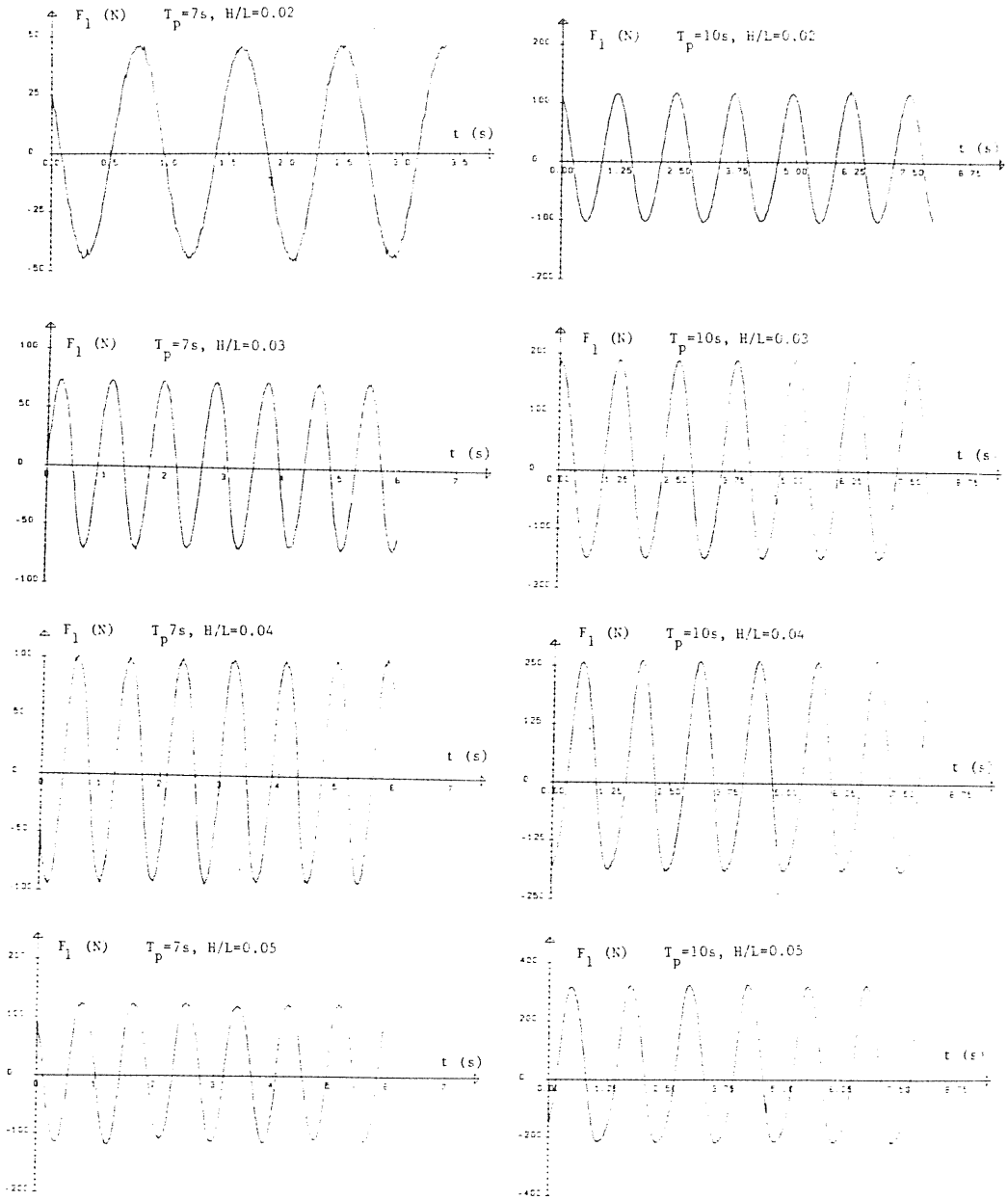

Figure 5.16a Horizontal force, as measured on a 1.99 m long model section of breakwater C. Left column: T_p=7 s, T_m=0.87 s. Right column: T_p=10 s, T_m=1.24 s.

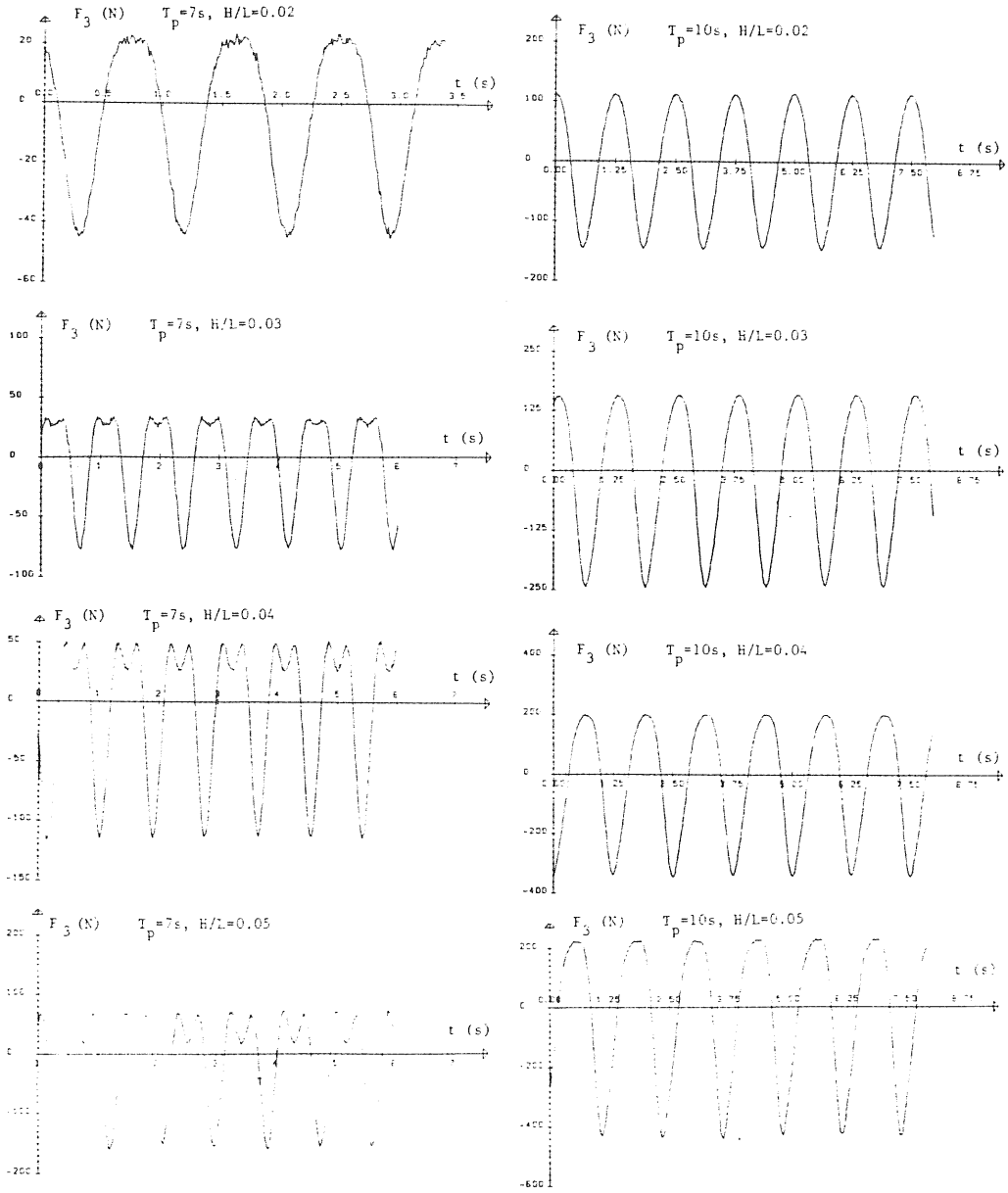

Figure 5.16b Vertical force, as measured on a 1.99 m long model section of breakwater C. Left column: T_p=7 s, T_m=0.87 s. Right column: T_p=10 s, T_m=1.24 s.

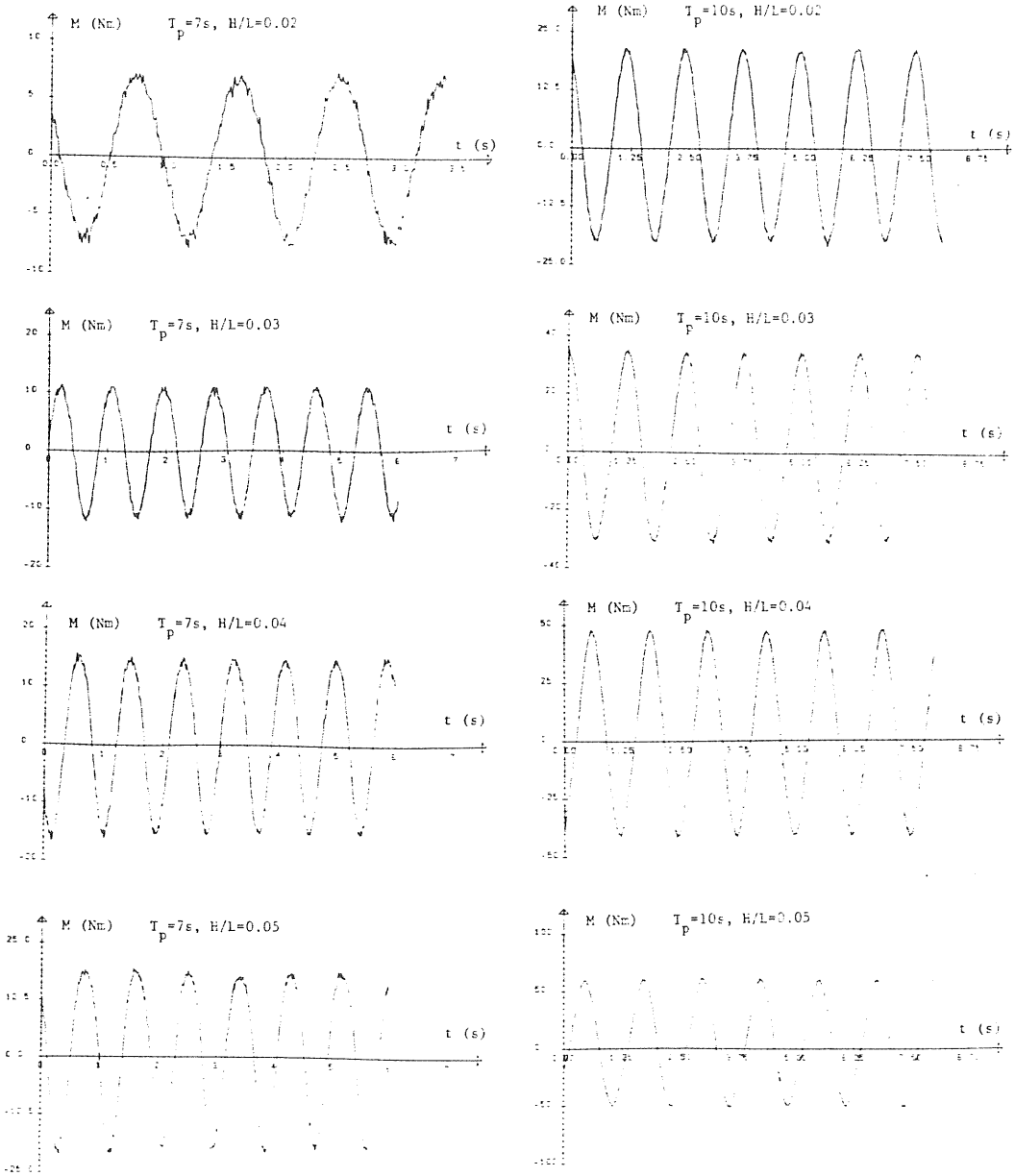

Figure 5.16c Moment about the centre of the bottom of the breakwater, as measured on a 1.99 m long model section of breakwater C. Left column: T_p=7 s, T_m=0.87 s. Right column: T_p=10s, T_m=1.24 s.

The ratio between the amplitude of the second order component and the first order component of the vertical force increases for short and steep waves. In Figure 5.17 the amplitude spectrum for the vertical force, as measured on a 1.99 m long model section of the breakwater is shown. The wave characteristics are T_p=7 s, T_m=0.87 s and H/L=0.04.

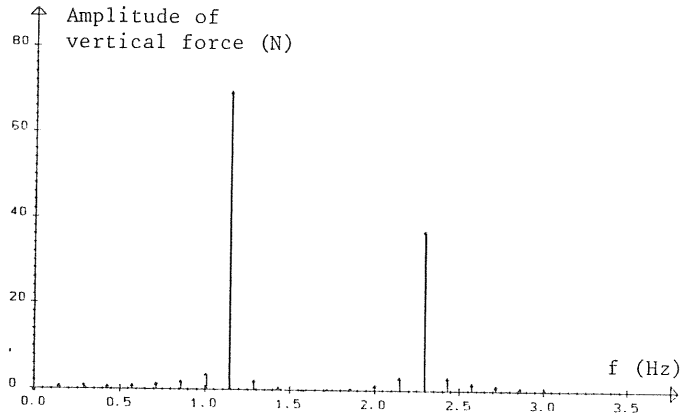

Figure 5.17 Amplitude spectrum of measured vertical force. T_p=7 s (T_m=0.87 s) and H/L=0.04.

The second–order characteristic of the vertical force cannot be modelled theoretically using a linear model. The vorticies shed at the corner facing the incident waves were generally small for short waves, when the second–order characteristics were at their strongest, and therefore concluded not to be the main reason for a second–order component. Whether a second–order wave/structure model could accurately simulate this characteristic has not been investigated. However, for a ship section in deep water with a draught to width ratio d/2b=0.4 Guoping (1987) found that the ratio between the second order component and the first order component of the vertical force significantly increases with decreasing wave period. The same trend has been found in the present experiments. Preliminary results from a second order solution for a rectangular horizontal cylinder by Sulisz (1989) also exhibit the same trends.

In a second order solution the force consists of three parts, i.e. a linear part oscillating at the frequency f, a non–oscillating steady part, and a bi–harmonic part oscillating at the frequency 2f.

In the present study the developed solution procedures concern the linear part of the problem. It is considered to be outside the scope to investigate wether or not a second order wave/structure model accurately can simulate the measured behaviour.

In order to get a first idea of the agreement between measurements and theory it is convenient to compare the maximum to minimum values of the measured forces with those obtained with the linear theoretical model. In Table 5.10 a, b and c, the maximum to minimum values of the horizontal force, vertical force and moment about the centre of the bottom of the breakwater are listed together with corresponding theoretical values. In Figures 5.18a, b and c, the same measured quantities for the smallest steepness H/L=0.02 are illustrated together with theoretically obtained values.

Table 5.10a Maximum to minimum value of the measured horisontal force divided by wave height. Scaled to prototype dimensions per metre breakwater ((kN/m)/m).

T_p(s)	H/L = 0.02	0.03	0.04	0.05	Theory
6	118	121	114	112	119.9
7	131	133	132	131	138.5
8	154	147	147	144	153.0
9	157	155	153	151	162.1
10	161	156	156	151	165.0
11	161	155	154	150	162.3
12	158	158	153	148	156.2

Table 5.10b Maximum to minimum value of the measured vertical force, divided by wave height. Scaled to prototype dimensions per metre breakwater ((kN/m)/m).

T_p(s)	H/L = 0.02	0.03	0.04	0.05	Theory
6	61	78	88	98	63.2
7	89	100	120	125	97.5
8	134	131	133	147	130.9
9	154	159	158	163	162.1
10	189	187	189	181	190.5
11	212	202	207	208	215.8
12	229	230	214	218	237.8

Table 5.10c Maximum to minimum value of the measured moment about the centre of the bottom of the breakwater divided by wave height. Scaled to prototype dimensions per metre breakwater ((kNm/m)/m).

T_p(s)	H/L = 0.02	0.03	0.04	0.05	Theory
6	1118	1138	1135	1100	1103
7	1303	1376	1380	1342	1377
8	1690	1656	1627	1668	1632
9	1869	1858	1882	1914	1840
10	1958	1962	2010	1967	1970
11	2097	2022	2016	2081	2021
12	2079	2090	2096	2099	2009

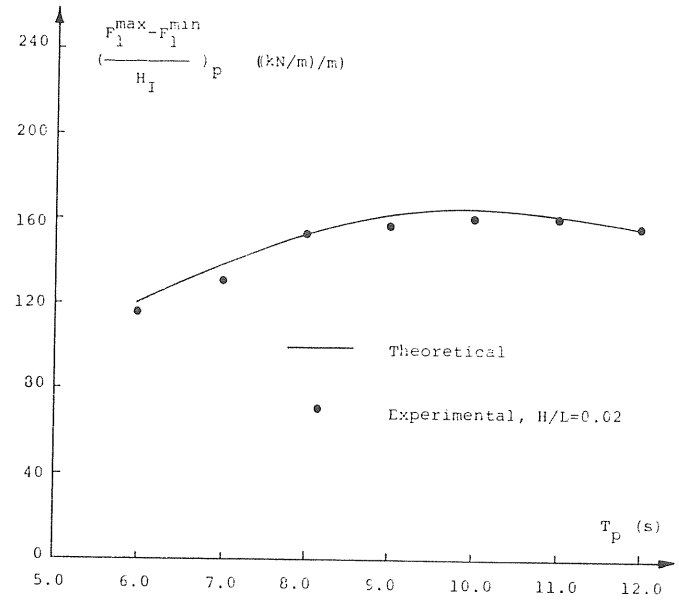

Figure 5.18a Maximum to minimum value of measured horizonal force divided by wave height. H/L=0.02. Scaled to prototype dimensions per metre breakwater ((kN/m)/m).

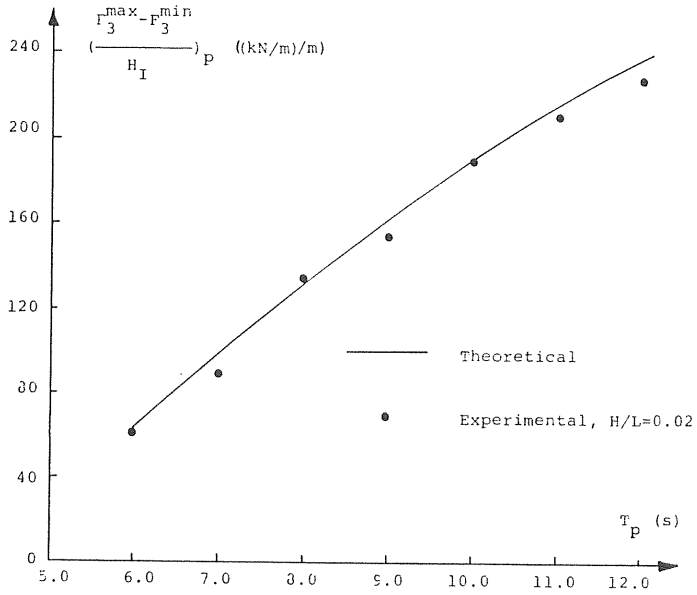

Figure 5.18b Maximum to minimum value of measured vertical force divided by wave height. H/L=0.02. Scaled to prototype dimensions per metre breakwater ((kN/m)/m).

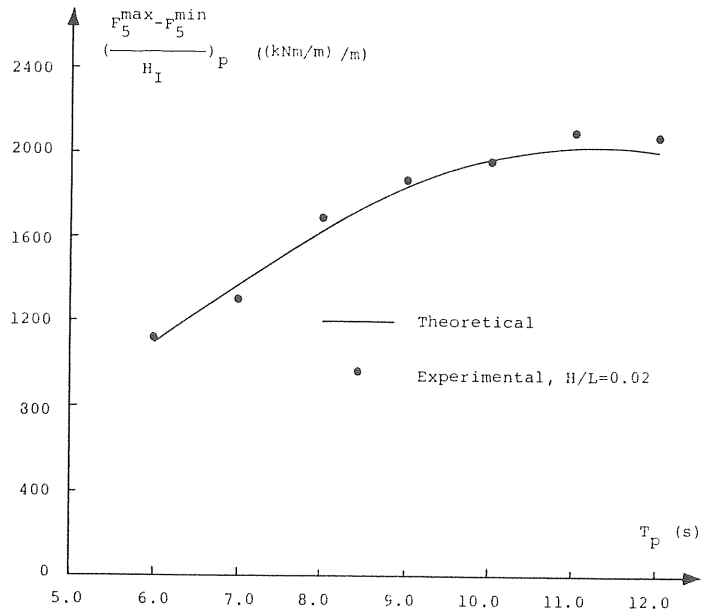

Figure 5.18c Maximum to minimum value of measured moment divided by wave height. H/L=0.02. Scaled to prototype dimensions per metre breakwater ((kNm/m)/m).

For small waves, H/L=0.02, the measurements agree well with the theory for all three quantities. For larger waves, the measured values are still close to the theoretical values for the horizontal force and the moment, while for the vertical force the deviation is significant.

The comparison with the vertical force is, of course, questionable especially for higher waves, since the measured quantities for higher waves contain a component of significant amplitude at twice the frequency of wave generation. A comparison which, mathematically, is more appropriate although probably of less practical interest is the one between the first order component of the measured vertical force and the amplitude of the force obtained using the linear theoretical model. In Table 5.11 the ratio between the amplitude of the first order component of the vertical force and the amplitude of the first order component of the incident wave is shown. Even for short and steep waves the agreement between measurements and theory is satisfactory. It is concluded that it is not sufficient to calculate the vertical force for short and steep waves using a linear model.

Table 5.11 First order component of measured vertical force divided by first order component of incident wave. Scaled to prototype dimensions per metre breakwater ((kN/m)/m).

T_p(s)	H/L = 0.02	0.03	0.04	0.05	Theory
7	92.6	95.3	93.7	94.6	97.5
10	187.1	185.3	187.6	182.7	190.5

Even if a complete second–order solution is not available it is possible to use the results from the first order solution in a momentum flux consideration in order to obtain the steady drift forces, correct to second order in wave amplitude. General expressions for the surge and sway drift forces were first derived by Maruo (1960) and subsequently extended to include the drift moment in yaw by Newman (1967). For 2D structures Longuet–Higgins (1977) expressed the horizontal drift force directly in terms of the reflection coefficient. The expression by Longuet–Higgins can be written as

$$\bar{F}_1 = \frac{E\ c_g}{c}(1+K_R^2-K_T^2) = \frac{E\ c_g}{c}2K_R^2 \qquad (5.5)$$

where

c_g = group velocity = $\frac{1}{2}(1 + \frac{2kh}{\sinh 2kh})\ c$

c = phase velocity

$E = \frac{1}{2}\rho g a_I^2$

a_I = amplitude of incident wave

The second equality in Eq. (5.5) is valid only when there is no energy absorbed or dissipated, i.e. when $K_R^2+K_T^2=1$. In Figure 5.19 the horizontal drift force obtained experimentally is compared with the force obtained with the Longuet–Higgins expression.

The drift force is plotted versus kb and made dimensionless by the factor $2Ec_g/c$. Since the drift force is equal to the change in momentum the factor equals the drift force obtained when the incident wave is totally reflected, i.e. when the incident wave carries the momentum Ec_g/c in the positive x–direction and the reflected wave carries the same quantity in the opposite direction. Consequently, the dimensionless drift force should be less or equal to unity. The drift force obtained experimentally was evaluated as the mean value of the time series of the force. The length of the times series were adjusted to be equal to an integer number times the wave period. The experimental results were obtained for steepnesses 3,4 and 5 %. No dependence on the wave heigth apart from the proportionality to the square of the wave heigth was identified. Although there are some scatter in the experimental results the agreement is considered as satisfactory since the drift force is a second–order effect.

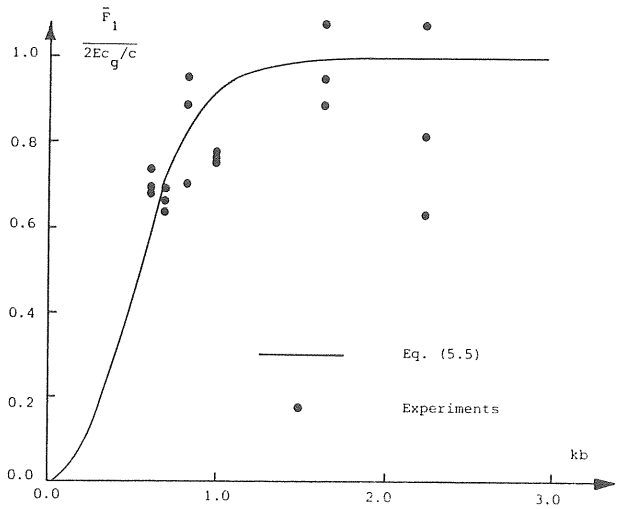

Figure 5.19 Horizontal drift force for breakwater C. Comparison between experiments and theory (procedure II).

Since the vertical forces measured directly with force probes exhibited a stronger second–order characteristic than expected, it was decided to verify the force by also measuring the pressure at the bottom of the breakwater. The force probes and pressure transducers were calibrated separately. The verification included two periods T_p=7 and 10 s and each of the 4 steepnesses. In all tested cases the agreement between integrated pressure and forces measured by force probes were excellent. Example of comparisons are shown in Figure 5.20.

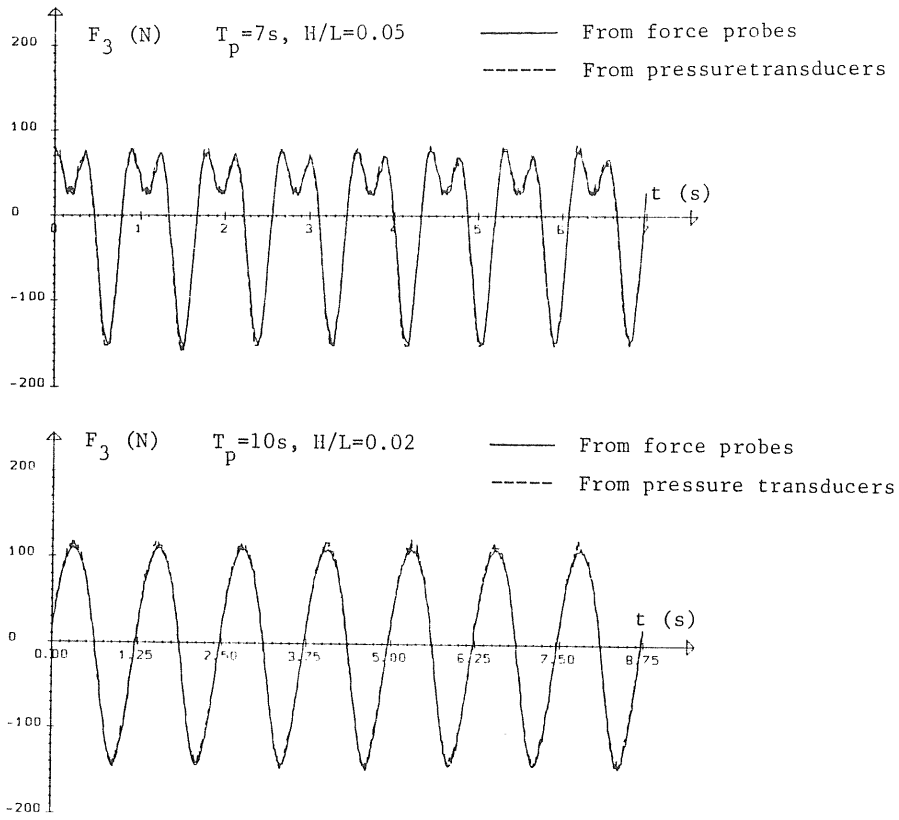

Figure 5.20 Comparison of pressure integrated over the bottom of the breakwater and the vertical force obtained from the force probes. The results are presented as they were measured on a 1.99 m long model section of breakwater C.

From the pressure measurements it also became clear that the second–order characteristics of the force could be traced in the pressure all over the bottom plate of the breakwater and not only from the transducers located close to the corner facing the incident waves. In Figure 5.21 the pressure measured by transducers nos. 1,2,4,5 and 6 are presented (their locations can be seen in Figure 4.14, transducer no. 3 did not work properly and was disregarded from the evaluation).

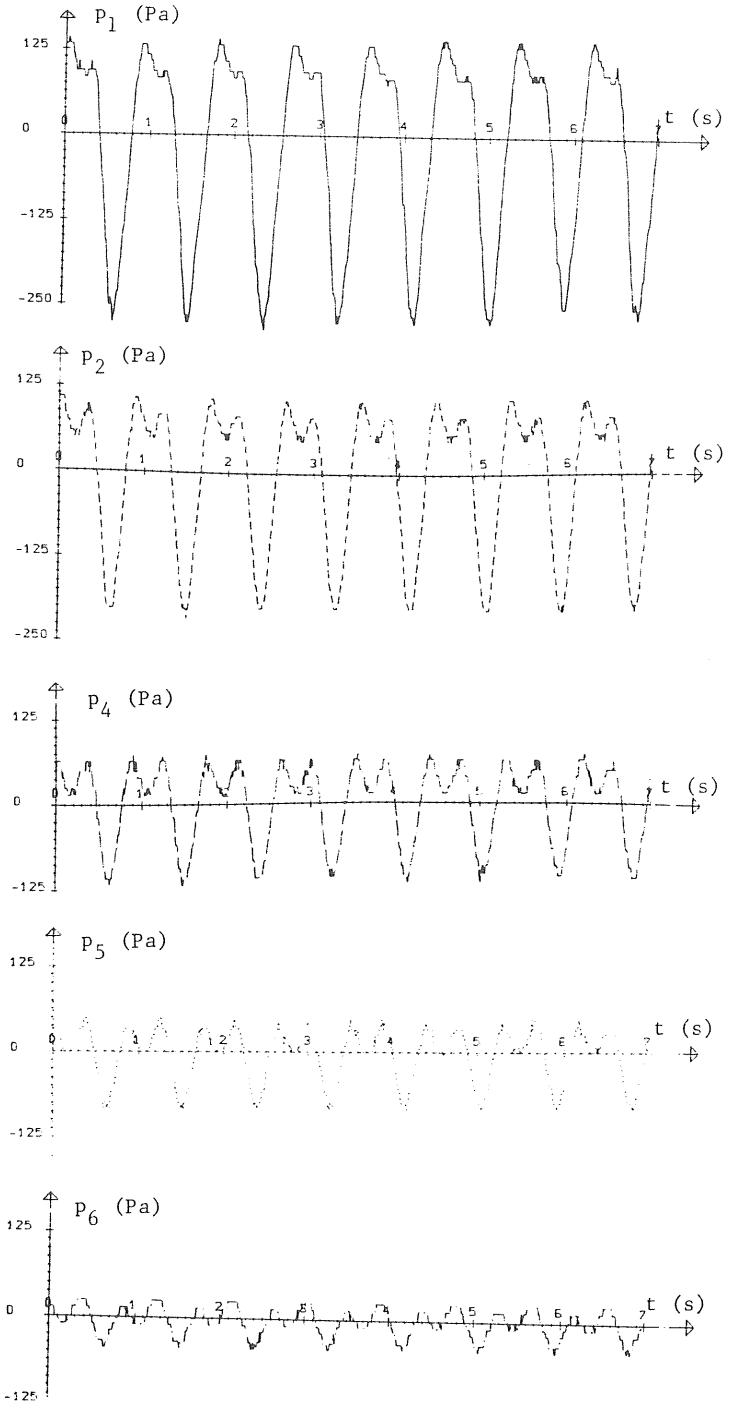

Figure 5.21 Pressure measured at the bottom plate of the breakwater. The locations of the transducers are given in Figure 4.14. The pressure is presented in model dimensions. T_p=7 s, T_m=0.87s, H/L=0.05.

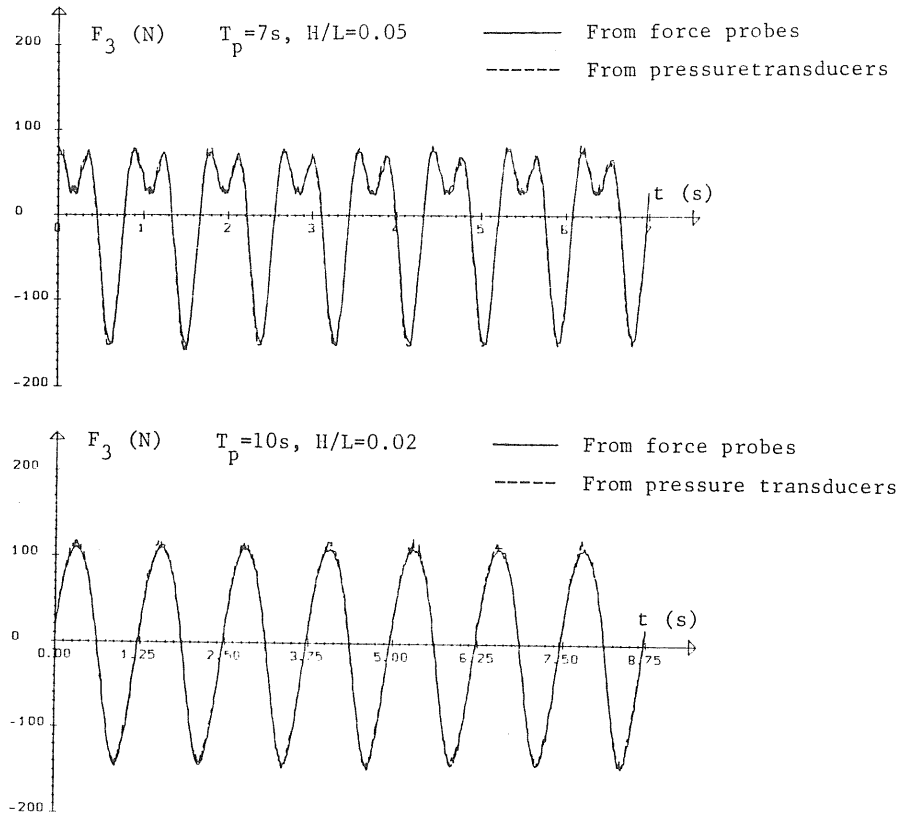

Figure 5.20 Comparison of pressure integrated over the bottom of the breakwater and the vertical force obtained from the force probes. The results are presented as they were measured on a 1.99 m long model section of breakwater C.

From the pressure measurements it also became clear that the second–order characteristics of the force could be traced in the pressure all over the bottom plate of the breakwater and not only from the transducers located close to the corner facing the incident waves. In Figure 5.21 the pressure measured by transducers nos. 1,2,4,5 and 6 are presented (their locations can be seen in Figure 4.14, transducer no. 3 did not work properly and was disregarded from the evaluation).

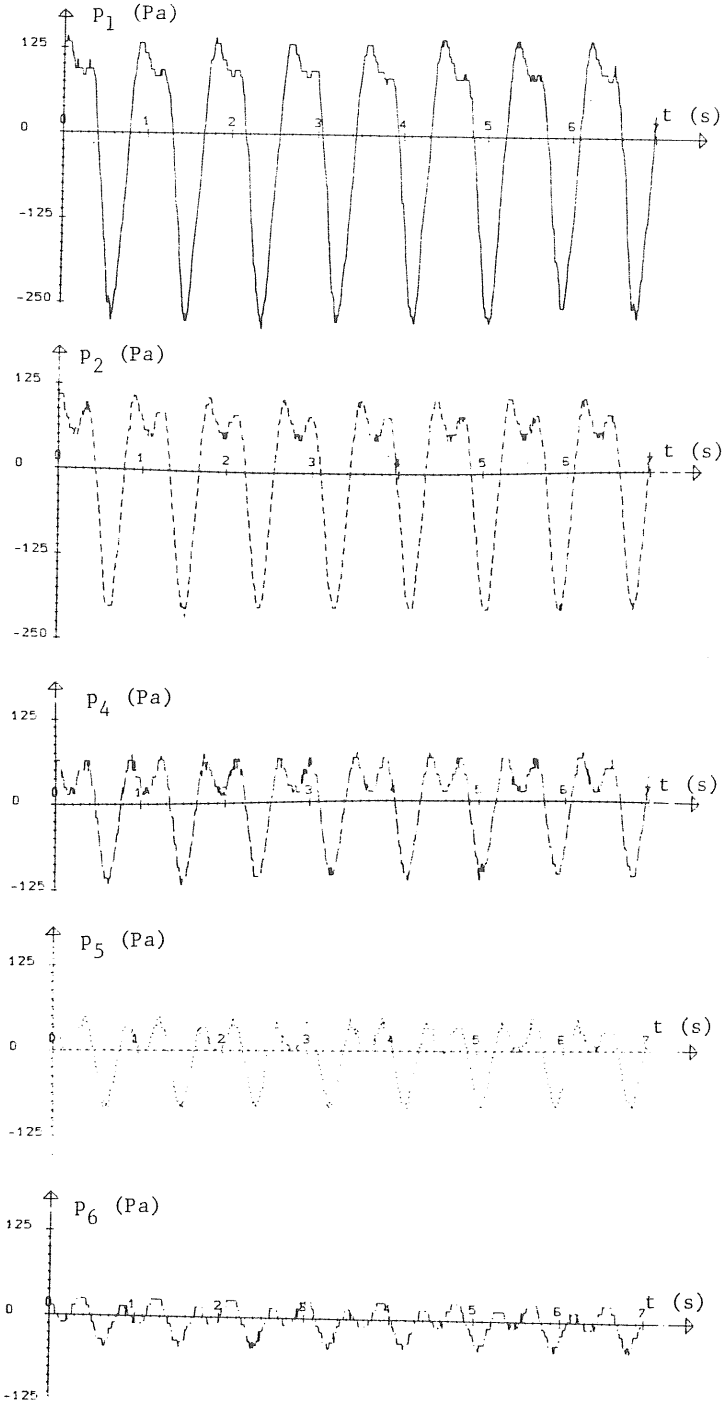

Figure 5.21 Pressure measured at the bottom plate of the breakwater. The locations of the transducers are given in Figure 4.14. The pressure is presented in model dimensions. T_p=7 s, T_m=0.87s, H/L=0.05.

6 CONCLUSIONS

6.1 The barrier type of breakwater

For certain dimensions, a barrier–type breakwater of limited draught can significantly reduce the waves. The geometry of the cross section of the breakwater strongly influences the size of transmission. For example, a breakwater with a protruding bottom plate (Principality of Monaco's patent no. F 85 15938) could significantly reduce the transmission compared with a rectangular cross–section type of breakwater of the same total width (Pincipality of Monaco's patent no. PCT/MC/86/00003). This is confirmed both by experiments and potential theory.

6.2. Theoretical study

A linear theoretical model is found to be a valuable tool in the design of a barrier–type breakwater. Different solution procedures could be selected. A procedure based on orthogonal series solutions in fluid subregions has the advantage of not being dependent on any discretization and therefore probably safer to use. Furthermore, it requires neither much core memory in a computer, nor much processing time, and is run with simple input data. It is also an excellent tool for checking numerical models based on discretization. One obvious disadvantage of the procedure is its lack of generality.

The numerical model based on the fundamental source function formulation agrees well with the procedures based on orthogonal series solutions as well as results presented by other authors. A price one has to pay for the generality is the time it requires, both in terms of time to establish input data and computer processing. For sharp edge models, the results seem to be sensitive to the discretization, requiring a more dense discretization close to the corners. This was found to be especially important for pitch quantities.

6.3 Experimental study

In the irregular wave tests, the technique by which fast wave components were successively delayed worked satisfactorily. The transmission coefficients obtained from the irregular wave tests agreed well with those obtained in regular waves. The reproducibility of the irregular waves was high.

Energy losses increased with increasing wave steepness. The increase in energy loss affected the reflection coefficients more than the transmission coefficients.

The anti–resonance characteristics theoretically obtained for the breakwater with protruding bottom plate could not be found in the experiments.

The transmission coefficients sometimes decreased for increasing steepness, while for other geometries and/or periods it increased. This is probably associated with the cancellation which appears in the theory. The ideal situation without viscous effects giving the appearance of cancellation is probably increasingly disturbed with increasing steepness, thus giving increasing transmission.

The maximum to minimum values of the horizontal force and the moment about the centre of the bottom of the breakwater agreed well with theory. The maximum to minimum value of the vertical force agreed well with theory for small waves, H/L=0.02. However, for short and steep waves the oscillation of the force contained a second–order component of significant amplitude. For these waves the first order component of the measured force, obtained by using an FFT–analysis, agreed well with the force obtained from the linear theoretical model. It was considered to be outside the scope of this study to investigate whether or not a second–order wave/structure interaction model could accurately simulate the behaviour.

In the experimental part of the thesis, results have been presented mainly for a breakwater with a rectangular cross section defined by a draught to water depth ratio d/h=10/50 and a draught to width ratio d/2b=10/40 (breakwater C). Although not presented here, transmission past breakwaters with other dimensions has been investigated. An idea of the span of the dimensions included in the experimental tests is given by the four breakwaters defined below.

1: d/h=10/50 and d/2b=10/30
2: d/h=10/50 and d/2b=10/50
3: d/h=7/50 and d/2b=7/40
4: d/h=13/50 and d/2b=13/40

For these breakwaters, all with rectangular cross section, the size of the deviations between the transmission coefficients obtained in regular wave tests, irregular wave tests, and theoretically are comparable to those obtained for breakwater C. These additional tests were performed only for a few periods and steepnesses, still they give an indication of what experimental results one can expect for these dimensions.

LIST OF SYMBOLS

a	wave amplitude
a_i	amplitude of wave component
a_{ij}	element of added mass matrix
a_I	amplitude of incident wave
A_I	complex amplitude of incident wave
A_R	complex amplitude of reflected wave
A_w	water plane area
b	half width of breakwater
b_1	horizontal distance from origin to region I (solution procedure III)
b_3	horizontal distance from origin to region III (solution procedure III)
b_{ij}	element of potential damping matrix
c	phase velocity of wave
c_g	group velocity of wave
c_{ij}	element of hydrostatic matrix
c_{gi}	group velocity of the i:th wave component
C	breakwater defined in Figure 5.9
C2	breakwater defined in Figure 5.9
C4	breakwater defined in Figure 5.9
C_j	complex amplitude of the j:th measured wave
d	draught of breakwater
e	distans defined in Figure 3.1
E	average energy per unit horizontal area
f	frequency
f_i	discrete frequency = $i\Delta f$
f_m	frequency in model dimension
f_p	frequency in prototype dimension
F_i	element of force vector
$\bar{F}_1$	horizontal drift force
g	acceleration of gravity

h	water depth
h_1	water depth (solution procedure I)
h_1	water depth at ocean side (solution procedure III)
h_2	water depth at protruding bottom plate (solution procedure I)
h_3	water depth at port side (solution procedure III)
H	wave height
H_A	wave height of antinod
H_I	incident wave height
H_N	wave height of nod
H_R	reflected wave height
H_s	significant wave height
H_{SI}	significant incident wave height
H_{ST}	significant transmitted wave height
$\underline{i}$	unit vector along the x–axis
$\underline{j}$	unit vector along the y–axis
J	moment of inertia of the water plane area about the y–axis.
k	wave number
$\underline{k}$	unit vector along the z–axis
k_l	wave number at the left side of the breakwater (ocean side)
k_r	wave number at the right side of the breakwater (port side)
K_R	reflection coefficient
$\bar{K}_R$	mean value of reflection coefficient
$\bar{K}_T$	transmission coefficient
$\bar{K}_T$	mean value of transmission coefficient
K_T^S	transmission coefficient based on significant wave height
L	wave length
L_m	wave length in model dimension
L_p	wave length in prototype dimension

m	mass of structure
m_{ij}	element of mass matrix
m_{0I}	zero order spectral moment of incident wave
m_{0T}	zero order spectral moment of transmitted wave
$\underline{n}$	generalized normal vector
n_i	element of generalized normal vector
N	number of components in spectrum
N	number of measurements
N	number of components in orthogonal series
N_6	number of elements in solution procedure III
Oxyz	Cartesian coordinate system
p	pressure
r	polar coordinate in the horizontal plane
r_p	pitch radius of gyration
$r(t)$	input signal to wave generator
R	wave making coefficient
Re{ }	real value of the complex quantity inside the braces
s	standard deviation
s	distance from wave generator to measuring point
S	boundary enclosing the fluid domain
S_∞	vertical boundary at infinity enclosing the fluid domain
S_1	boundary according to Figure 3.3
S_2	boundary according to Figure 3.3
S_3	boundary according to Figure 3.3
S_4	boundary according to Figure 3.3
S_5	boundary according to Figure 3.3
S_6	boundary according to Figure 3.3
$S(f)$	wave spectrum
$\bar{S}(f)$	smooth spectrum of measured wave
$S_I(f)$	wave spectrum of incident wave
$S_T(f)$	wave spectrum of transmitted wave

t	time
T	wave period
T_m	measuring period
T_m	wave period in model dimensions
T_p	wave period in prototype dimension
T_{si}	time for the i:th wave component to reach the measuring point
T_r	return period of time series
T_z	zero upcrossing period
u	velocity component along the x–axis
$\underline{u}$	fluid velocity vector
v	velocity component along the y–axis
$\forall$	water volume displaced by breakwater
w	velocity component along the z–axis
$\underline{x}$	vector of motion
x_c	x–coordinate of the center of gravity of the water plane area
x_i	element of the motion vector
x_j	x–coordinate of the j:th wave gague
$x_l(t)$	motion in the l:th mode as function of time
z_B	center of buoyancy
z_G	center of gravity
Δf	frequency spacing
ζ	wave elevation
ζ_I	elevation of incident wave
ζ_R	elevation of reflected wave
ζ_j^m	elevation of the i:th measured wave

θ_i	phase angle
$\theta(\tau)$	delay function defined by Eq. (4.5)
ρ	density of fluid
τ	time
ϕ	spatial velocity potential
ϕ_I	spatial velocity potential of incident wave
Φ	time dependent velocity potential
ω	angular frequency
∇	differential operator
$\int$	line integral
$\int\int$	surface integral
$\int\int\int$	volume integral

LIST OF FIGURES

LIST OF TABLES

LIST OF REFERENCES

Bai, K.J. and Yeung, R.W. (1974): Numerical solutions to free–surface flow problems. Tenth Naval Hydrodynamics Symposium, Massachusetts, pp. 609–633.

Bouchet, R. and Manzone, J.M. (1986): Le mur d'eau dispositif noveau de brise houle en eau profonde PIANC/AIPCN Bulletin 1986, No. 52, pp 60–77.

Chakrabarti, S.K. (1987): Hydrodynamics of offshore structures. Computational Mechanics Publications, Southampton.

Finnigan, T.D. and Yamamoto, T. (1979): Analysis of semi–submerged porous breakwaters. Proc. Civil Eng. in the Oceans, ASCE, San Fransisco. Vol. I, pp. 380–397.

Garret, C.J.R. (1971): Wave forces on a circular dock. J. Fluid Mech., Vol. 46.

Garrison, C.J. (1984): Interaction of oblique waves with an infinite cylinder. Applied Ocean Research, Vol. 6, No. 1.

Gaillard, P., Gauthier, M., and Holly, F. (1980): Method of analysis of random wave experiments with reflecting coastal structures. Proc. 17th Coastal Eng. Conf. Sydney, pp. 124–125.

Goda, Y. and Suzuki, Y. (1976): Estimation of incident and reflected waves in random wave experiments. Proc. 15th Coastal Eng. Conf., Hawaii, pp. 828–845.

Guoping, M. (1987): Second–order wave forces on bodies in regular waves. Thesis. Dept. Marine Hydrodynamics, Chalmers University of Technology, Sweden.

Ijima, T., Chou, C.R. and Yoshida, A. (1976): Method of analysis for two–dimensional water wave problems. Proc. 15th Coastal Eng. Conf., Honolulu, Vol. III, pp. 2717–2736.

International Ship Structures Congress (1964); Proceedings, Delft, The Netherlands.

Jolas, P. (1962): Contribution à l'étude des oscillations périodiques des liquides pesants, avec surface libre. La Houille Blance. No. 6, pp. 758–769.

Jones, D.B., Lee, J.–J., and Raichlen, F. (1979): A transportable breakwater for nearshore applications. Proc. Civil Eng. in the Oceans.

Keil, H. (1974): Discussion on the paper by Bai and Yeung (1974).

Kirby, J.T., and Dalrymple, R.A. (1983): Propagation of obliquely incident water waves over a trench. J. Fluid Mech., Vol. 133, pp. 47–63.

Kajima, R. (1969): Estimation of an incident wave spectrum under the influence of reflection. Proc. 13th IAHR Congr. Kyoto, pp. 285–288.

Lee, J–J. and Ayer, R.M. (1981): Wave propagation over a rectangular trench. J. Fluid Mech., vol. 110, pp. 335–347.

Leonard, J.W., Huang, M.–C., and Hudspeth, R.T. (1983): Hydrodynamic interference between floating cylinders in oblique seas. Applied Ocean Research, Vol. 5, No. 3.

Liu, P.L.–F., and Abbaspour, M. (1982): Wave scattering by a rigid thin barrier. J. Waterways, Port, Coastal and Ocean Division, Vol. 108, No. WW4.

Longuet–Higgins, M.S. (1977): The mean forces exerted by waves on floating or submerged bodies, with applications to sand bars and wave power machines. Proc. R. Soc., London.

Mansard, E.P.D. and Funke, E.R. (1980): The measurement of incident and reflected spectra using least squares method. Proc. 17th Coastal Eng. Conf. Sydney, pp. 154–172.

Maruo, H. (1960): The drift of a body floating on waves. J. Ship. Res., Vol. 4, pp. 1–10.

McIver, P. (1986): Wave forces on adjacent floating bridges. Applied Ocean Research, Vol. 8, No. 2.

Mei, C.C. (1983): The applied dynamics of ocean surface waves. Wiley–Interscience Publication.

Newman, J.N. (1962): The exciting forces on fixed bodies in waves. J. Ship. Res., Vol. 6, No. 3, pp. 10–17.

Newman, J.N. (1967): The drift force and moment on ships in waves. J. Ship. Res., Vol. 11, pp. 51–60.

Newman, J.N. (1977): Marine hydrodynamics. MIT Press.

Sarpkaya, T. and Isaacson, M. (1981): Mechanics of wave forces on offshore structures. Van Nostrand Reinhold, New York.

Sulisz, W. (1989): Private communication. Polish Academy of Sciences, Institute of Hydroengineering, Gdansk, Poland.

Thorton, E.B. and Calhoun, R.J. (1972): Spectral resolution of breakwater reflected waves. J. Waterways, Harbour, Coastal Eng. Div. ASCE, 1972. Vol. 98, WW4, pp. 443–460.

Wu, J. and Liu, P.L.–F. (1988): Interaction of obliquely incident water waves with to vertical obstacles. Applied Ocean Research, Vol. 10, No. 2.

Wu, X.–J. and Price, W.G (1987): A multiple Green's function expression for the hydrodynamic analysis of multiple–hull structures. Applied Ocean Research, Vol. 9, No. 2.

Yamamoto, T. (1981): Moored floating breakwater response to regular and irregular waves. Applied Ocean Research, Vol. 3, No. 1.

Yeung, R.W. (1981): Added mass and damping of a vertical cylinder of finite depth water. Applied Ocean Research. Vol. 3, No. 3

APPENDIX I

SOLUTION OF THE DIFFRACTION PROBLEM FOR A BREAKWATER WITH A RECTANGULAR CROSS SECTION AND A PROTRUDING BOTTOM PLATE FACING THE INCIDENT WAVES

The problem is solved using the method of separation of variables. The fluid domain is divided into four regions, see Figure A1.1.

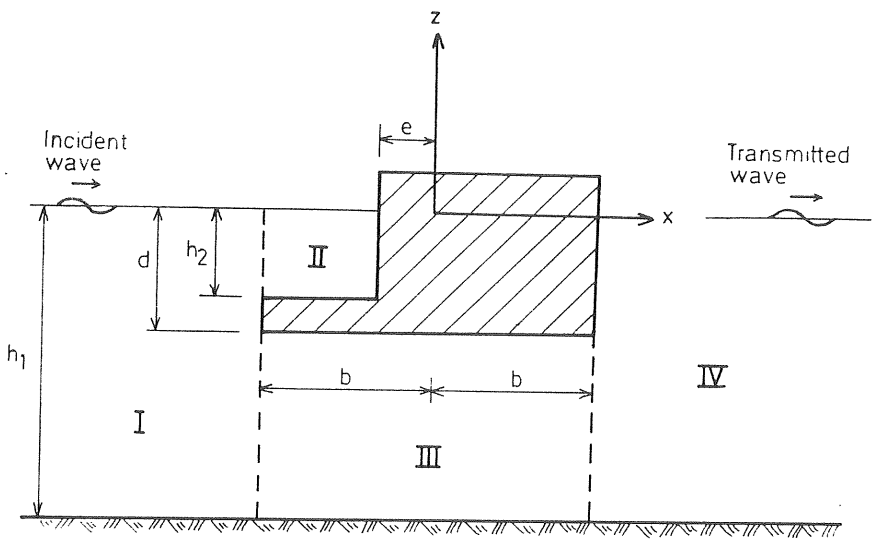

Figure A1.1 Definition of fluid regions and geometrical properties.

The method of separation of variables is applied in each region in order to obtain expressions for the unknown function, i.e. the velocity potential. Expressions valid in the respective region are obtained as infinite series of orthogonal functions. These expressions are developed to satisfy all boundary conditions except those at the common boundary between the regions. It then remains to determine a number of unknown coefficients in the series. This is done by imposing the condition of continuity of pressure and normal velocity at the common boundary between the regions. Mathematically this is fulfilled by matching the potentials and the normal derivatives of the potentials.

A formulation of the diffraction problem starting from the potentials in each region is given below.

Let

$$\Phi_j(x,z,t) = \mathrm{Re}\{\phi_j(x,z)e^{-i\omega t}\},\ j=1,2,3,4 \tag{A1.1}$$

Applying the method of separation of variables gives the complex valued spatial potentials in each region expressed in terms of orthogonal series as below

$$\phi_1 = \phi_I - \frac{iR_1 g}{\omega} e^{-ik_1(x+b)} \frac{\cosh k_1(z+h_1)}{\cosh k_1 h_1} +$$

$$+ \sum_{n=2}^{\infty} -\frac{iR_n g}{\omega} e^{\alpha_n(x+b)} \frac{\cos \alpha_n(z+h_1)}{\cos \alpha_n h_1} \tag{A1.2}$$

$$\phi_2 = -\frac{iP_1 g}{\omega} \frac{\cosh k_2(z+h_2)}{\cosh k_2 h_2} \cos k_2(x+e) +$$

$$+ \sum_{n=2}^{\infty} -\frac{iP_n g}{\omega} \frac{\cos \gamma_n(z+h_2)}{\cos \gamma_n h_2} \cosh \gamma_n(x+e) \tag{A1.3}$$

$$\phi_3 = -\frac{igA_1 x}{\omega b} - \frac{igB_1}{\omega} + \sum_{n=2}^{\infty} -\frac{ig}{\omega}(A_n e^{\lambda_n x} + B_n e^{-\lambda_n x}) \cos \lambda_n(z+h_1) \tag{A1.4}$$

$$\phi_4 = -\frac{igT_1}{\omega} e^{ik_1(x-b)} \frac{\cosh k_1(z+h_1)}{\cosh k_1 h_1} +$$

$$+ \sum_{n=2}^{\infty} -\frac{iT_n g}{\omega} e^{-\beta_n(x-b)} \frac{\cos \beta_n(z+h_1)}{\cos \beta_n h_1} \tag{A1.5}$$

where the incident spatial potential for a wave with amplitude a is given by

$$\phi_I = -\frac{iga}{\omega} e^{ik_1(x+b)} \frac{\cosh k_1(z+h_1)}{\cosh k_1 h_1} \tag{A1.6}$$

In region III the eigenvalues are given explicitly while in regions I, II and IV they are given implicitly by the dispersion relation. We have the following relations

$$k_1 \tanh k_1 h_1 = \nu \tag{A1.7a}$$
$$\alpha_n \tan \alpha_n h_1 = -\nu, \quad n=2,3,... \tag{A1.7b}$$

$$k_2 \tanh k_2 h_2 = \nu \tag{A1.8a}$$
$$\gamma_n \tan \gamma_n h_2 = -\nu, \quad n=2,3,... \tag{A1.8b}$$

$$\lambda_n = (n-1)\pi/(h_1-d), \quad n=1,2,3,... \tag{A1.9}$$

$$k_1 \tanh k_1 h_1 = \nu \tag{A1.10a}$$
$$\beta_n \tan \beta_n h_1 = -\nu, \quad n=2,3,... \tag{A1.10b}$$

where

$$\nu = \omega^2/g$$

The potentials given above describe the flow in the respective region and satisfy all boundary conditions except those at the common boundary. For example in region I the potential satisfies the linear free surface boundary condition, the impermeable bottom condition and the radiation condition when $x \to -\infty$.

The remaining problem is mainly to determine the five sets of unknown coefficents $\{(R_n, P_n, A_n, B_n, T_n), n=1,2,...\}$. The five sets are found by imposing the boundary conditions at the common boundaries. The requirements of continuity of pressure and normal velocity give the following conditions. At x=–b we get

$$\phi_1 = \phi_2 \ , \ -h_2 \le z \le 0 \tag{A1.11}$$

$$\phi_1 = \phi_3 \ , \ -h_1 \le z \le -d \tag{A1.12}$$

$$\frac{\partial \phi_1}{\partial x} = \begin{cases} \dfrac{\partial \phi_2}{\partial x} & , -h_2 \le z \le 0 \\ 0 & , -d \le z \le -h_2 \\ \dfrac{\partial \phi_3}{\partial x} & , -h_1 \le z \le -d \end{cases} \tag{A1.13}$$

and at x=b

$$\phi_3 = \phi_4 \ , \ -h_1 \le z \le -d \tag{A1.14}$$

$$\frac{\partial \phi_4}{\partial x} = \begin{cases} 0 & , -d \le z \le 0 \\ \dfrac{\partial \phi_3}{\partial x} & , -h_1 \le z \le -d \end{cases} \tag{A1.15}$$

The boundary conditions given above are satisfied over the z interval in a least square sense by multiplying each side of the boundary condition by a proper set of eigenfunctions and then by integrating them over the interval in question. Before we proceed with the evaluation of the matching integrals it is suitable to introduce some simplifications. Let

$$\alpha_1 = -ik_1$$
$$\gamma_1 = -ik_2$$
$$\beta_1 = -ik_1$$

and make use of the relation between the cosine function and the hyperbolic cosine function

$$\cos(-ix) = \cosh(x)$$

The potentials and the sets of eigenfunctions can then be written more comprehensively. Using the above mentioned simplifications, matching at the common boundaries is achieved with the integrals below.

Boundary condition 1 (A1.11):

$$\int_{-h_2}^{0} \phi_1 \{\cos \gamma_m (z+h_2), m=1,2,...\} dz = \int_{-h_2}^{0} \phi_2 \{\cos \gamma_m (z+h_2), m=1,2,...\} dz \tag{A1.16}$$

Boundary condition 2 (A1.12):

$$\int_{-h_1}^{-d} \phi_1 \{\cos \lambda_m (z+h_1), m=1,2, ...\} dz = \int_{-h_1}^{-d} \phi_3 \{\cos \lambda_m (z+h_1), m=1,2,...\} dz \tag{A1.17}$$

Boundary condition 3 (A1.13):

$$\int_{-h_1}^{0} \frac{\partial \phi_1}{\partial x} \{\cos \alpha_m (z+h_1),\ m=1,2,...\}dz =$$

$$= \int_{-h_1}^{0} \begin{Bmatrix} \frac{\partial \phi_2}{\partial x},\ -h_2 \le z \le 0 \\ 0\ ,\ -d \le z < -h_2 \\ \frac{\partial \phi_3}{\partial x},\ -h_1 \le z < -d \end{Bmatrix} \{\cos \alpha_m (z+h_1),\ m=1,2,..\}dz \qquad \text{(A1.18)}$$

Boundary condition 4 (A1.14):

$$\int_{-h_1}^{-d} \phi_3 \{\cos \lambda_m (z+h_1),\ m=1,2,...\}\ dz = \int_{-h_1}^{-d} \phi_4 \{\cos \lambda_m (z+h_1),\ m=1,2,...\}dz \qquad \text{(A1.19)}$$

Boundary condition 5 (A1.15):

$$\int_{-h_1}^{0} \frac{\partial \phi_4}{\partial x} \{\cos \beta_m (z+h_1),\ m=1,2,\ ..\}dz =$$

$$= \int_{-h_1}^{0} \begin{Bmatrix} 0\ ,\ -d \le z \le\ 0 \\ \\ \frac{\partial \phi_3}{\partial x},\ -h_1 \le z < -d \end{Bmatrix} \{\cos \beta_m (z+h_1),\ m=1,2,..\}dz \qquad \text{(A1.20)}$$

Furthermore, define two matching functions. The first function is defined as

$$E(\alpha_n, \beta_m, h_\alpha, h_\beta, z_1, z_2) = \int_{z_1}^{z_2} \cos \alpha_n(z+h_\alpha) \cos \beta_m(z+h_\beta)\, dz$$

$$= \left[\frac{\sin\,[(\alpha_n + \beta_m)z + \alpha_n h_\alpha + \beta_m h_\beta]}{2(\alpha_n + \beta_m)} + \right.$$

$$\left. \frac{\sin\,[(\alpha_n - \beta_m)z + \alpha_n h_\alpha - \beta_m h_\beta]}{2(\alpha_n - \beta_m)} \right]_{z_1}^{z_2} \qquad \text{(A1.21)}$$

where $\{\alpha_n,\ n=1,2,...\}$ and $\{\beta_m,\ m=1,2,...\}$ are two different sets of eigenvalues. The second matching function is defined as

$$N(\alpha_n, h_\alpha, z_1, z_2) = \int_{z_1}^{z_2} (\cos \alpha_n (z + h_\alpha))^2\, dz$$

$$= \begin{cases} z_2 - z_1\ , & \alpha_n = 0 \\ \frac{1}{2} \left[(z + h_\alpha) + \frac{\sin(2\alpha_n(z+h_\alpha))}{2\alpha_n} \right]_{z_1}^{z_2}\ , & \alpha_n \neq 0 \end{cases} \qquad \text{(A1.22)}$$

Now, rewrite the matching integrals, Eqs. (A1.16) to (A1.17) and introduce the matching functions (A1.21) and (A1.22). The following five sets of equations are then obtained:

Boundary condition 1:

$$\sum_{n=1}^{\infty} \left[\frac{R_n}{\cos\ \alpha_n h_1} E(\alpha_n, \gamma_m, h_1, h_2, -h_2, 0) \right] - \frac{P_m N(\gamma_m, h_2, -h_2, 0)}{\cos\ \gamma_m h_2} \cosh\ \gamma_m (e-b)$$

$$= - \frac{a\ E(\alpha_1, \gamma_m, h_1, h_2, -h_2, 0)}{\cos\ \alpha_1 h_1} \qquad \text{(A1.23)}$$

Boundary condition 2:

$$\sum_{n=1}^{\infty}\left[\frac{R_n}{\cos\ \alpha_n h_1}\,E(\alpha_n,\lambda_m,h_1,h_1,-h_1,-d)\right]-(\theta_m^{(1)}A_m e^{-\lambda_m b}+B_m e^{\lambda_m b})\,N(\lambda_m,h_1,-h_1,-d)$$
$$=-\frac{a\ E(\alpha_1,\lambda_m,h_1,h_1,-h_1,-d)}{\cos\ \alpha_1 h_1} \qquad \text{(A1.24)}$$

where

$$\theta_m^{(1)}=\begin{cases}-1, & m=1\\ 1, & m\geq 2\end{cases}$$

Boundary condition 3:

$$\sum_{n=1}^{\infty}\left[(\theta_n^{(2)}A_n e^{-\lambda_n b}-\lambda_n B_n e^{\lambda_n b})\,E(\lambda_n,\alpha_m,h_1,h_1,-h_1,-d)+\right.$$
$$\left.+P_n\frac{\gamma_n}{\cos\ \gamma_n h_2}\sinh\gamma_n(e-b)\,E(\gamma_n,\alpha_m,h_2,h_1,-h_2,0)\right]-$$
$$\frac{R_m\alpha_m}{\cos\ \alpha_m h_1}\,N(\alpha_m,h_1,-h_1,0)=-\theta_m^{(3)}a\,\alpha_m\frac{N(\alpha_m,h_1,-h_1,0)}{\cos\ \alpha_m h_1} \qquad \text{(A1.25)}$$

where

$$\theta_m^{(2)}=\begin{cases}\frac{1}{b}, & m=1\\ \lambda_m, & m\geq 2\end{cases}$$

$$\theta_m^{(3)}=\begin{cases}1, & m=1\\ 0, & m\geq 2\end{cases}$$

Boundary condition 4:

$$\sum_{n=1}^{\infty}\left[\frac{T_n E(\beta_n,\lambda_m,h_1,h_1,-h_1,-d)}{\cos\ \beta_n h_1}\right]-(A_m e^{\lambda_m b}+B_m e^{-\lambda_m b})\,N(\lambda_m,h_1,-h_1,-d)=0 \qquad \text{(A1.26)}$$

Boundary condition 5:

$$\sum_{n=1}^{\infty} \left[(\theta_n^{(2)} A_n e^{\lambda_n b} - \lambda_n B_n e^{-\lambda_n b}) E(\lambda_n,\beta_m,h_1,h_1,-h_1,-d) \right] + \frac{T_m \beta_m}{\cos \beta_m h_1} N(\beta_m,h_1,-h_1,0) = 0 \qquad \text{(A1.27)}$$

In order to find a solution, we must truncate the infinite series of orthogonal functions. Assume that N is the number of considered orthogonal functions. We then get a system of 5N complex equations and an equal number of unknown coefficients. Organizing the equations in matrices gives

$$\underline{\underline{S}}\,\underline{X} = \underline{F} \qquad \text{(A1.28)}$$

where

$$\underline{X} = (R_1,R_2,..,R_N, P_1,P_2,..,P_N, A_1,A_2,..,A_N, B_1,B_2,..,B_N, T_1,T_2,..,T_N)^T \qquad \text{(A1.29)}$$

Let the elements in the system matrix be denoted by S_{ji} and the elements in the right hand side matrix by F_j, where i,j = 1,2,...,5N. The elements in the two matrices are given by the boundary conditions as follows below, with local indices running according to n,m = 1,2,...,N.

Boundary condition 1:

$$S_{mn} = \frac{E(\alpha_n,\gamma_m,h_1,h_2,-h_2,0)}{\cos \alpha_n h_1} \qquad \text{(A1.30a)}$$

$$S_{m(N+m)} = -N(\gamma_m,h_2,-h_2,0) \frac{\cosh \gamma_m (e-b)}{\cos \gamma_m h_2} \qquad \text{(A1.30b)}$$

$$F_m = -\frac{aE(\alpha_1,\gamma_m,h_1,h_2,-h_2,0)}{\cos \alpha_1 h_1} \qquad \text{(A1.30c)}$$

Boundary condition 2:

$$S_{(N+m)n} = \frac{E(\alpha_n,\lambda_m,h_1,h_1,-h_1,-d)}{\cos\ \alpha_n h_1} \qquad \text{(A1.30d)}$$

$$S_{(N+m)(2N+m)} = -\theta_m^{(1)} e^{-\lambda_m b}\ N(\lambda_m,h_1,-h_1,-d) \qquad \text{(A1.30e)}$$

$$S_{(N+m)(3N+m)} = -e^{\lambda_m b}\ N(\lambda_m,h_1,-h_1,-d) \qquad \text{(A1.30f)}$$

$$F_{(N+m)} = -\frac{a\ E(\alpha_1,\lambda_m,h_1,h_1,-h_1,-d)}{\cos\ \alpha_1 h_1} \qquad \text{(A1.30g)}$$

Boundary condition 3:

$$S_{(2N+m)(2N+n)} = \theta_n^{(2)} e^{-\lambda_n b}\ E\ (\lambda_n,\alpha_m,h_1,h_1,-h_1,-d) \qquad \text{(A1.30h)}$$

$$S_{(2N+m)(3N+n)} = -\lambda_n\ e^{\lambda_n b}\ E(\lambda_n,\alpha_m,h_1,h_1,-h_1,-d) \qquad \text{(A1.30i)}$$

$$S_{(2N+m)(N+n)} = \frac{\gamma_n}{\cos\ \gamma_n h_2} \sinh\ \gamma_n\ (e-b)\ E(\gamma_n,\alpha_m,h_2,h_1,-h_2,0) \qquad \text{(A1.30j)}$$

$$S_{(2N+m)m} = -\frac{\alpha_m}{\cos\ \alpha_m h_1} N(\alpha_m,h_1,-h_1,0) \qquad \text{(A1.30k)}$$

$$F_{(2N+m)} = -\theta_m^{(3)}\ a\ \frac{\alpha_m}{\cos\ \alpha_m h_1} N(\alpha_m,h_1,-h_1,0) \qquad \text{(A1.30l)}$$

Boundary condition 4:

$$S_{(3N+m)(4N+n)} = \frac{E(\beta_n,\lambda_m,h_1,h_1,-h_1,-d)}{\cos\ \beta_n h_1} \qquad \text{(A1.30m)}$$

$$S_{(3N+m)(2N+m)} = -e^{\lambda_m b}\ N(\lambda_m,h_1,-h_1,-d) \qquad \text{(A1.30n)}$$

$$S_{(3N+m)(3N+m)} = -e^{-\lambda_m b}\ N(\lambda_m,h_1,-h_1,-d) \qquad \text{(A1.30o)}$$

$$F_{(3N+m)} = 0 \tag{A1.30p}$$

Boundary condition 5:

$$S_{(4N+m)(2N+n)} = \theta_n^{(2)} e^{\lambda_n b} E(\lambda_n,\beta_m,h_1,h_1,-h_1,-d) \tag{A1.30q}$$

$$S_{(4N+m)(3N+n)} = -\lambda_n e^{-\lambda_n b} E(\lambda_n,\beta_m,h_1,h_1,-h_1,-d) \tag{A1.30r}$$

$$S_{(4N+m)(4N+m)} = \frac{\beta_m}{\cos \beta_m h_1} N(\beta_m,h_1,-h_1,0) \tag{A1.30s}$$

$$F_{(4N+m)} = 0 \tag{A1.30t}$$

Solving the complex system of equations gives the unknown coefficients in the orthogonal series and thereby also the potentials in each respective region.

From the velocity potential in region I, Eq. (A1.2), it is seen that the orthogonal series consists of both a propagating component and a series of evanescent components. The evanescent components vanish far away from the structure. Hence, the amplitude of the reflected wave is given directly from the coefficient of the propagating component, i.e. R_1. Analogously, the amplitude of the transmitted wave is given by the coefficient of the harmonic component in region IV, i.e. T_1.

The forces caused by the waves are calculated by integration of the dynamic pressure given by the Bernoulli equation. In order to be consistent with the linear formulation the pressure is given by

$$p = -\rho \frac{\partial \phi}{\partial t} = i\omega\rho\phi e^{-i\omega t} \tag{A1.31}$$

Integration of the complex valued pressure gives the complex valued forces, including information of both amplitudes and phases.

The horizontal force:

$$F_1 = \rho g \sum_{n=1}^{N} (a\theta_n^{(3)} + R_n) \frac{\sin \alpha_n (h_1-h_2) - \sin \alpha_n(h_1-d)}{\alpha_n \cos \alpha_n h_1}$$

$$+ \rho g \sum_{n=1}^{N} P_n \frac{\tan \gamma_n h_2}{\gamma_n}$$

$$+ \rho g \sum_{n=1}^{N} T_n \frac{\sin \beta_n(h_1-d) - \sin \beta_n h_1}{\beta_n \cos \beta_n h_1} \qquad \text{(A1.32)}$$

The vertical force:

$$F_3 = \rho g \sum_{n=1}^{N} P_n \frac{\sin \gamma_n(e-b)}{\gamma_n \cos \gamma_n h_2}$$

$$+ \rho g \left[2B_1 b + \sum_{n=2}^{N} \frac{2}{\lambda_n} (A_n+B_n) \sinh \lambda_n b \cos \lambda_n(h_1-d)\right] \qquad \text{(A1.33)}$$

The moment about x=z=0:

$$F_5 = \rho g \sum_{n=1}^{N} \left[\frac{(a\theta_n^{(3)} + R_n)}{\cos \alpha_n h_1} \left(\frac{\cos \alpha_n(h_1-h_2) - \cos \alpha_n(h_1-d)}{\alpha_n^2} \right.\right.$$

$$\left.\left. - \frac{h_2 \sin \alpha_n(h_1-h_2) - d \sin \alpha_n(h_1-d)}{\alpha_n} \right) \right]$$

$$+ \rho g \sum_{n=1}^{N} \left[\frac{P_n}{\cos \gamma_n h_2} \left(\frac{\cos \gamma_n h_2 + \cosh \gamma_n(e-b) - 2}{\gamma_n^2} + \frac{b \sinh \gamma_n(e-b)}{\gamma_n} \right) \right]$$

$$- \rho g \left(\frac{2}{3} A_1 b^2 + \sum_{n=2}^{N} \left[\left((A_n - B_n) \frac{(\lambda_n b - 1)}{\lambda_n^2} e^{\lambda_n b} \right.\right.\right.$$

$$\left.\left.\left. + (A_n - B_n) \frac{(\lambda_n b + 1)}{\lambda_n^2} e^{-\lambda_n b} \right) \cos \lambda_n(h_1-d) \right] \right)$$

$$- \rho g \sum_{n=1}^{N} \left[\frac{T_n}{\cos \beta_n h_1} \left(\frac{\cos \beta_n h_1 - \cos \beta_n(h_1-d)}{\beta_n^2} + \frac{d \sin \beta_n(h_1-d)}{\beta_n} \right) \right] \quad \text{(A1.34)}$$

APPENDIX II

SOLUTION OF THE DIFFRACTION AND RADIATION PROBLEMS FOR A BREAKWATER WITH A RECTANGULAR CROSS SECTION

In the present appendix the method of separation of variables is used to solve both the diffraction problem, when the fixed structure is exposed to regular waves, and the radiation problem, when the structure is forced to move in the absence of waves.

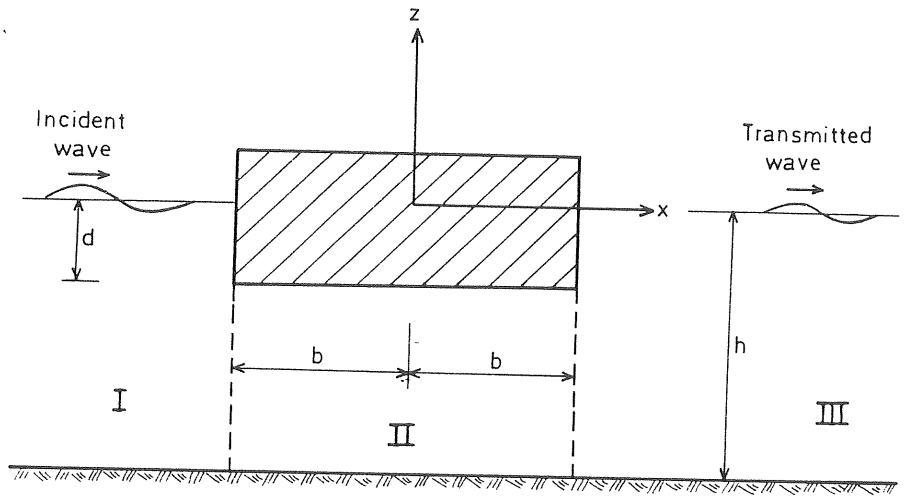

Figure A2.1 Definition of fluid regions and geometrical properties.

Solution of the diffraction problem gives the wave exciting forces in the horizontal and vertical directions as well as the wave exciting moment. Solution of the radiation problem in surge, heave and pitch gives the hydrodynamic coefficients, i.e. the added mass coefficients and the radiation damping coefficients. Once the diffraction problem and the radiation problems are solved the motions of the structure can be calculated as well as the reflection and transmission coefficients.

The solving procedure applied is basically the same as the one given in Appendix I. The difference between the diffraction problem and the radiation problem appears in the type of excitation applied. In the diffraction problem the excitation is caused by an incident propagating wave while in the radiation problem the excitation is introduced by

moving boundaries. If the motion of the structure is assumed to be small the boundary conditions for the radiation problem can be applied when the structure is in its equilibrium position. This assumption makes the mathematical formulation of the diffraction problem and the radiation problem quite similar, and in fact they differ only in terms of a non–homogeneous boundary condition. Owing to the mathematical similarities the solutions of the problems are presented together.

For the structure with a rectangular cross section the fluid domain is divided into three regions according to Figure A2.1.

The method of separation of variables is then applied in each region in order to obtain expressions for the unknown function, i.e. the velocity potential. Expressions valid in each respective region are obtained as infinite series of orthogonal functions. These expressions are developed to satisfy all boundary conditions except those at the common boundaries between the regions. It then remains to determine a number of unknown coefficients in the series. This is done by imposing the condition of continuity of pressure and normal velocity at the common boundary between the regions. Mathematically this is fulfilled by matching the potentials and the normal derivatives of the potentials respectively.

A formulation of the diffraction problem as well as the radiation problem for motions in surge, heave and pitch respectively is given below. The formulation starts from the potentials developed independently in each region.

Let

$$\Phi_j^{(l)}(x,z,t) = \mathrm{Re}\{\phi_j^{(l)}(x,z)\dot{x}_l\}, \quad \begin{matrix} j=1,2,3 \\ l=1,3,5,7 \end{matrix} \qquad \text{(A2.1)}$$

where $\dot{x}_l$ is the velocity of the l:th mode for the radiation problems and $e^{-i\omega t}$ for the diffraction problem.

Applying the method of separation of variables gives the complex valued spatial potentials in each region expressed in terms of orthogonal series as below

$$\phi_1^{(l)} = \phi_I^{(l)} - \frac{iR_{1g}}{\omega} e^{-ik(x+b)} \frac{\cosh k(z+h)}{\cosh kh} -$$

$$- \sum_{n=2}^{\infty} \frac{iR_{ng}}{\omega} e^{\alpha_n(x+b)} \frac{\cos \alpha_n(z+h)}{\cos \alpha_n h} \qquad \text{(A2.2)}$$

$$\phi_2^{(l)} = -\frac{igA_1 x}{\omega b} - \frac{igB_1}{\omega} + \sum_{n=2}^{\infty} -\frac{ig}{\omega}(A_n e^{\lambda_n x} + B_n e^{-\lambda_n x}) \cos \lambda_n(z+h) + \phi_{2p}^{(l)}$$

(A2.3a)

where the particular solution in region two is

$$\phi_{2p}^{(l)} = \begin{cases} 0 & , l = 1 \\ \dfrac{(z+h)^2 - x^2}{2(h-d)} & , l = 3 \\ -\dfrac{3x(z+h)^2 - x^3}{6(h-d)} & , l = 5 \\ 0 & , l = 7 \end{cases} \qquad \text{(A2.3b)}$$

$$\phi_3^{(l)} = -\frac{igT_1}{\omega} e^{ik(x-b)} \frac{\cosh k(z+h)}{\cosh kh} +$$

$$+ \sum_{n=2}^{\infty} -\frac{iT_{ng}}{\omega} e^{-\beta_n(x-b)} \frac{\cos \beta_n(z+h)}{\cos \beta_n h} \qquad \text{(A2.4)}$$

The incident spatial potential $\phi_I^{(l)} = 0$ except for l=7 when

$$\phi_I^{(7)} = -\frac{iga}{\omega} e^{ik(x+b)} \frac{\cosh k(z+h)}{\cosh kh} \qquad \text{(A2.5)}$$

In region II the eigenvalues are given explicitly while in regions I and III they are given implicitly by the dispersion relation. We have the following relations

$$k \tanh kh = \nu \qquad \text{(A2.6a)}$$

$$\alpha_n \tan \alpha_n h = -\nu, \quad n=2,3,... \qquad \text{(A2.6b)}$$

$$\lambda_n = (n-1)\pi/(h-d), \quad n=1,2,3,... \qquad \text{(A2.7)}$$

$$k \tanh kh = \nu \tag{A2.8a}$$

$$\beta_n \tan \beta_n h = -\nu, \quad n=2,3,... \tag{A2.8b}$$

where

$$\nu = \omega^2/g$$

The potentials given above describe the flow in each respective region and satisfy all boundary conditions except those at the common boundaries. For example in region I the potential satisfies the linear free surface boundary condition, the impermeable bottom condition and the radiation condition when $x \to -\infty$.

The remaining problem is mainly to determine the four sets of unknown coefficents $\{(R_n, A_n, B_n, T_n), n=1,2,...\}$. It should be pointed out that the units of the coefficients vary for different modes due to the definition of the spatial velocity potential made in Eq. A2.1. The four sets are found by imposing the boundary conditions at the common boundaries. The requirements of continuity of pressure and normal velocity give the following conditions. At x=–b we obtain

$$\phi_1^{(l)} = \phi_2^{(l)}, \quad -h \le z \le -d \tag{A2.9}$$

$$\frac{\partial \phi_1^{(l)}}{\partial x} = \begin{cases} V_2^{(l)}, & -d \le z \le 0 \\ \dfrac{\partial \phi_2^{(l)}}{\partial x}, & -h \le z \le -d \end{cases} \tag{A2.10a}$$

where $V_2^{(l)}$ is the moving boundary condition for the vertical wall at x=–b. This condition becomes

$$V_2^{(l)} = \begin{cases} 1, & l = 1 \\ 0, & l = 3 \\ z, & l = 5 \\ 0, & l = 7 \end{cases} \tag{A2.10b}$$

At x=b the matching conditions are

$$\phi_2^{(l)} = \phi_3^{(l)}, \quad -h \le z \le -d \tag{A2.11}$$

$$\frac{\partial \phi_3^{(l)}}{\partial x} = \begin{cases} V_4^{(l)}, & -d \le z \le 0 \\ \dfrac{\partial \phi_2^{(l)}}{\partial x}, & -h \le z \le -d \end{cases} \tag{A2.12a}$$

where $V_4^{(l)}$ is the moving boundary condition for the vertical wall at x=b. This condition becomes

$$V_4^{(l)} = \begin{cases} 1 \ , \ l = 1 \\ 0 \ , \ l = 3 \\ z \ , \ l = 5 \\ 0 \ , \ l = 7 \end{cases} \qquad \text{(A2.12b)}$$

The boundary conditions above are satisfied over the z interval in a least square sence by multiplying each side of the boundary condition by a proper set of eigenfunctions and then by integrating them over the interval in question. Before we proceed with the evaluation of the matching integrals it is suitable to introduce some simplifications. Let

$$\alpha_1 = -ik_1$$
$$\beta_1 = -ik_1$$

and make use of the relation between the cosine function and the hyperbolic cosine function

$$\cos(-ix) = \cosh(x)$$

Then, the potentials and the sets of eigenvalues can be written more comprehensively. Using the simplifications given above, matching at the common boundaries is achieved by the integrals below.

Boundary condition 1 (A2.9):

$$\int_{-h}^{-d} \phi_1^{(l)} \{\cos \lambda_m(z+h), m=1,2, ...\} \, dz = \int_{-h}^{-d} \phi_2^{(l)} \{\cos \lambda_m(z+h), m=1,2,...\} dz \qquad \text{(A2.13)}$$

Boundary condition 2 (A2.10):

$$\int_{-h}^{0} \frac{\partial \phi_1^{(l)}}{\partial x} \{\cos \alpha_m (z+h),\ m=1,2,\ldots\}dz =$$

$$= \int_{-h}^{0} \begin{cases} V_2^{(l)}, & -d \le z \le 0 \\ \dfrac{\partial \phi_2^{(l)}}{\partial x}, & -h \le z < -d \end{cases} \{\cos \alpha_m (z+h),\ m=1,2,..\}dz \qquad \text{(A2.14)}$$

Boundary condition 3 (A2.11):

$$\int_{-h}^{-d} \phi_2^{(l)} \{\cos \lambda_m (z+h),\ m=1,2,\ldots\}\ dz = \int_{-h}^{-d} \phi_3^{(l)} \{\cos \lambda_m (z+h),\ m=1,2,\ldots\}dz \qquad \text{(A2.15)}$$

Boundary condition 4 (A2.12):

$$\int_{-h}^{0} \frac{\partial \phi_3^{(l)}}{\partial x} \{\cos \beta_m (z+h),\ m=1,2,\ ..\}dz =$$

$$= \int_{-h}^{0} \begin{cases} V_4^{(l)}, & -d \le z \le 0 \\ \dfrac{\partial \phi_2^{(l)}}{\partial x}, & -h \le z < -d \end{cases} \{\cos \beta_m (z+h),\ m=1,2,..\}dz \qquad \text{(A2.16)}$$

Furthermore, define the following five matching functions,

$$E(\alpha_n, \beta_m, h_\alpha, h_\beta, z_1, z_2) = \int_{z_1}^{z_2} \cos \alpha_n(z+h_\alpha) \cos \beta_m(z+h_\beta)\, dz \qquad (A2.17)$$

$$N(\alpha_n, h_\alpha, z_1, z_2) = \int_{z_1}^{z_2} (\cos \alpha_n (z + h_\alpha))^2\, dz \qquad (A2.18)$$

$$G_1(\alpha_n, h_\alpha, z_1, z_2) \int_{z_1}^{z_2} (z + h_\alpha)^2 \cos \alpha_n (z + h_\alpha)\, dz \qquad (A2.19)$$

$$G_2(\alpha_n, h_\alpha, z_1, z_2) = \int_{z_1}^{z_2} z \cos \alpha_n (z + h_\alpha)\, dz \qquad (A2.20)$$

$$G_3(\alpha_n, h_\alpha, z_1, z_2,) = \int_{z_1}^{z_2} \cos \alpha_n (z + h_\alpha)\, dz \qquad (A2.21)$$

where $\{\alpha_n, n=1,2,...\}$ and $\{\beta_m, m=1,2,...\}$ are two different sets of eigenvalues.

Now, rewrite the matching integrals, Eqs. (A2.13) to (A2.16) and introduce the matching functions (A2.17) to (A2.21). The following four sets of equations are then obtained:

Boundary condition 1:

$$\sum_{n=1}^{\infty} \left[\frac{R_n}{\cos\ \alpha_n h} E(\alpha_n, \lambda_m, h, h, -h, -d) \right] - (\theta_m^{(1)} A_m e^{-\lambda_m b} + B e^{\lambda_m b})\, N(\lambda_m, h, -h, -d)$$

$$= \frac{i\omega}{g} H_{1m}^{(I)} \qquad (A2.22)$$

where

$$\theta_m^{(1)} = \begin{cases} -1, & m = 1 \\ 1, & m \geq 2 \end{cases}$$

$$H_{1m}^{(l)} = \begin{cases} 0 \ , & l=1 \\ \dfrac{G_1(\lambda_m, h, -h, -d) - b^2 G_3(\lambda_m, h, -h, -d)}{2(h-d)} \ , & l=3 \\ \dfrac{3bG_1(\lambda_m, h, -h, -d) - b^3 G_3(\lambda_m, h, -h, -d)}{6(h-d)} \ , & l=5 \\ \dfrac{iga}{\omega} \dfrac{E(\alpha_1, \lambda_m, h, h, -h, -d)}{\cos \alpha_1 h} \ , & l=7 \end{cases}$$

Boundary condition 2:

$$\sum_{n=1}^{\infty} \left[-(\theta_n^{(2)} A_n e^{-\lambda_n b} - \lambda_n B_n e^{\lambda_n b}) E(\lambda_n, \alpha_m, h, h-h, -d) \right] +$$

$$\frac{R_m \alpha_m}{\cos \alpha_m h} N(\alpha_m, h, -h, 0) = \frac{i\omega}{g} H_{2m}^{(l)} \qquad \text{(A2.23)}$$

where

$$\theta_m^{(2)} = \begin{cases} \dfrac{1}{b} \ , & m = 1 \\ \lambda_m, & m \geq 2 \end{cases}$$

$$\theta_m^{(3)} = \begin{cases} 1, & m = 1 \\ 0, & m \geq 2 \end{cases}$$

$$H_{2m}^{(l)} = \begin{cases} G_3(\alpha_m, h, -d, 0) & , l=1 \\ \dfrac{b}{h-d} G_3(\alpha_m, h, -h, -d) & , l=3 \\ G_2(\alpha_m, h, -d, 0) - \dfrac{G_1(\alpha_m, h, -h, -d) - b^2 G_3(\alpha_m, h, -h, -d)}{2(h-d)} & , l=5 \\ -\dfrac{ig}{\omega} \theta_m^{(3)} a\alpha_m \dfrac{N(\alpha_m, h, -h, 0)}{\cos \alpha_m h} & , l=7 \end{cases}$$

Furthermore, define the following five matching functions,

$$E(\alpha_n, \beta_m, h_\alpha, h_\beta, z_1, z_2) = \int_{z_1}^{z_2} \cos \alpha_n(z+h_\alpha) \cos \beta_m(z+h_\beta)\, dz \qquad (A2.17)$$

$$N(\alpha_n, h_\alpha, z_1, z_2) = \int_{z_1}^{z_2} (\cos \alpha_n (z + h_\alpha))^2\, dz \qquad (A2.18)$$

$$G_1(\alpha_n,h_\alpha,z_1,z_2 \int_{z_1}^{z_2} (z + h_\alpha)^2 \cos \alpha_n (z + h_\alpha)\, dz \qquad (A2.19)$$

$$G_2(\alpha_n,h_\alpha,z_1,z_2) = \int_{z_1}^{z_2} z \cos \alpha_n (z + h_\alpha)\, dz \qquad (A2.20)$$

$$G_3(\alpha_n,h_\alpha,z_1,z_2,) = \int_{z_1}^{z_2} \cos \alpha_n (z + h_\alpha)\, dz \qquad (A2.21)$$

where $\{\alpha_n, n=1,2,...\}$ and $\{\beta_m, m=1,2,...\}$ are two different sets of eigenvalues.

Now, rewrite the matching integrals, Eqs. (A2.13) to (A2.16) and introduce the matching functions (A2.17) to (A2.21). The following four sets of equations are then obtained:

Boundary condition 1:

$$\sum_{n=1}^{\infty}\left[\frac{R_n}{\cos\ \alpha_n h} E(\alpha_n,\lambda_m,h,h,-h,-d)\right] - (\theta_m^{(1)} A_m e^{-\lambda_m b} + B e^{\lambda_m b})\, N(\lambda_m,h,-h,-d)$$

$$= \frac{i\omega}{g} H_{1m}^{(I)} \qquad (A2.22)$$

where

$$\theta_m^{(1)} = \begin{cases} -1, & m = 1 \\ 1, & m \geq 2 \end{cases}$$

$$H_{1m}^{(l)} = \begin{cases} 0 \quad , & l=1 \\ \dfrac{G_1(\lambda_m, h, -h, -d) - b^2 G_3(\lambda_m, h, -h, -d)}{2(h-d)} & , l=3 \\ \dfrac{3bG_1(\lambda_m, h, -h, -d) - b^3 G_3(\lambda_m, h, -h, -d)}{6(h-d)} & , l=5 \\ \dfrac{iga}{\omega} \dfrac{E(\alpha_1, \lambda_m, h, h, -h, -d)}{\cos \alpha_1 h} & , l=7 \end{cases}$$

Boundary condition 2:

$$\sum_{n=1}^{\infty} \left[-(\theta_n^{(2)} A_n e^{-\lambda_n b} - \lambda_n B_n e^{\lambda_n b}) E(\lambda_n, \alpha_m, h, h-h, -d) \right] +$$

$$\frac{R_m \alpha_m}{\cos \alpha_m h} N(\alpha_m, h, -h, 0) = \frac{i\omega}{g} H_{2m}^{(l)} \qquad \text{(A2.23)}$$

where

$$\theta_m^{(2)} = \begin{cases} \dfrac{1}{b}, & m = 1 \\ \lambda_m, & m \geq 2 \end{cases}$$

$$\theta_m^{(3)} = \begin{cases} 1, & m = 1 \\ 0, & m \geq 2 \end{cases}$$

$$H_{2m}^{(l)} = \begin{cases} G_3(\alpha_m, h, -d, 0) & , l=1 \\ \dfrac{b}{h-d} G_3(\alpha_m, h, -h, -d) & , l=3 \\ G_2(\alpha_m, h, -d, 0) - \dfrac{G_1(\alpha_m, h, -h, -d) - b^2 G_3(\alpha_m, h, -h, -d)}{2(h-d)} & , l=5 \\ -\dfrac{ig}{\omega} \theta_m^{(3)} a\alpha_m \dfrac{N(\alpha_m, h, -h, 0)}{\cos \alpha_m h} & , l=7 \end{cases}$$

Boundary condition 3:

$$\sum_{n=1}^{\infty}\left[\frac{T_n E(\beta_n,\lambda_m,\ h,h,-h,-d)}{\cos\beta_n h}\right] - (A_m e^{\lambda_m b} + B_m e^{-\lambda_m b})\, N(\lambda_m,h,-h,-d) = \frac{i\omega}{g} H_{3m}^{(l)} \tag{A2.24}$$

where

$$H_{3m}^{(l)} = \begin{cases} 0 & , l = 1 \\ H_{1m}^{(l)} & , l = 3 \\ -H_{1m}^{(l)} & , l = 5 \\ 0 & , l = 7 \end{cases}$$

Boundary condition 4:

$$\sum_{n=1}^{\infty}\left[-(\theta_n^{(2)} A_n e^{\lambda_n b} - \lambda_n B_n e^{-\lambda_n b})\, E(\lambda_n,\beta_m,h,h,-h,-d)\right] - \frac{T_m\beta_m}{\cos\beta_m h} N(\beta_m,h,-h,0) = \frac{i\omega}{g} H_{4m}^{(l)} \tag{A2.25}$$

where

$$H_{4m}^{(l)} = \begin{cases} H_{2m}^{(l)} & , l = 1 \\ -H_{2m}^{(l)} & , l = 3 \\ H_{2m}^{(l)} & , l = 5 \\ 0 & , l = 7 \end{cases}$$

In order to find a solution we must truncate the infinite series of orthogonal functions. Assume that N is the number of orthogonal functions considered. We then get a system of 4N complex equations and an equal number of unknown coefficients. Organizing the equations in matrices gives

$$\underline{\underline{S}}\,\underline{X} = \underline{F} \qquad \text{(A2.26)}$$

where

$$\underline{X} = -\frac{i\,g}{\omega}\,(R_1,R_2,..,R_N,\ A_1,A_2,..,A_N,\ B_1,B_2,..,B_N,\ T_1,T_2,..,T_N)^T$$

Let the elements in the system matrix be denoted by S_{ij} and the elements in the right hand side matrix by F_j, where i,j = 1,2,..., 4N. The elements in the two matrices are given by the boundary conditions as follows below, with local indices running according to n,m = 1,2,..., N.

Boundary condition 1:

$$S_{mn} = \frac{E(\alpha_n,\lambda_m,h,\ h,-h,-d)}{\cos\,\alpha_n h} \qquad \text{(A2.27a)}$$

$$S_{m(N+m)} = -\,\theta_m^{(1)} e^{-\lambda_m b}\,N(\lambda_m,h,-h,-d) \qquad \text{(A2.27b)}$$

$$S_{m(2N+m)} = -\,e^{\lambda_m b}\,N(\lambda_m,h,-h,-d) \qquad \text{(A2.27fc}$$

$$F_m = H_{1m}^{(I)} \qquad \text{(A2.27d)}$$

Boundary condition 2:

$$S_{(N+m)(N+n)} = -\,\theta_n^{(2)} e^{-\lambda_n b}\,E\,(\lambda_n,\alpha_m,h,h,-h,-d) \qquad \text{(A2.27e)}$$

$$S_{(N+m)(2N+n)} = \lambda_n\,e^{\lambda_n b}\,E(\lambda_n,\alpha_m,h,h,-h,-d) \qquad \text{(A2.27f)}$$

$$S_{(N+m)m} = \frac{\alpha_m}{\cos\ \alpha_m h}\,N(\alpha_m,h,-h,0) \qquad \text{(A2.27g)}$$

$$F_{(N+m)} = H_{2m}^{(I)} \qquad \text{(A2.27h)}$$

Boundary condition 3:

$$S_{(2N+m)(3N+n)} = \frac{E(\beta_n,\lambda_m,h,h,-h,-d)}{\cos\ \beta_n h} \qquad \text{(A2.27i)}$$

$$S_{(2N+m)(N+m)} = -\,e^{\lambda_m b}\,N(\lambda_m,h,-h,-d) \qquad \text{(A2.27j)}$$

$$S_{(2N+m)(2N+m)} = -\,e^{-\lambda_m b}\,N(\lambda_m,h,-h,-d) \qquad \text{(A2.27k)}$$

$$F_{(2N+m)} = H_{3m}^{(l)} \qquad \text{(A2.27l)}$$

Boundary condition 4:

$$S_{(3N+m)(N+n)} = -\,\theta_n^{(2)}\,e^{\lambda_n b}\,E(\lambda_n,\beta_m,h,h,-h,-d) \qquad \text{(A2.27m)}$$

$$S_{(3N+m)(2N+n)} = \lambda_n\,e^{-\lambda_n b}\,E(\lambda_n,\beta_m,h,h,-h,-d) \qquad \text{(A2.27n)}$$

$$S_{(3N+m)(3N+m)} = -\,\frac{\beta_m}{\cos\ \beta_m h}\,N(\beta_m,h,-h,0) \qquad \text{(A2.27o)}$$

$$F_{(3N+m)} = H_{4m}^{(l)} \qquad \text{(A2.27p)}$$

Solving the complex system of equations gives the unknown coefficients in the orthogonal series and thereby also the potentials valid in each respective region.

The forces caused by the motion of the structure or the waves are calculated by integration of the dynamic pressure given by the Bernoulli equation. In order to be consistent with the linear formulation the pressure is given by

$$p^{(l)} = -\rho\,\frac{\partial \Phi^{(l)}}{\partial t} = i\omega\rho\phi^{(l)}\,\dot{x}_l \quad , l=1,3,5 \qquad \text{(A2.28)}$$

$$p^{(7)} = -\rho\,\frac{\partial \Phi^{(7)}}{\partial t} = i\omega\rho\phi^{(7)}\,e^{-i\omega t},\ l=7$$

Integration of the pressure over the wet surface of the structure gives forces and moments associated either with the diffraction problem or one of the radiation problems. Let us start with the diffraction problem.

Integration of the complex valued pressure gives the complex valued wave exciting forces including information of both amplitudes and phases.

The horizontal force:

$$F_1 = \rho g \sum_{n=1}^{N} (a\theta_n^{(3)} + R_n - T_n) \frac{\sin \alpha_n h - \sin \alpha_n(h-d)}{\alpha_n \cos \alpha_n h} \tag{A2.29}$$

The vertical force:

$$F_3 = \rho g \left[2B_1 b + \sum_{n=2}^{N} \frac{2}{\lambda_n} (A_n + B_n) \sinh \lambda_n b \cos \lambda_n (h-d) \right] \tag{A2.30}$$

The moment about x=z=0:

$$F_5 = \rho g \sum_{n=1}^{N} \left[\frac{(a\theta_n^{(3)} + R_n - T_n)}{\cos \alpha_n h} \left(\frac{\cos \alpha_n h - \cos \alpha_n (h-d)}{\alpha_n^2} + \frac{d \sin \alpha_n (h-d)}{\alpha_n} \right) \right]$$

$$- \rho g \left(\frac{2}{3} A_1 b^2 + \sum_{n=2}^{N} \left[(A_n - B_n) \frac{(\lambda_n b - 1)}{\lambda_n^2} e^{\lambda_n b} \right. \right.$$

$$\left. \left. + (A_n - B_n) \frac{(\lambda_n b + 1)}{\lambda_n^2} e^{-\lambda_n b} \right) \cos \lambda_n (h-d) \right] \right) \tag{A2.31}$$

The hydrodynamic reaction force associated with the radiation problem can be written as one part proportional to the acceleration of the structure and one part porportional to the velocity as follows:

$$F_j = - a_{jl} \ddot{x}_l - b_{jl} \dot{x}_l \tag{A2.32}$$

The coefficients introduced, a_{jl} and b_{jl}, are the added mass and radiation damping coefficients respectively. Integration of the pressure associated with the radiation problems yields expressions for the hydrodynamic coefficients a_{jl} and b_{jl} presented below.

The surge radiation problem:

$$a_{11} + \frac{ib_{11}}{\omega} = -\frac{i\rho g}{\omega}\sum_{n=1}^{N}(R_n - T_n)\frac{\sin\alpha_n h - \sin\alpha_n(h-d)}{\alpha_n \cos\alpha_n h} \qquad \text{(A2.33)}$$

$$a_{51} + \frac{ib_{51}}{\omega} = -\frac{i\rho g}{\omega}\sum_{n=1}^{N}\left[\frac{R_n - T_n}{\cos\alpha_n h}\left(\frac{\cos\alpha_n h - \cos\alpha_n(h-d)}{\alpha_n^2} + \frac{d\sin\alpha_n(h-d)}{\alpha_n}\right)\right]$$

$$+\frac{i\rho g}{\omega}\left(\frac{2}{3}A_1 b^2 + \sum_{n=2}^{N}\left[\left((A_n - B_n)\frac{(\lambda_n b-1)}{\lambda_n^2}e^{\lambda_n b}\right.\right.\right.$$

$$\left.\left.\left. + (A_n - B_n)\frac{(\lambda_n b+1)}{\lambda_n^2}e^{-\lambda_n b}\right)\cos\lambda_n(h-d)\right]\right) \qquad \text{(A2.34)}$$

The heave radiation problem:

$$a_{33} + \frac{ib_{33}}{\omega} = -\frac{i\rho g}{\omega}\left[2B_1 b + \sum_{n=2}^{N}\frac{2}{\lambda_n}(A_n + B_n)\sinh\lambda_n b\cos\lambda_n(h-d)\right]$$

$$+\rho\frac{3(h-d)^2 b - b^3}{3(h-d)} \qquad \text{(A2.35)}$$

The pitch radiation problem:

$$a_{55} + \frac{ib_{55}}{\omega} = -\frac{i\rho g}{\omega}\sum_{n=1}^{N}\left[\frac{R_n - T_n}{\cos\ \alpha_n h}\left(\frac{\cos\ \alpha_n h\ -\ \cos\ \alpha_n(h-d)}{\alpha_n^2} + \frac{d\ \sin\ \alpha_n(h-d)}{\alpha_n}\right)\right]$$

$$+\frac{i\rho g}{\omega}\left(\frac{2}{3}A_1 b^2 + \sum_{n=2}^{N}\left[\left((A_n - B_n)\frac{(\lambda_n b-1)}{\lambda_n^2}e^{\lambda_n b}\right.\right.\right.$$

$$\left.\left.\left. + (A_n - B_n)\frac{(\lambda_n b+1)}{\lambda_n^2}e^{-\lambda_n b}\right)\cos\ \lambda_n(h-d)\right]\right) + \rho\frac{5(h-d)^2 b^3 - b^5}{15(h-d)} \qquad \text{(A2.36)}$$

$$a_{15} + \frac{ib_{15}}{\omega} = -\frac{i\rho g}{\omega}\sum_{n=1}^{N}(R_n - T_n)\frac{\sin\ \alpha_n h\ -\ \sin\ \alpha_n(h-\ d)}{\alpha_n\ \cos\ \alpha_n h} \qquad \text{(A2.37)}$$

If we are interested in the diffraction forces but not in the reflected and transmitted waves, it is possible to use the radiation solutions to obtain the diffraction forces. This is a consequence of Green's second identity and the applied boundary conditions. It is usually called the Haskind relation, see Newman (1962). Making use of the relation we obtain the following expression for the diffraction forces:

$$F_l = -\frac{\rho g^2 a}{\omega} k R_1^{(l)} \frac{h\left(1 + \frac{\sinh\ 2kh}{2kh}\right)}{(\cosh\ kh)^2}\ ,\ l=1,3,5 \qquad \text{(A2.38)}$$

When the diffraction problem and the radiation problems are solved we can apply Newton's second law to calculate the motions of the structure caused by the waves. Substituting the wave exciting forces and the hydrodynamic reaction forces into Newton's law gives the following form of the equation of motion:

$$\sum_{j=1,3,5}\left[-\omega^2(m_{ij} + a_{ij}) - i\omega b_{ij} + c_{ij}\right]x_j = F_i\ ,\ i=1,3,5 \qquad \text{(A2.39)}$$

where

x_j is the complex valued motion of the structure in the j:th mode of motion and m_{ij}, a_{ij}, b_{ij}, c_{ij} are elements in the mass, added mass, radiation damping and hydrostatic matrix, respectively.

All non–zero elements in the mass matrix and the hydrostatic matrix are given below

$$m_{11} = m_{33} = m$$
$$m_{15} = m_{51} = mz_G$$
$$m_{55} = mr_p^2$$
$$c_{33} = \rho g 2b$$
$$c_{55} = \rho g \forall z_B - mgz_G + \rho g J$$

where

m = mass of structure
z_G = z–coordinate of centre of gravity
r_p = pitch radius of gyration
$\forall$ = volume displaced by structure
z_B = z–coordinate of center of buoyancy
J = moment of inertia of the water plane area

Solution of Eq. (2.39) gives the complex valued motion in surge, heave, and pitch including both information on amplitudes and phases.

APPENDIX III

SOLUTION OF THE DIFFRACTION AND RADIATION PROBLEMS FOR A BREAKWATER WITH A CROSS SECTION OF GENERAL SHAPE.

In the present appendix the diffraction problem and the radiation problems are solved for a breakwater with a cross section of general shape. The formulation also allows the water depth to vary in the vicinity of the cylinder.

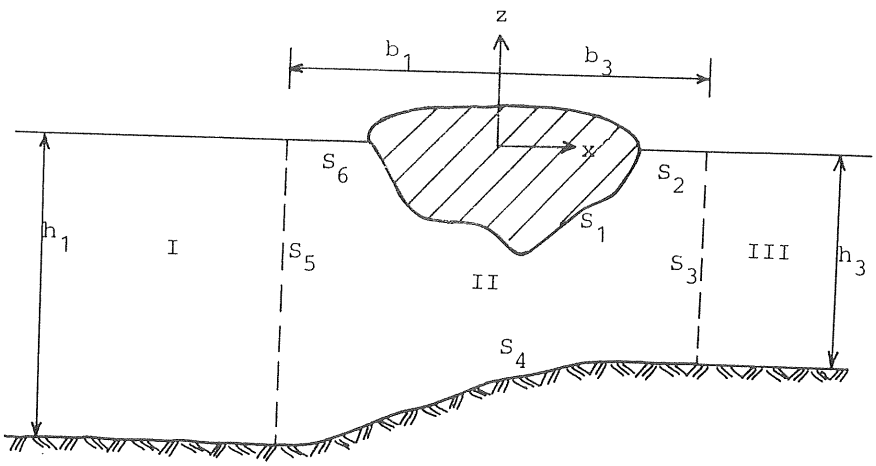

Figure A3.1 Definition of fluid regions.

The method used is an integral equation method based on Green's theorem. The integral equation is applied to a fluid region close to the cylinder (region II), see Figure A3.1. Outside this region, at each side, the water depth is assumed to be constant. Series solutions are developed in the outer regions and subsequently introduced in the integral equation as boundary conditions. The series solutions are simply obtained by separating the variables in the respective region.

Let

$$\Phi_j^{(l)}(x,z,t) = \mathrm{Re}\{\phi_j^{(l)}(x,z)\dot{x}_l\}, \quad \begin{matrix} j = 1,2,3 \\ l = 1,3,5,7 \end{matrix} \qquad \text{(A3.1)}$$

where

$\dot{x}_l$ is the velocity of the l:th mode for the radiation problems and $e^{-i\omega t}$ for the diffraction problem.

The complex valued spatial velocity potential in region I and region III are then obtained as

$$\phi_1^{(l)} = \phi_I^{(l)} - \frac{iR_1 g}{\omega} e^{-ik_1(x+b_1)} \frac{\cosh k_1(z+h_1)}{\cosh k_1 h_1} - \\ - \sum_{n=2}^{\infty} \frac{iR_n g}{\omega} e^{\alpha_n(x+b_1)} \frac{\cos \alpha_n(z+h_1)}{\cos \alpha_n h_1} \qquad \text{(A3.2)}$$

$$\phi_3^{(l)} = -\frac{igT_1}{\omega} e^{ik_3(x-b_3)} \frac{\cosh k_3(z+h_3)}{\cosh k_3 h_3} + \\ + \sum_{n=2}^{\infty} -\frac{iT_n g}{\omega} e^{-\beta_n(x-b_3)} \frac{\cos \beta_n(z+h_3)}{\cos \beta_n h_3} \qquad \text{(A3.3)}$$

where the incident spatial potential $\phi_I^{(l)} = 0$ for $l = 1,\ 3,\ 5$ and

$$\phi_I^{(7)} = -\frac{iga}{\omega} e^{ik_1(x+b_1)} \frac{\cosh k_1(z+h_1)}{\cosh k_1 h_1} \qquad \text{(A3.4)}$$

where a is the amplitude of the incident wave. In regions I and III the eigenvalues are given implicitly by the dispersion relation.

$$k_1 \tanh k_1 h_1 = \nu \qquad \text{(A3.5a)}$$
$$\alpha_n \tan \alpha_n h_1 = -\nu, \quad n=2,3,... \qquad \text{(A3.5b)}$$

$$k_3 \tanh k_3 h_3 = \nu \qquad \text{(A3.6a)}$$
$$\beta_n \tan \beta_n h_3 = -\nu, \quad n=2,3,... \qquad \text{(A3.6b)}$$

where

$\nu = \omega^2/g$

The potentials above describe the flow in the respective region and satisfy all boundary conditions except those at the boundaries to region II. For example in region I the potential satisfies the linear free surface boundary condition, the impermeable bottom condition and the radiation condition when $x \to -\infty$.

Let us continue the formulation of the problem letting the potential in region II, ϕ_2, be expressed in terms of potentials of 2D–sources according to Green's theorem. The potential of a field point (P) inside the fluid region is then given by

$$2\pi\phi_2(P) = \int_S \left[\phi_2 \frac{\partial}{\partial n} \ln r - \frac{\partial \phi_2}{\partial n} \ln r \right] ds \qquad \text{(A3.7)}$$

where S is the line enclosing the fluid region II and

$$r = ((x - \xi)^2 + (z - \zeta)^2)^{1/2}$$

is the distance from the source point $Q = (\xi,\zeta)$ to the field point $P = (x,z)$. Let the field point coincide with the closed boundary S. The Green's theorem then slightly changes and becomes

$$\pi\phi_2(P) = \int_S \left[\phi_2 \frac{\partial}{\partial n} \ln r - \frac{\partial \phi_2}{\partial n} \ln r \right] ds \qquad \text{(A3.8)}$$

Before we solve Eq. (A3.8) let us introduce the different conditions along the boundary S enclosing the fluid region II. They are

$$\frac{\partial \phi_2}{\partial n} = V_n^{(l)} \quad , \quad \text{at } S_1 \qquad \text{(A3.9a)}$$

$$V_n^{(l)} = \begin{cases} n_x & , l = 1 \\ n_z & , l = 3 \\ -(xn_z - (z - z_c)n_x), & l = 5 \\ 0 & , l = 7 \end{cases}$$

$$\frac{\partial \phi_2}{\partial n} = \frac{\omega^2}{g} \phi_2 \quad , \text{ at } S_2 \text{ and } S_6 \qquad \text{(A3.9b)}$$

$$\left.\begin{aligned}\phi_2 &= \phi_3 \\ \frac{\partial\phi_2}{\partial n} &= \frac{\partial\phi_3}{\partial n}\end{aligned}\right\}, \text{ at } S_3 \qquad \text{(A3.9c)}$$

$$\frac{\partial\phi_2}{\partial n} = 0 \quad , \text{ at } S_4 \qquad \text{(A3.9d)}$$

$$\left.\begin{aligned}\phi_2 &= \phi_1 \\ \frac{\partial\phi_2}{\partial n} &= \frac{\partial\phi_1}{\partial n}\end{aligned}\right\}, \text{ at } S_5 \qquad \text{(A3.9e)}$$

By substituting the boundary conditions above into the integral equation we obtain

$$\pi\phi_2(P) = \int_{S_1}\left[\phi_2\frac{\partial}{\partial n}(\ln r) - V_n \ln r\right] dS + \int_{S_2}\phi_2\left[\frac{\partial}{\partial n}(\ln r) - \frac{\omega^2}{g}\ln r\right] dS$$

$$+ \int_{S_3}\left[\phi_3\frac{\partial}{\partial n}(\ln r) - \frac{\partial\phi_3}{\partial n}\ln r\right] dS$$

$$+ \int_{S_4}\phi_2\frac{\partial}{\partial n}(\ln r)\, dS + \int_{S_5}\left[\phi_1\frac{\partial}{\partial n}(\ln r) - \frac{\partial\phi_1}{\partial n}\ln r\right] dS$$

$$\int_{S_6}\phi_2\left[\frac{\partial}{\partial n}(\ln r) - \frac{\omega^2}{g}\ln r\right] dS \qquad \text{(A3.10)}$$

The integral equation above is solved numerically by discretising the boundary S into elements according to Figure A3.2.

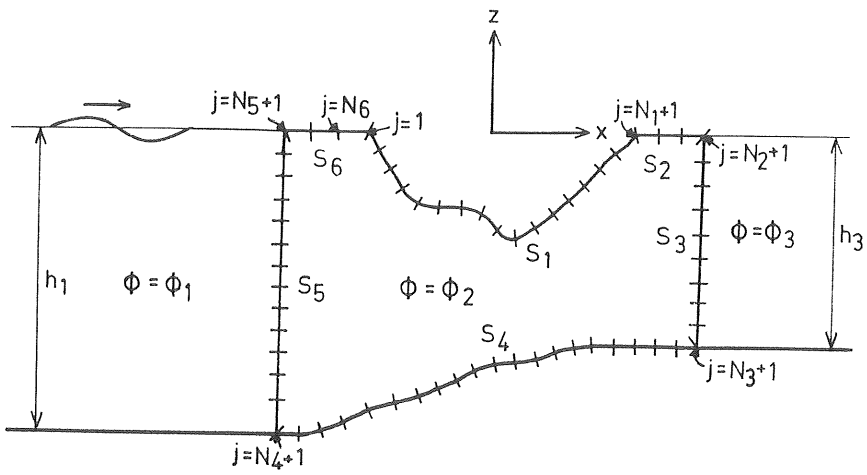

Figure A3.2 Discretisation of boundary enclosing region II.

Assuming the velocity potentials ϕ_1, ϕ_2, ϕ_3 and ϕ_I to be constant over the elements, the integral equation can be written in a discretised form

$$\pi\phi_2(P) = \sum_{S_1}\left[\phi_2(Q)\int_{\Delta S}\frac{\partial}{\partial n}(\ln r) - V_n(Q)\int \ln r\right]ds$$

$$+ \sum_{S_2}\phi_2(Q)\left[\int_{\Delta S}\frac{\partial}{\partial n}(\ln r)dS - \frac{\omega^2}{g}\int_{\Delta S}\ln r\, dS\right]$$

$$+ \sum_{S_3}\left[\phi_3(Q)\int_{\Delta S}\frac{\partial}{\partial n}(\ln r)dS - \frac{\partial\phi_3}{\partial n}(Q)\int_{\Delta S}\ln r\, dS\right]$$

$$+ \sum_{S_4}\phi_2(Q)\int_{\Delta S}\frac{\partial}{\partial n}(\ln r)\, dS$$

$$+ \sum_{S_5}\left[\phi_1(Q)\int_{\Delta S}\frac{\partial}{\partial n}(\ln r)dS - \frac{\partial\phi_1}{\partial n}(Q)\int_{\Delta S}\ln r\, dS\right]$$

$$+ \sum_{S_6} \phi_2(Q) \left[\int_{\Delta S} \frac{\partial}{\partial n}(\ln r)\,dS - \frac{\omega^2}{g} \int_{\Delta S} \ln r\, dS \right] \qquad (A3.11)$$

If we now apply Eq. (A3.11) to calculate the unknown velocity potential $\phi_2(P)$ for the midpoint of each element we get N equations where N is the number of elements. If we assume that the number of components included in the series solutions in region I and region III is truncated at the same number as the number of elements at boundaries S_3 and S_5 respectively, the number of unknown will equal the number of equations. Let us organise the system of equations in matrices using the notation

$$\underline{\underline{S}}\,\underline{X} = \underline{F} \qquad (A3.12)$$

where the elements of the unknown matrix are

$$x_j = \begin{cases} \phi_{2j} & ,j = (1, N_2),(N_3+1, N_4),(N_5+1, N_6) \\ T_j\text{-}N_2 & ,j = N_2+1, N_3 \\ R_j\text{-}N_4 & ,j = N_4+1, N_5 \end{cases} \qquad (A3.13)$$

Define the following integrals

$$E_{ij} = \int_{(\xi,\zeta)_j}^{(\xi,\zeta)_{j+1}} \ln r\, dS \qquad (A3.14a)$$

$$\bar{E}_{ij} = \int_{(\xi,\zeta)_j}^{(\xi,\zeta)_{j+1}} \frac{\partial}{\partial n}(\ln r)\, dS \qquad (A3.14b)$$

and the following functions

$$C_{ni} = -\frac{ig}{\omega} \frac{\cos \alpha_n(z_i + h_1)}{\cos \alpha_n h_1} \qquad (A3.15a)$$

$$\bar{C}_{ni} = \frac{ig}{\omega} \alpha_n \frac{\cos \alpha_n(z_i + h_1)}{\cos \alpha_n h_1} \qquad (A3.15b)$$

$$D_{ni} = -\frac{ig}{\omega} \frac{\cos \beta_n(z_i + h_3)}{\cos \beta_n h_3} \qquad (A3.15c)$$

$$\bar{D}_{ni} = \frac{ig}{\omega}\beta_n \frac{\cos\beta_n(z_i + h_3)}{\cos\beta_n h_3} \qquad \text{(A3.15d)}$$

$$\theta^{(1)}_{ij} = \begin{cases} 1 & \text{if } \begin{cases} 1\le i\le N_2 \text{ or } N_3+1\le i\le N_4 \text{ or } N_5+1\le i\le N_6 \\ i=j \end{cases} \\ 0 & \text{else} \end{cases} \qquad \text{(A3.16a)}$$

$$\theta^{(2)}_{ij} = \begin{cases} 1 & \text{if } N_2+1\le i,\ j\le N_3 \\ 0 & \text{else} \end{cases} \qquad \text{(A3.16b)}$$

$$\theta^{(3)}_{ij} = \begin{cases} 1 & \text{if } N_4+1\le i,\ j\le N_5 \\ 0 & \text{else} \end{cases} \qquad \text{(A3.16c)}$$

Using the definitions given above, the elements of the system matrix are

$$S_{ij} = -\pi\left[\theta^{(1)}_{ij} + \theta^{(2)}_{ij} D_{(j-N_2)i} + \theta^{(3)}_{ij} C_{(j-N_4)i}\right] + \qquad \text{(A3.17)}$$

$$\begin{cases} \bar{E}_{ij}\ , & 1\le j\le N_1 \\ \bar{E}_{ij} - \dfrac{\omega^2}{g} E_{ij}\ , & \begin{cases} N_1+1\le j\le N_2 \\ N_5+1\le j\le N_6 \end{cases} \\ \displaystyle\sum_{n=N_2+1}^{N_3}\left[D_{(j-N_2)n}\,\bar{E}_{in} - \bar{D}_{(j-N_2)n}E_{in}\right], & N_2+1\le j\le N_3 \\ \bar{E}_{ij}\ , & N_3+1\le j\le N_4 \\ \displaystyle\sum_{n=N_4+1}^{N_5}\left[C_{(j-N_4)n}\,\bar{E}_{in} - \bar{C}_{(j-N_4)n}\,E_{in}\right], & N_4+1\le j\le N_5 \end{cases}$$

Finally, the elements of the exciting matrix become

$$F_i = \left[\pi C_{1i} - \sum_{n=N_4+1}^{N_5}(C_{1n}\bar{E}_{in} + \bar{C}_{1n}E_{in})\right] a^{(l)} + \sum_{k=1}^{N_1} V^{(l)}_{nk} E_{ik} \qquad \text{(A3.18)}$$

Solving the system of complex equations, (A3.12), gives the unknown velocity potential along boundaries S_1, S_2, S_4 and S_6 directly while at S_3 and S_5 it can be calculated using the series solutions Eq. (A3.3) and Eq. (A3.2), respectively.

Once the velocity potential is known the desired quantities such as wave exciting forces added masses, potential damping, wave pattern, and motions are calculated in a straightforward way following the equations given in Chapter 2.

CHALMERS TEKNISKA HÖGSKOLA
Institutionen för vattenbyggnad

Report Series A

A:1 Bergdahl, L.: Physics of ice and snow as affects thermal pressure. 1977.

A:2 Bergdahl, L.: Thermal ice pressure in lake ice covers. 1978.

A:3 Häggström, S.: Surface Discharge of Cooling Water. Effects of Distortion in Model Investigations. 1978.

A:4 Sellgren, A.: Slurry Transportation of Ores and Industrial Minerals in a Vertical Pipe by Centrifugal Pumps. 1978.

A:5 Arnell, V.: Description and Validation of the CTH–Urban Runoff Model. 1980.

A:6 Sjöberg, A.: Calculation of Unsteady Flows in Regulated Rivers and Storm Sewer Systems. 1976.

A:7 Svensson, T.: Water Exchange and Mixing in Fjords. Mathematical Models and Field Studies in the Byfjord. 1980.

A:8 Arnell, V.: Rainfall Data for the Design of Sewer Pipe Systems. 1982.

A:9 Lindahl, J., Sjöberg, A.: Dynamic Analysis of Mooring Cables. 1983.

A:10 Nilsdal, J–A.: Optimeringsmodellen ILSD. Beräkning av topografins inverkan på ett dagvattensystems kapacitet och anläggningskostnad. 1983.

A:11 Lindahl, J.: Implicit numerisk lösning av rörelseekvationerna för en förankringskabel. 1984.

A:12 Lindahl, J.: Modellförsök med en förankringskabel. 1985.

A:13 Lyngfelt, S.: On Urban Runoff Modelling. The Application of Numerical Models Based on the Kinematic Wave Theory. 1985.

A:14 Johansson, M.: Transient Motions of Large Floating Structures. 1986.

A:15 Mårtensson, N., Bergdahl, L.: On the Wave Climate of the Southern Baltic. 1987.

A:16 Moberg, G.: Wave Forces on a Vertical Slender Cylinder. 1988.

A:17 Perrusquía González, G.S.: Part–Full Flow in Pipes with a Sediment Bed. Part one: Bedform dimensions. Part two: Flow resistance. 1988.

A:18 Nilsdal, J–A.: Bedömning av översvämningsrisken i dagvattensystem. Kontrollberäkning med typregn. 1988.

A:19 Johansson, M.: Barrier–Type Breakwaters. Transmission, Reflection and Forces. 1989.

A:20 Rankka, W.: Estimating the Time to Fatigue Failure of Mooring Cables. 1989.

CHALMERS TEKNISKA HÖGSKOLA
Institutionen för vattenbyggnad

Report Series B

B:1 Bergdahl, L.: Beräkning av vågkrafter. (Ersatts med 1979:07) 1977.

B:2 Arnell, V.: Studier av amerikansk dagvattenteknik. 1977.

B:3 Sellgren, A.: Hydraulic Hoisting of Crushed Ores. A feasibility study and pilot–plant investigation on coarse iron ore transportation by centrifugal pumps. 1977.

B:4 Ringesten, B.: Energi ur havsströmmar. 1977.

B:5 Sjöberg, A., Asp, T.: Brukar–anvisning för ROUTE–S. En matematisk modell för beräkning av icke–stationära flöden i floder och kanaler vid strömmande tillstånd. 1977.

B:6 Annual Report 1976/77. 1977.

B:7 Bergdahl, L., Wernersson, L.: Calculated and Expected Thermal Ice Pressures in Five Swedish Lakes. 1977.

B:8 Göransson, C–G., Svensson, T.: Drogue Tracking – Measuring Principles and Data Handling. 1977.

B:9 Göransson, C–G.: Mathematical Model of Sewage Discharge into confined, stratified Basins – Especially Fjords. 1977.

B:10 Arnell, V., Lyngfelt, S.: Beräkning av dagvattenavrinning från urbana områden. 1978.

B:11 Arnell, V.: Analysis of Rainfall Data for Use in Design of Storm Sewer Systems. 1978.

B:12 Sjöberg, A.: On Models to be used in Sweden for Detailed Design and Analysis of Storm Drainage Systems. 1978.

B:13 Lyngfelt, S.: An Analysis of Parameters in a Kinematic Wave Model of Overland Flow in Urban Areas. 1978.

B:14 Sjöberg, A., Lundgren, J., Asp, T., Melin, H.: Manual för ILLUDAS (Version S2). Ett datorprogram för dimensionering och analys av dagvattensystem. 1979.

B:15 Annual Report 1978/79. 1979.

B:16 Nilsdal, J–A., Sjöberg, A.: Dimensionerande regn vid höga vattenstånd i Göta älv. 1979.

B:17 Stöllman, L–E.: Närkes Svartå. Hydrologisk inventering. 1979.

B:18 Svensson, T.: Tracer Measurements of Mixing in the Deep Water of a Small, Stratified Sill Fjord. 1979.

B:19 Svensson, T., Degerman, E., Jansson, B.,Westerlund, S.: Energiutvinning ur sjö– och havssediment. En förstudie. R76:1980. 1979.

B:20 Annual Report 1979. 1980.

B:21 Stöllman, L–E.: Närkes Svartå. Inventering av vattentillgång och vattenanvändning. 1980.

Report Series B

B:22 Häggström, S., Sjöberg, A.: Effects of Distortion in Physical Models of Cooling Water Discharge. 1979.

B:23 Sellgren, A.: A Model for Calculating the Pumping Cost of Industrial Slurries. 1981.

B:24 Lindahl, J.: Rörelseekvationen för en kabel. 1981.

B:25 Bergdahl, L., Olsson, G.: Konstruktioner i havet. Vågkrafter–rörelser. En inventering av datorprogram. 1981.

B:26 Annual Report 1980. 1981.

B:27 Nilsdal, J–A.: Teknisk–ekonomisk dimensionering av avloppsledningar. En litteraturstudie om datormodeller. 1981.

B:28 Sjöberg, A.: The Sewer Network Models DAGVL–A and DAGVL–DIFF. 1981.

B:29 Moberg, G.: Anläggningar för oljeutvinning till havs. Konstruktionstyper, dimensioneringskriterier och positioneringssystem. 1981.

B:30 Sjöberg, A., Bergdahl, L.: Förankringar och förankringskrafter. 1981.

B:31 Häggström, S., Melin, H.: Användning av simuleringsmodellen MITSIM vid vattenresursplanering för Svartån. 1982.

B:32 Bydén, S., Nielsen, B.: Närkes Svartå. Vattenöversikt för Laxå kommun. 1982.

B:33 Sjöberg, A.: On the stability of gradually varied flow in sewers. 1982.

B:34 Bydén, S., Nyberg, E.: Närkes Svartå. Undersökning av grundvattenkvalitet i Laxå kommun. 1982.

B:35 Sjöberg, A., Mårtensson, N.: Regnenveloppmetoden. En analys av metodens tillämplighet för dimensionering av ett 2–års perkolationsmagasin. 1982.

B:36 Svensson, T., Sörman, L–O.: Värmeupptagning med bottenförlagda kylslangar i stillastående vatten. Laboratorieförsök. 1982.

B:37 Mattsson, A.: Koltransporter och kolhantering. Lagring i terminaler och hos storförbrukare. (Delrapport). 1983.

B:38 Strandner, H.: Ett datorprogram för sammankoppling av ILLUDAS och DAGVL–DIFF. 1983.

B:39 Svensson, T., Sörman, L–O.: Värmeupptagning med bottenförlagda slangar i rinnande vatten. Laboratorieförsök. 1983.

B:40 Mattsson, A.: Koltransporter och kolhantering. Lagring i terminaler och hos storförbrukare. Kostnader. Delrapport 2. 1983.

B:41 Häggström, S., Melin, H.: Närkes Svartå. Simuleringsmodellen MITSIM för kvantitativ analys i vattenresursplanering. 1983.

B:42 Hård, S.: Seminarium om miljöeffekter vid naturvärmesystem. Dokumentation sammanställd av S. Hård, VIAK AB. BFR–R60:1984. 1983.

B:43 Lindahl, J.: Manual för MODEX–MODIM. Ett datorprogram för simulering av dynamiska förlopp i förankringskablar. 1983.